

CHARACTERIZING THE MN(II) OXIDIZING ENZYME  
FROM THE MARINE BACILLUS SP. PL-12 SPORE

By

Cristina N. Butterfield

A THESIS/DISSERTATION

Presented to the Division of Environmental and Biomolecular Systems

and

Oregon Health & Science University

in partial fulfillment of

the requirements for the degree of

Doctor of Philosophy

September 2014

Oregon Health & Science University  
School of Medicine  
Institute of Environmental Health  
Division of Environmental and Biomolecular Systems

---

CERTIFICATE OF APPROVAL

---

This is to certify that the Ph.D. dissertation of  
Cristina N. Butterfield  
has been approved

---

Bradley M. Tebo, Ph.D.  
Professor and Research Advisor

---

Ninian J. Blackburn, Ph.D.  
Professor and Examination Committee Chair

---

Pierre Moenne-Loccoz, Ph.D.  
Associate Professor and Committee Member

---

Martina Ralle, Ph.D.  
Assistant Professor, Molecular and Medical Genetics, External Examiner

---

Thomas G. Spiro, Ph.D.  
Professor, University of Washington, External Examiner

## Table of Contents

Acknowledgments .....	ivv
Abstract .....	v
Chapter 1. Mn oxidation by <i>Bacillus</i> sp. spores.....	1
Chapter 2. Mn(II, III) oxidation and MnO <sub>2</sub> mineralization by an expressed bacterial multicopper oxidase (published in PNAS July 2013) .....	25
Chapter 3. Substrate kinetics and Cu binding characteristics of the Mn oxidizing Mnx complex from <i>Bacillus</i> sp. PL-12.....	37
Chapter 4. Spectroscopic studies reveal novel type 2 Cu and heme binding in subunits of a multicopper oxidase-containing complex .....	55
Chapter 5. Conclusions and Future Directions .....	72
References .....	81
Appendices.....	93

## **Acknowledgments**

I would like to thank my family and friends for their support and encouragement throughout my graduate career, especially Robert, Kelly, and my parents. I am forever changed by the experiences of failing and succeeding during my tenure on this project and will always be indebted to Brad for allowing me to take that path. I also want to thank Tom and Pierre for challenging me and pushing me beyond what I thought I was capable of.

Thanks also to my high school summer interns Gloria Kim and Katherine Osterlund for helping with protein preparation and keeping enthusiasm up.

I am grateful to the various funding sources for making this work possible: Oregon Opportunity Fund, Vertex Pharmaceuticals Graduate Fellowship, and the NSF Grants OCE-1154307 and OCE-1129553.

## Abstract

On Earth, the Mn geochemical cycle is becoming increasingly recognized as playing a significant role in the cycling of other elements. Especially reactive are the oxidized Mn species (Mn(III, IV)) in MnO<sub>2</sub> minerals which are abundant in the environment. Bacteria are believed to be the main driver in Mn oxidation catalysis so the mechanism of this process is of great scientific interest. The premier Mn oxidizing microbes in the laboratory have been the marine *Bacillus* species that mineralize Mn on the outside layer of their spores, the exosporium. In this thesis, the expression, purification, and characterization of the active Mn(II, III) oxidase from *Bacillus* sp. PL-12 is described. Several biochemical and bioinorganic methods, both straightforward and sophisticated, are employed to investigate the basic structural, metal binding, and catalytic features of the oxidase. The purified protein is a complex, named “Mnx”, composed of the multicopper oxidase, MnxG, and MnxE and MnxF, previously “hypothetical proteins” but herein suggested as a novel Cu binding oligomer also capable of binding Fe heme. As a complex, Mnx is able to catalyze the most efficient enzymatic Mn oxidation described in addition to the oxidation of common MCO substrates, Fe and phenolic compounds. This work facilitates the investigation into the mechanism of Mn mineralization in the environment on the molecular level and the elucidation of unusual bioinorganic chemistry.

## Chapter 1. Mn oxidation by *Bacillus* sp. spores

It is estimated that 30% of all proteins use transition metals as catalytic cofactors for activity. The naturally occurring transition metal cofactors include V, Cr, Co, Mo, Ni, Zn, Cd, W, Fe, Mn, and Cu and the oxidation state of these metals greatly impacts their chemistry and bioavailability. In the environment, these elements cycle via biotic and abiotic properties, influencing other chemical cycles as well as biological abundance and diversity by limiting metabolic processes. This thesis focuses on the enzymatic mechanism of Mn biomineralization by bacteria, one of many biotransformations responsible for catalyzing the transitions of metals through their biotic/abiotic phases (Fig. 1). Elucidating the mechanisms behind transition metal cycling processes in nature will further the understanding of some fundamental biogeochemical questions like how life evolved with the changes in Earth's atmosphere and how humans contribute to global climate change.

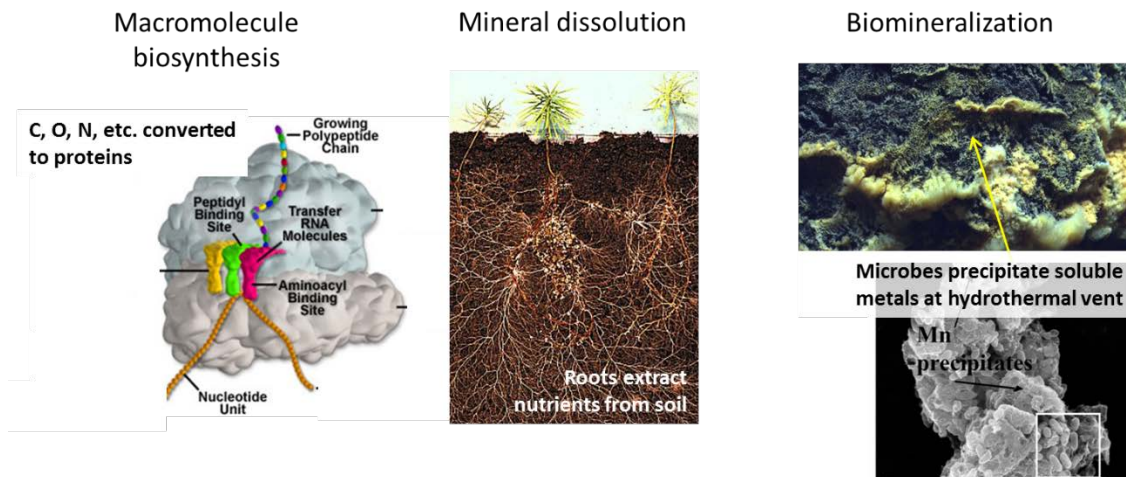


Figure 1. Examples of biotransformations and their mechanisms. From left to right: Proteins are synthesized by the ribosome, plant roots liberate nutrients from the rhizosphere, and microbes deposit Mn and Fe oxides at the sea floor (MARUM, 2012).

## *Mn biogeochemistry*

Manganese is ubiquitous in the environment and abundant in the Earth's crust, comprising about 0.1% of average crustal rocks (Turekian and Wedepohl, 1961). It cycles primarily between soluble Mn(II) and insoluble Mn(III,IV) oxides (collectively referred to as "Mn oxides") with a ligand-stabilized soluble Mn(III) intermediate occurring as a transient state (Fig. 2).

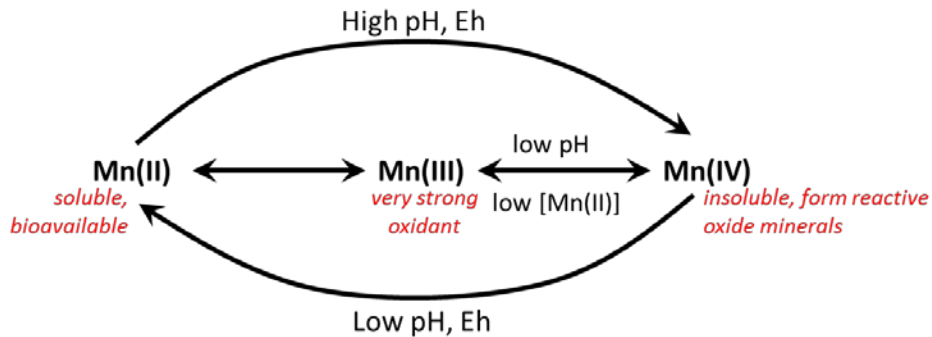
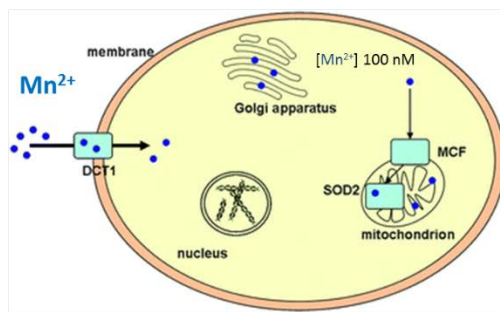


Figure 2. Mn cycles between three oxidation states in the environment.

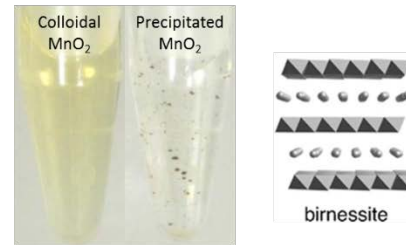
Mn(II) is released from igneous and metamorphic rocks by interactions with surface water and groundwater either through reductive dissolution of Mn(III,IV) oxides or leaching of Mn(II) from rocks. In this bioavailable state, Mn(II) is taken up by cells through transporters up to concentrations over 100 nM and incorporated into proteins to perform many different processes (Fig. 3) (Ba et al., 2009). In photosynthesizing organisms, a multinuclear Mn-Ca site is the catalytic center for H<sub>2</sub>O oxidation to O<sub>2</sub> in Photosystem II. In superoxide dismutase (SOD), Mn is used to catalyze the formation of O<sub>2</sub> and H<sub>2</sub>O<sub>2</sub> from O<sub>2</sub><sup>-</sup>, a potent antimicrobial used by the immune system to kill pathogenic cells.

Bioavailable  $Mn^{2+}$  is incorporated into proteins, much more stable than Fe and Cu



Aicha Ba et al. 2009

Insoluble  $Mn^{4+}$  precipitates into minerals



Ferromanganese nodules cover 30% of deep ocean floor!

Figure 3. Left: soluble  $Mn^{2+}$  is available for incorporation into cells and proteins. Right: Insoluble  $Mn^{4+}$  aggregates to form birnessite sheets at the atomic level and eventually large nodules.

Mn oxides are insoluble, have high surface area, and are abundant in depositions such as nodules, microconcretions, coatings, and crusts in soil as Mn hydrous oxides and on the ocean floor in ferromanganese nodules (Post, 1999). They form about 30 different types of oxide/hydroxide minerals with tunnel and layered structures that contain vacancies in which other metals can sorb, such as Ra, Pb, and Po (Towler et al., 1996; Post, 1999). Mn and Fe oxides readily incorporate radionuclides including  $^{234}Th$ ,  $^{228}Th$ ,  $^{228}Ra$ , and  $^{226}Ra$  (Todd et al., 1988b; Wei and Murray, 1991). The detoxifying properties of the Mn oxides inspired their description as “scavengers of the sea” (Goldberg, 1954).

$Mn(III,IV)$  oxides are some of nature’s strongest oxidants; this property makes them attractive for removing contaminants immobilized on the mineral surface. In fact,



Mn oxides are already used in drinking water treatment facilities (Prasad and Chaudhuri, 1995). They can oxidize both simple organic matter including phenols and quinones (Stone and Morgan, 1984a; Stone and Morgan, 1984b; Lehmann et al., 1987) and recalcitrant organic matter, forming low molecular weight organic compounds (Sunda and Kieber, 1994) that could be used as microbial food. They also oxidize metals such as Se(IV) to Se(VI) (Scott and Morgan, 1996), Cr(III) to Cr(VI) (Manceau and Charlet, 1992), and As(III) to As(V) (Huang, 1991). Additionally, synthetic contaminants like Bisphenol A (Davis-Kaplan et al., 1998), polychlorinated biphenyls, chlorinated anilines, and atrazine are all degraded by Mn oxides (Stone and Morgan, 1984a; Stone and Morgan, 1984b; Stone, 1987b; Ulrich and Stone, 1989). A review by Tebo et al. (Tebo et al., 2004) highlights the mechanisms by which these compounds are degraded: free radical oxidation, nucleophilic addition of the substrate to o-quinones (Park et al., 1999), oxidation and release of CO<sub>2</sub> without organic intermediates (Cheney et al., 1996; Nasser et al., 2000), and dealkylation at Mn oxide surfaces (Cheney et al., 1998). At low pH, these mechanisms are enhanced (Stone, 1987a; Laha and Luthy, 1990; Davis-Kaplan et al., 1998).

#### *Bacterial Manganese(II) oxidation*

Chemical Mn(II) oxidation is thermodynamically favorable but kinetically very slow at pH < ~8.5 (Morgan, 2000). It is likely that the environmentally relevant mechanism of mineralization is through microbial (bacterial and fungal) activities which is several orders of magnitude faster than abiotic autocatalysis on the surface of Mn oxides (Hastings and Emerson, 1986). Low G + C Firmicutes, high G + C Gram-positive, and alpha, beta, and gamma Proteobacteria all have Mn(II)-oxidizing members, and many

of them catalyze this oxidative reaction in their vegetative form, including *Pseudomonas*, *Aurantimonas*, *Roseobacter*, *Leptothrix*, *Pedomicrobium*, and *Erythrobacter* (Tebo et al., 2004).

Biogenic oxides tend to localize to the outer layers of the cell, often with the extracellular polysaccharide matrix. Mn oxides likely template on the organic matter by direct and indirect processes (Richardson et al., 1988; Hullo et al., 2001) forming predominately birnessite minerals (Tebo et al., 2004). The evolutionary purpose of Mn(II) oxidation remains a mystery. Bacteria do not require the process for survival, yet one can imagine that a Mn mineral coat may deter predation, act as UV protection, or degrade recalcitrant organic matter for nutrition for the microbe. That dormant spores from some *Bacillus* species can also oxidize Mn(II) to form Mn oxides, makes the role of Mn(II) oxidation even more inexplicable for these organisms.

#### *Bacillus* spores and Mn(II) oxidation

Bacteria have been linked to Mn(II) oxidation since the beginning of the 20th century but it was not until the 1970s that a spore had been linked to this important process. Transmission electron microscopy captured the first images of a bacterial spore, *Bacillus* sp. SG-1, isolated from an



Figure 4. Transmission electron micrograph of *Bacillus* sp. SG-1 spore with spiny MnO<sub>2</sub> oxides localized on the exosporium (from (Rosson and Nealson, 1982)).

enrichment culture of near-shore sediments from San Diego and encased in a web of Mn oxides (Fig. 4) (Nealson, 1978). Rosson and Nealson proposed that an enzyme on the spore surface was the Mn oxide deposition culprit since azide and cyanide inhibited Mn(II) binding and oxidation (Rosson and Nealson, 1982). Since then, work has been continued to determine how the bacteria generate these oxides and what effects these Mn oxides have on geochemical cycling of Mn and other elements.

Mn(II)-oxidizing spores are not uncommon. Although it may be difficult to analyze the abundance of spores and their activity in the environment, our lab has demonstrated the diversity and pervasiveness of Mn(II) oxidizing *Bacillus* spores through isolation from a variety of environments (Lee, 1994; Francis and Tebo, 2002; Templeton et al., 2005; Dick et al., 2006). Mn(II) oxidizing spores are isolated by diluting a soil or water sample, heating it to 80°C for 10-20 min, and spreading it onto Mn(II) containing solid media. Colonies that sporulate and become encrusted with brown Mn oxides are cultured for DNA extraction and 16s rRNA gene sequence analysis. In 2002, Francis and Tebo (2002) reported the isolation of 13 different species in near-shore sediments around San Diego, CA that formed three phylogenetically distinct groupings (Francis and Tebo, 2002). These included isolates from various environments grouping with strain SG-1, the MB-7 cluster that were similar to moderately halophilic or halotolerant species, and the PL-12 cluster. The PL-12 cluster was similar to strains isolated from a variety of sources including a Korean traditional fermented seafood, a uranium mine tailings pile near Dresden, Germany, a hydrocarbon seep, and rice paddy-associated anoxic bulk soil. Clearly, Mn(II)-oxidizing activity of *Bacillus* spores is present in phylogenetically and

environmentally diverse *Bacillus* species, suggesting that Mn(II) oxidizing *Bacillus* spores are common and widespread in the environment.

If Mn oxides are the “scavengers of the sea” (Goldberg, 1954) and Mn(II) oxidizing spores are widespread, then Mn(II) oxidizing spores should impact the Mn biogeochemical cycle in the oceans. Dick and colleagues were also able to map out the diversity of 20 more isolates of Mn(II) oxidizing *Bacillus* spores, which fall into two clusters in the water column of the Guaymas Basin, a semi-enclosed basin with a sediment-covered hydrothermal system (Dick et al., 2006). Mn(II) oxidizing activity was associated with the spores and could occur at high temperatures, as high as 70 °C. Their study suggested that bacterial spores play a role in the short Mn residence time in the Guaymas Basin and that rapid and stable Mn(II) oxidizing spores at hydrothermal sediments and plumes could be the mechanism of elemental scavenging as put forth by Cowen (Cowen et al., 1986; Cowen et al., 1990; Cowen and Li, 1991).

Metals like Cr(III), Co(II), and U(IV) are oxidized in the presence of Mn(II) oxidizing spores (Fig. 5). An exciting prospect was the possibility that the spores directly oxidized these metals, but, alas, these metals were not oxidized by stringently washed *Bacillus* sp. SG-1 spores without added Mn (Murray and Tebo, 2007), nor they competed with Mn(II) for sites within the same enzyme (Murray and Tebo, 2007; Murray et al., 2007). Cr(III), Co(II), and U(IV) have been shown to be oxidized abiotically by synthetic Mn oxides,  $\delta$ -MnO<sub>2</sub> (Fendorf and Zamoski, 1992; Fredrickson et al., 2002; Murray et al., 2007), leading to the speculation that the Mn oxides are the oxidant. Indeed, newly formed biogenic MnO<sub>2</sub> oxidize these metals faster than synthetic oxides: seven times faster for Cr(III) (Murray and Tebo, 2007), two to five times faster for Co(II)

(Murray et al., 2007), and almost two times faster for U(IV) (Chinni et al., 2008). The higher reactivity of the biogenic nanoparticulate MnO<sub>2</sub> oxides can be attributed to their mixed valence Mn(II, III, IV) (Bargar et al., 2000) and vacancies within the structure (Tebo et al., 2004). Clearly, determining the mechanism of generating reactive biogenic MnO<sub>2</sub> oxides is linked to understanding the cycling of other metals.

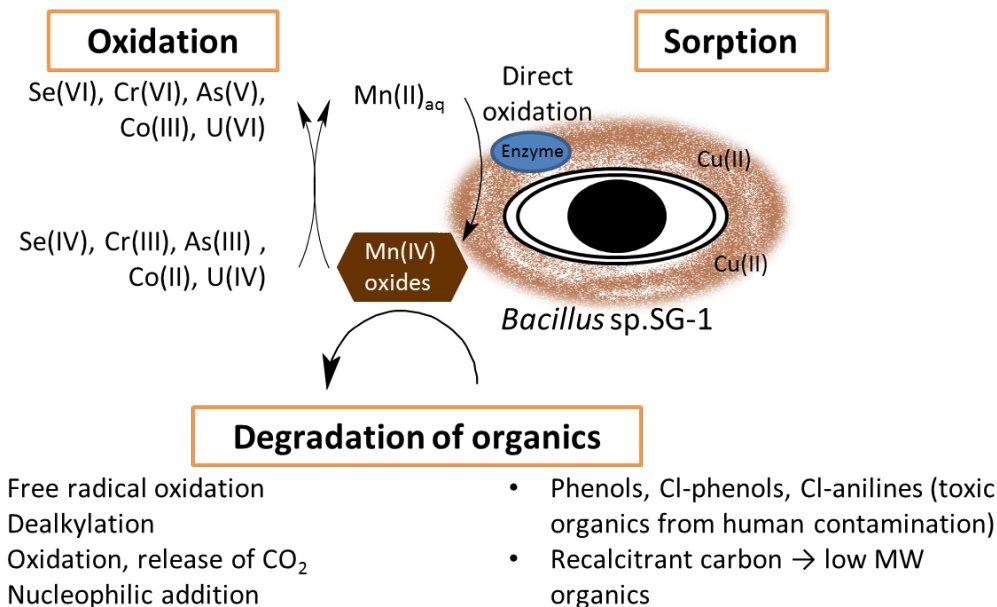


Figure 5. Proposed functions and applications of bacteriogenic Mn oxides.

#### *Proposed mechanisms of bacterial Mn oxidation*

Although the bacteria that oxidize Mn are ubiquitous and phylogenetically diverse, only a handful of Mn oxidation mechanisms have been proposed. Mn(II) to Mn(IV) oxidation can be catalyzed directly by metallo-enzymes from the multicopper oxidase and animal heme peroxidase families (*in vide infra*). Multicopper oxidases (MCOs) have been linked to activity in *Leptothrix discophora*, *Pseudomonas putida*, and diverse marine *Bacillus* spp. (Van Waasbergen et al., 1993; Corstjens et al., 1997; Geszvain et al., 2013). MCOs contain four Cu atoms that oxidize a substrate and reduce

O<sub>2</sub> to H<sub>2</sub>O. The animal heme peroxidase in *Pseudomonas putida* is also implicated in Mn oxidation along with *Erythrobacter* sp. strain SD-21 and *Aurantimonas manganoxydans* strain SI85-9A1 (Anderson et al., 2009). This enzyme utilizes Fe-heme to oxidize a substrate, reducing H<sub>2</sub>O<sub>2</sub> in the process. Mn oxides may also form from indirect processes. The generation of Mn(III) by white rot fungi during the breakdown of plant matter by their Mn peroxidases is a source of Mn(IV) by disproportionation and superoxide from various metabolic and reproductive processes facilitate oxidation in *Roseobacter* sp. AzwK-3b and Ascomycete filamentous fungi even in low pH conditions (Hansel and Francis, 2006; Hansel et al., 2012). The challenge throughout this project has been to provide evidence for direct Mn oxidation by enzymes designed for this process specifically because no Mn oxidizing MCO or animal heme peroxidase has been purified to the quantity necessary for detailed studies.

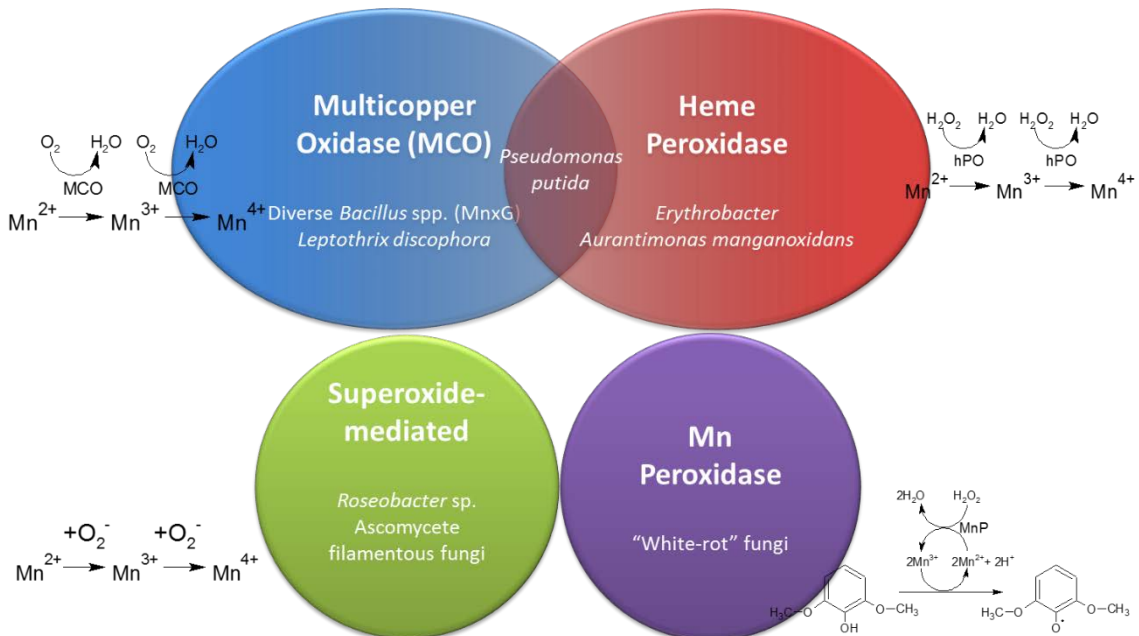


Figure 6. Mn oxidation: mechanisms and microbes. See text for details.

The redox reactivity and stability characteristics of Mn oxidizing proteins make them especially conducive to extracellular catalysis. The intrinsic redox potential of MCOs and heme peroxidases and their reliance on O species to provide oxidant as opposed to metabolic products NAD and NADPH are the properties that make these proteins able to function independently from the vegetative cell's activities. MCOs are especially hardy as well, even reaching optimal activity at 70 °C (Reiss et al., 2011) which is advantageous when the localization to the outer cell surfaces or extra-cellular matrix such as the spore coat or exosporium requires direct interaction with harsh environments. The heme center of horseradish peroxidase also aids in stability of the protein structure at low pH (Carvalho et al., 2003).

*Proteins bind metal for catalysis*

As mentioned previously, it is estimated that 1/3 of all proteins contain transition metals for catalysis so it is not entirely surprising that metalloproteins are implicated in the process of Mn oxidation. Enzymes that utilize metal cofactors for redox chemistry have evolved active sites designed to bind cofactor and substrate in such a way as to tune reduction potential and lower the reorganization energy towards electron transfer (Gray et al., 2000). "This entactic" state theory helps explain how metalloproteins perform unique chemistry (Vallee and Williams, 1968). Characterizing the metal binding and kinetic features of these centers links common mechanisms to disparate enzymes and reactions, thus harnessing physical reality to obtain metabolic diversity of life on Earth.

When evaluating a newly purified protein, one can predict metal binding ligands based on Lewis hard-soft theory of acids and bases (Table 1) and on sequence similarity to known proteins. Cu is incorporated into three spectroscopically distinct centers within

the MCOs as well as in other configurations in cytochrome c oxidase (Fig. 7) and nitrous oxide reductase (Solomon et al., 1996). These centers are highly conserved among the various members of the protein families. Cu is usually bound by the borderline and soft bases of the functional groups centered on N(His), N(amide backbone), S(Cys), and S(Met). Fe can be found in the form of Fe-S(elemental and Cys) clusters and in protoporphyrin rings stabilized by one or two N(His) in proteins of the electron transport chain (Fig. 7). Mn is often housed in multinuclear sites of such proteins as those in photosystem II at the O<sub>2</sub> evolving complex, Mn-catalase, and ribonucleotide reductase and ligated with borderline and hard Lewis bases centered on O(Asp), O(Glu), and N(His).

**Hard-soft acid-base classification of metal ions and ligands important to bioinorganic chemistry**

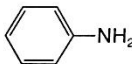
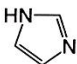
Metals			Ligands		
<b>Hard</b>					
H <sup>+</sup>	Mn <sup>2+</sup>	Cr <sup>3+</sup>	H <sub>2</sub> O	CO <sub>3</sub> <sup>2-</sup>	NH <sub>3</sub>
Na <sup>+</sup>	Al <sup>3+</sup>	Co <sup>3+</sup>	OH <sup>-</sup>	NO <sub>3</sub> <sup>-</sup>	RNH <sub>2</sub>
K <sup>+</sup>	Ga <sup>3+</sup>	Fe <sup>3+</sup>	CH <sub>3</sub> CO <sub>2</sub> <sup>-</sup>	ROH	N <sub>2</sub> H <sub>4</sub>
Mg <sup>2+</sup>	Ca <sup>2+</sup>	Tl <sup>3+</sup>	PO <sub>4</sub> <sup>3-</sup>	R <sub>2</sub> O	RO <sup>-</sup>
			ROPO <sub>3</sub> <sup>2-</sup>	(RO) <sub>2</sub> PO <sub>2</sub> <sup>-</sup>	Cl <sup>-</sup>
<b>Borderline</b>					
Fe <sup>2+</sup>	Ni <sup>2+</sup>	Zn <sup>2+</sup>	NO <sub>2</sub> <sup>-</sup>		
Co <sup>2+</sup>	Cu <sup>2+</sup>		N <sub>2</sub>		
			SO <sub>3</sub> <sup>2-</sup>		
			Br <sup>-</sup>		
			N <sub>3</sub> <sup>-</sup>		
<b>Soft</b>					
Cu <sup>+</sup>	Pt <sup>2+</sup>	Pt <sup>4+</sup>	R <sub>2</sub> S	R <sub>3</sub> P	
Au <sup>+</sup>	Tl <sup>+</sup>	Hg <sup>2+</sup>	RS <sup>-</sup>	CN <sup>-</sup>	
Cd <sup>2+</sup>	Pb <sup>2+</sup>		RSH	RNC	
			(RS) <sub>2</sub> PO <sub>2</sub> <sup>-</sup>	(RO) <sub>2</sub> P(O)S <sup>-</sup>	
			SCN <sup>-</sup>	CO	
			H <sup>-</sup>	R <sup>-</sup>	

Table 1. Metals are Lewis acids that bind to corresponding hard or soft Lewis bases, chemical species in proteins. (Table from Principles of Bioinorganic Chemistry (Lippard and Berg, 1994).)



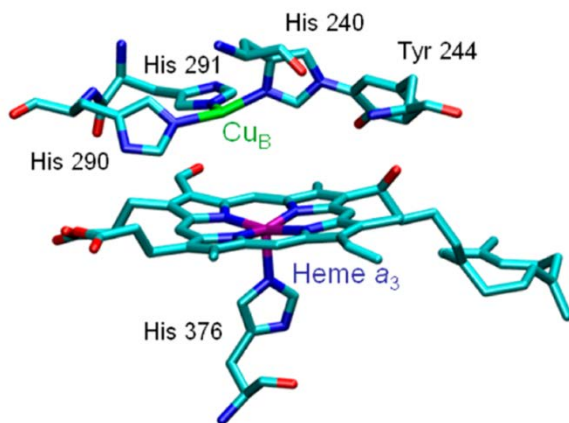


Figure 7. Cytochrome c oxidase has multiple metal centers, type 2 Cu and Fe-heme (Figure from “Copper active sites in biology” (Solomon et al., 2014).)

### *Physical methods to analyze metalloproteins*

The metal binding described above was made possible by the direct evidence of covalent binding obtained from advances in spectroscopic techniques. Several spectroscopic techniques have been developed during the last century to analyze the metal centers of highly concentrated (up to mM) proteins including electron paramagnetic resonance spectroscopy (EPR), nuclear magnetic resonance spectroscopy, resonance Raman spectroscopy, Mössbauer spectroscopy, X-ray absorption spectroscopy (XAS), Fourier transform infrared spectroscopy, circular dichroism, optical spectroscopy, etc. They have been optimized from earlier, cruder instrumentation that was originally developed for solid samples. One such advancement resulted from the increase in X-ray beam intensity and tunability achieved through synchrotron radiation sources, allowing for higher resolution and lower sample concentration. Each technique has its weaknesses depending on the sensitivity of the instruments and the electrochemical features of the metals. For example, when analyzing a complex sample containing the similar metals Fe and Mn by XAS, one might observe an overlap in signals because their absorption edge

energies are so close to each other (approx. 640 eV for Mn and 710 eV for Fe). EPR is limited by detecting only metals with unpaired electrons and those that are not antiferromagnetically coupled. Finally, if a protein has more than one type of center binding the same metal, the spectrum will be too complex for interpretation and effort must be taken to eliminate all but one signal at a time. Of the several techniques mentioned, EPR, XAS, and electronic spectroscopy (UV-vis) will be used in this dissertation research to characterize the Mn oxidase, and the following paragraphs will provide a primer on those approaches.

#### UV-visible absorption spectrophotometry

Metal centers are often colored because of their d-d charge transfer characteristics when bound to the protein. The spectrophotometer is a simple but powerful bench top instrument allowing the rapid evaluation of metal binding and oxidation state based on known absorbance features of metalloproteins. Type 1 Cu absorbs light at around 600 nm because of the Cu-S-Cys bond and type 3 Cu absorbs at 330 nm because of the Cu-OH-Cu bond (Fig. 8) (Solomon et al., 1996). A simple way to validate these features is reduction of the metal with a reductant like sodium hydrosulfite. When type 1 Cu<sup>2+</sup> is reduced to Cu<sup>1+</sup>, the 600 nm band is quenched. Fe in heme also has characteristic color and charge transfer UV-visible absorption spectrum peak, the Soret band, due to the four or six coordinate binding of Fe to the protoporphyrin heme cofactor. Heme-bound protein has visible peaks at around 400 (Soret) and two at around 550 nm due to the  $\pi$ - $\pi$  interactions (Fig. 9) (Luthra et al., 2011). When Fe in heme is reduced, there is a characteristic shift to the right of the Soret band and the visible bands become resolved.

#### Electron paramagnetic resonance

EPR is used to gain experimental evidence for covalent bonding of paramagnetic species, or those elements with an unpaired electron. From EPR, information about the spin state, oxidation state, and protein ligand environment of transition metal centers are yielded. Several metal centers are EPR detectable like Co(II), Fe(III), Mn(II), and Ni(I, III). Cu(II) centers are also well studied, including type 1 and type 2, but not type 3 because the two Cu are antiferromagnetically coupled (Fig. 8). The type 1 and type 2 Cu first derivative spectra have characteristic banding patterns associated with the Cu-N bonds; there are four hyperfine splitting peaks, typical of Cu(II), and superhyperfine splitting, indicative of two or three equivalent N-Cu bonds.

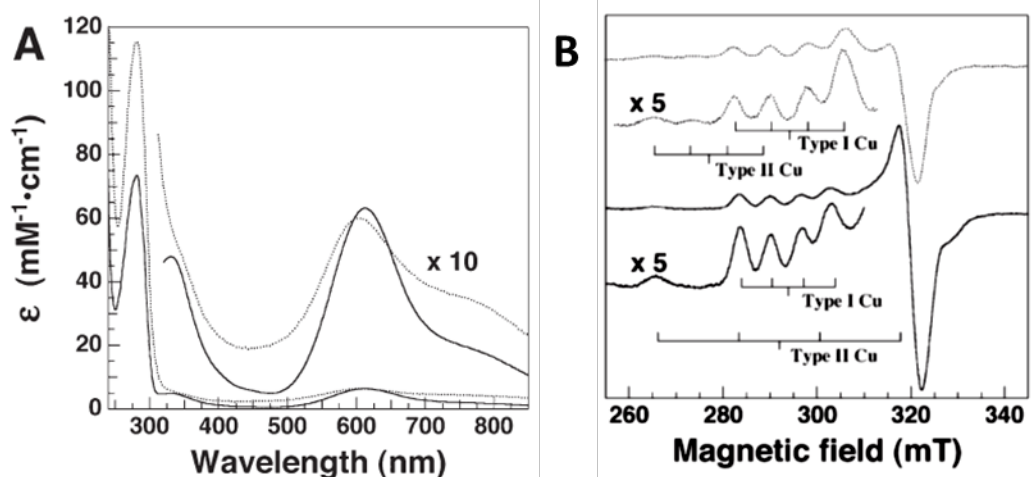


Figure 8. Absorption (A) and EPR spectra (X-band) (B) of the different types of MCO Cu CueO solid line. Bilirubin oxidase dotted line (Sakurai and Kataoka, 2007).

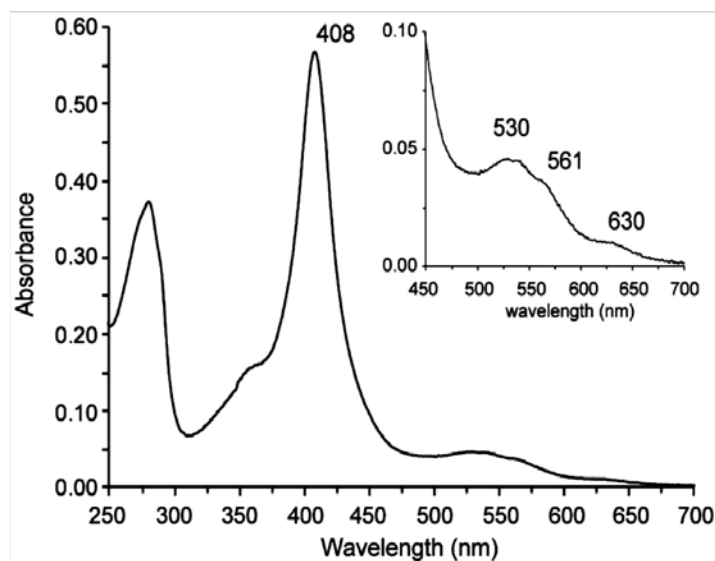


Figure 9. Absorption spectrum of heme peroxidase. Figure from “A heme peroxidase with a functional role as an l-tyrosine hydroxylase in the biosynthesis of anthramycin” (Connor et al., 2011)

### X-ray Absorption Spectroscopy

The oxidation state and binding environment can be obtained through X-ray absorption near-edge structure (XANES) and extended X-ray absorption fine structure (EXAFS), respectively. The 1s (K edge) or 2s,2p (L edge) electrons can be excited by the absorption of X-rays to empty localized orbitals. At the onset of this edge is where one can determine the oxidation state of the metal. The rest of the spectrum will reflect the binding environment since the electrons are scattered based on the neighboring atoms. One can fit the spectrum to a geometric model of the site to validate a metal binding hypothesis as shown in the case of the Fe-S clusters in Fig. 10. The same technique and analysis can be used as solids as well for such goals as determining the binding geometry of minerals.

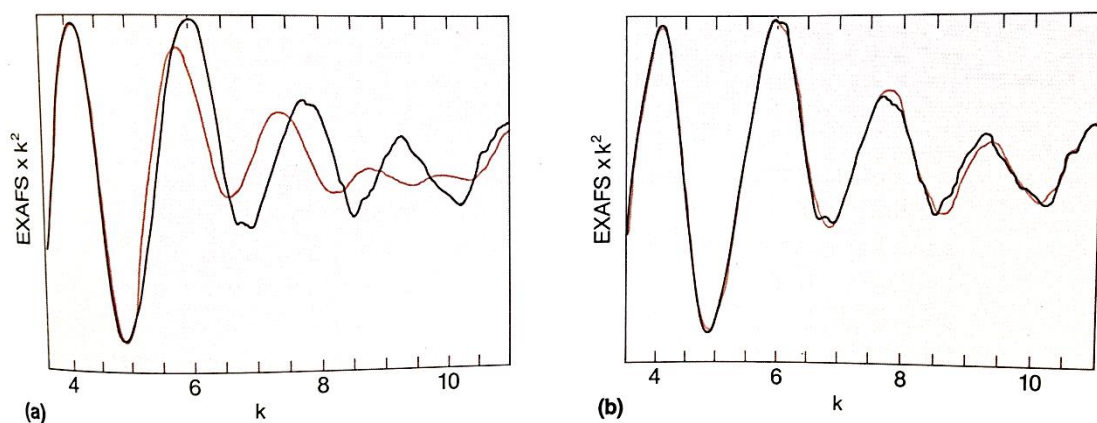


Figure 10. Extended X-ray absorption fine structure of Fe-S cluster in rubredoxin. A) Experimental spectrum (red) and crystallographic distances (black). B) Experimental spectrum (red) compared to model distances (black). Figure from Principles of Bioinorganic Chemistry (Lippard and Berg, 1994), originally published in Shulman et al., 1975 (Shulman et al., 1975).

#### History of the research on *Bacillus* sp. mechanism

Discovery of the Mn oxidizing MCO in *Bacillus* sp. SG-1 by mutagenesis was difficult because the development of a genetic system in *Bacillus* sp. SG-1 to alter its genomic DNA was not trivial. van Waasbergen attempted many transformation techniques with several plasmids (Van Waasbergen et al., 1993) before finally conceiving a protoplast preparation transformation of the pLTV1 plasmid with a modified *Streptococcus faecalis* transposon to disrupt the gene responsible for Mn(II) oxidation. Van Waasbergen identified the 7 gene cluster called *mnxA- mnxG* (Fig. 11) (Van Waasbergen et al., 1993; Van Waasbergen et al., 1996). Twenty years later and still only *Bacillus* SG-1 MnxC and MnxG primary sequences have enough amino acid sequence similarity to known proteins to predict function. MnxC shows similarity to a Cu loading protein folding chaperone, Sco, which is thought to be responsible for Cu loading in the synthesis of cytochrome c oxidase. MnxG is similar to another Cu containing protein,

ceruloplasmin, a large 6-domain multicopper oxidase that oxidizes Fe(II) to Fe(III) and is involved in Fe transport in the bloodstream (Van Waasbergen et al., 1996).

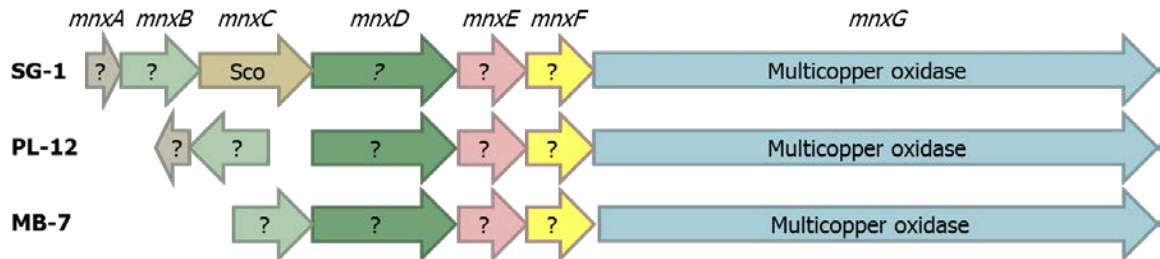


Figure 11. Marine Mn oxidizing *Bacillus* sp. SG-1, PL-12, and MB-7 have homologous *mnx* genes.

Further evidence that the *mnx* gene products are linked to spore Mn(II) oxidation activity soon followed. The *mnxD-lac* gene reporter activity assay localized gene expression to around stage III of sporulation, peaking between stages IV and V, suggesting regulation of *mnx* genes by the late sporulation sigma factor K (Fig. 12) (Van Waasbergen et al., 1996). The Cu-binding regions in the *mnxG* gene were used to design degenerate primers to amplify a region of DNA to be used in phylogenetic analysis of environmental isolates because the rest of the gene was too divergent from one isolate to the next (Francis and Tebo, 2002). *mnxG* genes clustered with their respective 16s rRNA genes, indicating little horizontal gene transfer of *mnxG*. Further, detection of *mnxG* correlated to Mn(II) oxidizing activity in the endospore, and because the exosporium retains Mn(II) oxidizing activity after being removed by high pressure with the French press, the activity was localized to this layer (Francis et al., 2002).

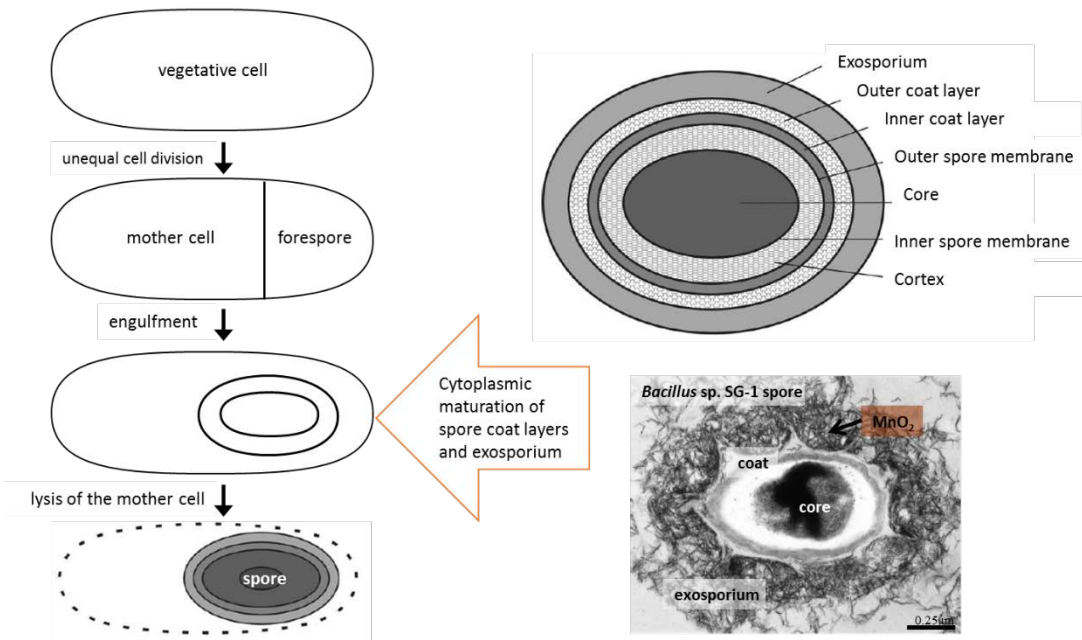


Figure 12. *Bacillus* spore generation and morphology. The exosporium is deposited on the spore coat surface while still engulfed in the mother cell (Kim and Schumann, 2009). The Mn-oxidase is therefore controlled by sigma K transcription factor and matures in the soluble cytoplasmic environment. Lower right transmission electron microscopy image of *Bacillus* SG-1 with Mn oxides localized in the “hairy nap” of the exosporium (Rosson and Neelson, 1982).

Direct evidence of Mnx proteins catalyzing Mn(II) oxidation came after isolating activity from the exosporium to a single protein band in non-denaturing sodium dodecyl sulfide-polyacrylamide gel electrophoresis (SDS-PAGE) and analyzing the peptides by tandem mass spectrometry (Dick et al., 2008). Only peptides matching MnxF and MnxG amino acid sequences were identified from the exosporium preparation of three diverse *Bacillus* spp., whose *mnxD*, *mnxE*, *mnxF*, and *mnxG* genes were well conserved among the sequenced Mn(II) oxidizing *Bacillus* species SG-1, PL-12, and MB-7.

The Mn(II) oxidation reaction was inactivated by multicopper oxidase inhibitors, azide and cyanide, further implicating a Cu protein in catalysis (Dick et al., 2008).

Multicopper oxidases contain at least four Cu atoms that facilitate the single electron

oxidation of a substrate with the reduction of  $O_2$  to  $H_2O$ . The four Cu sites are made up of one type 1 center consisting of two S ligands from Cys and Met, and two imidazole ligands from His, and the trinuclear center (TNC), made up of one type 2 center consisting of two imidazole ligands and two type 3 centers consisting of three imidazole ligands each. Multicopper oxidase binds a substrate, either a phenolic compound or metal, at a binding site proximal to the type 1 Cu. The type 1 Cu contains enough redox potential to rip a single electron off the substrate and send it  $\sim 10 \text{ \AA}$  down a proton bonding network to the TNC where the remaining Cu centers lie and are ready to transfer the electron to  $O_2$  creating  $H_2O$  (Fig. 13) (Solomon et al., 1996). Thus, it appeared that the multicopper oxidase, MnxG, was the Mn(II) oxidase with MnxF playing an unknown role.

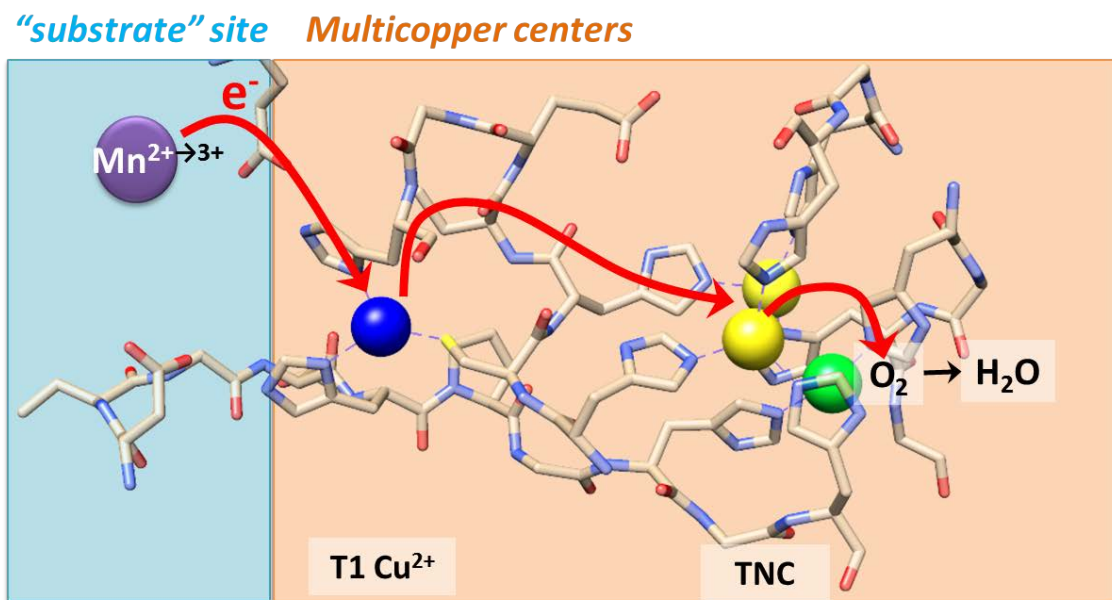


Figure 13. Electron flow through the MCO catalytic center.

There is a precedent for multicopper oxidases to be localized to the outer layer of the *Bacillus* spore. *Bacillus subtilis* coat protein, CotA, is a well-studied multicopper



oxidase located in the thick, striated outer coat capable of generating a brown pigment (not Mn oxides) around the spore, which it uses for UV protection (Moeller et al., 2012). CotA is a 67 kDa 3-domain protein encoded by a single gene and is most similar to *E. coli*'s Cu(I) oxidizing CueO multicopper oxidase. CotA is also heat resistant and even fully active at 80 °C (Martins et al., 2002). It has a flexible, lid-like region near the substrate binding region that can play a role in binding larger substrates than CueO is able to. CotA and CueO are very dissimilar to MnxG in sequence and in length, so comparisons are limited.

*Mn(II) oxidation mechanism and implications of Mn(III) intermediate*

X-ray absorption spectroscopy techniques determined that the primary product of Mn(II) oxidation and the most environmentally relevant mineral produced by *Bacillus* sp. SG-1 (and other Mn(II)-oxidizing bacteria) is closely similar to hexagonal birnessite (Mn(IV)O<sub>2</sub>) (Bargar et al., 2000; Villalobos et al., 2003; Bargar et al., 2005b). Experiments spectrophotometrically measuring the trapping of Mn(III) with pyrophosphate using purified exosporium from *Bacillus* sp. SG-1 and purified Mn oxidase from *Bacillus* sp. PL-12 confirmed the two single electron sequential oxidation steps (Webb et al., 2005a; Soldatova et al., 2012). The reaction could be initiated with Mn(II) or Mn(III)-pyrophosphate to produce brown Mn(IV) oxides, implying that the enzyme may have two binding sites for different Mn species.

Spiro and co-authors put forward a mechanistic model to rationalize these results within the thermodynamic limitations (Figure 14) (Soldatova et al., 2012). They postulate that Mn(II) is oxidized at the substrate site proximal to the Type 1 Cu just as in other multicopper oxidases. The Mn(III) product is then held in a holding site away from the

substrate site, akin to ceruloplasmin's Fe(III) holding site, before it is transferred to a Mn(III) binuclear site. Newly oxidized Mn(III) drives the formation of oxo bridges in the binuclear site to form Mn(IV)O<sub>2</sub>. The binuclear site may nucleate MnO<sub>2</sub> formation by following one of the mechanisms put forward for the ferritin Fe(II) to Fe(III) oxidation (Honarmand Ebrahimi et al., 2012), such as stabilizing the binuclear Mn(IV) until a new Mn(III) ion triggers sequential displacement of Mn(IV) and oxidation of the displacing Mn(III).

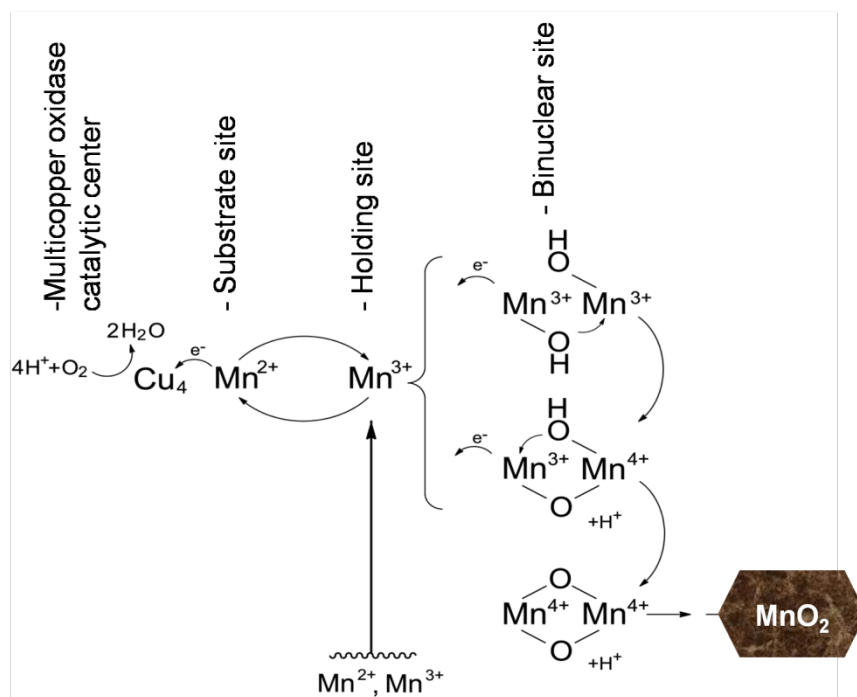


Figure 14: Mn oxidation model by Soldatova et al. 2012

As an intermediate in oxidation of Mn(II) to Mn(IV), Mn(III) is a powerful oxidant and its lability in this reaction could have interesting environmental implications. In the absence of chelators, Mn(III) species rapidly disproportionate to Mn(II) and Mn(IV) oxides. In the environment, however, a variety of Mn(III) chelators is available, such as oxalate, citrate, pyrophosphate or even organic matter. It is possible that Mn(III)

could be trapped by a natural chelator for other purposes such as competing with Fe(III) for complexation with siderophores (Parker et al., 2004), degrading lignin (Glenn et al., 1986; Perez and Jeffries, 1992; Höfer and Schlosser, 1999; Schlosser and Höfer, 2002), or oxidizing sulfur and nitrogen compounds (Kostka et al., 1995; Klewicki and Morgan, 1998; Luther III et al., 1998; Klewicki and Morgan, 1999). Thus, Mn(II) oxidation by “dormant” spores can impact Earth’s biogeochemistry through a catalytic effect on a variety of other major elemental cycles.

#### *Mnx protein expression*

Isolation of the native protein from the exosporium yields a very small amount of impure protein, so heterologous expression is preferred. Bacterial multicopper oxidases are typically expressed and purified from single gene MCO genes in *E. coli* expression hosts. In order to activate the MCO, Cu(II) is added directly after purification to fill the Cu binding sites. For the published *Bacillus* MCOs, however, the stoichiometric addition of Cu(II) does not fill the sites completely; for example, an “as-isolated aerobic” CotA from *B. subtilis* binds only 0.5 mol Cu per mol protein. Incubation with four-fold Cu(II) increases Cu(II) loading to 2.5:1, and an anaerobic addition of Cu(I) in the form of  $[\text{Cu(I)(MeCN)}_4]\text{PF}_6$  in Ar-purged acetonitrile results in 4.2 mol Cu per mol protein. A simpler and more effective method to fill Cu binding sites *in vivo* is microaerobic protein expression, as demonstrated by Durão and colleagues by loading the *E. coli* with 0.25 mM  $\text{CuCl}_2$  during *cotA* expression and achieving 3.7 Cu/protein with no further Cu incubation. Specifically, Cu(II) is added after expression, the shaking function of the incubator is stopped, and the static culture is allowed to sit for at least 22 hours. The whole cell content of Cu increases 10 fold over the duration of the static culture

incubation, resulting in about 2.5 mg Cu per g cell mass, whereas a no Cu control has essentially 0 mg Cu per g cell mass (Durão et al., 2008). The current hypothesis for how toxic levels of Cu enter the *E. coli* cytoplasm is that Cu export, in part, relies on CueO to oxidize Cu(I) to Cu(II) and exportation by the Cus protein complex. Without this oxidation, Fenton chemistry-reactive Cu(I) leaks across the inner membrane into the cytoplasm (Beswick et al., 1976; Grass and Rensing, 2001; Outten et al., 2001). Being an MCO itself, CueO cannot oxidize Cu(I) in the absence of O<sub>2</sub>, so Cu(I) accumulates in the cytoplasm under microaerobic conditions, effectively loading the heterologous MCO during biosynthesis.

Expressing and purifying MnxG alone from an *E. coli* expression host does not result in active protein even when the *in vivo* Cu loading method is implemented. Several attempts were made to isolate the Mn oxidase in this way, including heroic efforts with the latest technology such as the co-expression of protein folding chaperones, cloning in different purification tags, and transforming into special *E. coli* strains that are meant to increase protein solubility. A protein band corresponding to MnxG was observed by SDS-PAGE of the cell extract in these trials, but because the purification tag could not be cleaved, it was concluded that the MnxG product was probably aggregated, thus inactive.

#### Summary of thesis

The mechanism of microbial Mn oxidation is poorly understood and sometimes thought to occur through nonspecific side reactions facilitated by normal metabolic processes. The goal of this project was to determine the mechanism of Mn oxidation in the environment by demonstrating the direct and specific Mn oxidation by the Mnx protein from *Bacillus* sp. PL-12. In order to this, the catalytic center must be validated

and the activity specifically linked to it. Chapter 2 was published in PNAS in July 2013 and describes the breakthrough of protein production, the co-purification of MCO and small proteins MnxE and MnxF, and verifies that the activity is consistent with an MCO mechanism and the MnO<sub>2</sub> product is consistent with that found on the *Bacillus* spore. Chapter 3 completes the Cu binding characterization of the type 1 and type 2 sites within MnxG and also a survey of different substrates to determine that the active site has been optimized for Mn oxidation. Chapter 4 highlights the interesting heme and Cu binding characteristics of MnxEF, suggestive of possible redox activity within the MCO subunits. Chapter 5 summarizes the results and suggests future directions of the project including the elucidation of structural information and the detection of reaction intermediates along the course of Mn oxidation. In summary, this thesis describes the heterologous expression, purification, and characterization of a metalloprotein from a marine Mn(II) oxidizing *Bacillus* sp. spore. This thesis dissertation work marks the beginning of an in depth study of an important player in the Mn biogeochemistry cycle on Earth.

**Chapter 2. Mn(II, III) oxidation and MnO<sub>2</sub> mineralization by an expressed bacterial multicopper oxidase** (published in PNAS July 2013)

Cristina N. Butterfield, Alexandra V. Soldatova, Sung-Woo Lee, Thomas G.

Spiro, Bradley M. Tebo

Abstract:

Reactive Mn(IV) oxide minerals are ubiquitous in the environment, and control the bioavailability and distribution of many toxic and essential elements and organic compounds. Their formation is thought to be dependent on microbial enzymes, because spontaneous Mn(II) to Mn(IV) oxidation is slow. Several species of marine *Bacillus* spores oxidize Mn(II) on their exosporium, the outermost layer of the spore, encrusting them with Mn(IV) oxides. Molecular studies have identified the *mnx* (Mn oxidation) genes, including *mnxG*, a putative multicopper oxidase (MCO), as responsible for this two-electron oxidation, a surprising finding since MCOs only catalyze single electron transfer reactions. Characterization of the enzymatic mechanism has been hindered by the lack of purified protein. By purifying active protein from the *mnxDEFG* expression construct, we found that the resulting enzyme is a blue (Abs max 590 nm) complex containing MnxE, MnxF, and MnxG proteins. Further, by analyzing the Mn(II)- and (III)-oxidizing activity in the presence of a Mn(III) chelator, pyrophosphate, we found that the complex facilitates both electron transfers from Mn(II) to Mn(III) and from Mn(III) to Mn(IV). X-ray absorption spectroscopy of the Mn mineral product confirmed its similarity to Mn(IV) oxides generated by whole spores. Our results demonstrate that Mn oxidation from soluble Mn(II) to Mn(IV) oxides is a two step reaction catalyzed by an MCO-containing complex. With the purification of active Mn oxidase, we will be able to

uncover its mechanism, broadening our understanding of Mn mineral formation and the bioinorganic capabilities of MCOs.

## **Introduction**

Enzymatic Mn oxidation on the *Bacillus* spore surface overturns the widely held perception that bacterial spores are inactive, dormant cells. In fact, the *Bacillus* exosporium is made up of a highly ordered matrix of proteins and sugars responsible for interacting with the environment and conferring pathogenesis (Kailas et al., 2011). Many attempts have been made to purify the Mn-oxidizing exosporium protein, but it is in low abundance and difficult to solubilize. Exosporium preparation and extraction takes about two weeks and yields very little, impure protein, whereas the expression system described here produces about 2mg of purified *Bacillus* sp. strain PL-12 Mn(II) oxidase per liter of *E. coli* culture in five days.

## **Materials and Methods**

### *mnxDEFG gene cloning*

*Bacillus* sp. PL-12 genomic DNA was isolated with DNeasy kit (Qiagen).

*mnxDEFG* was amplified with Pfu Phusion high fidelity DNA polymerase (New England Biosciences) using forward primer 5'-

**GCTAGCATGCGTCATTCGGATTATTTGAAAAATTTGT**-3' and reverse primer, 5'-

**CTCGAGTTATGCCTTTTCTTCATTGTCCCACCCC**-3', including *mnxG* stop codon

and bolded restriction enzyme sites. This amplicon was subcloned into pJet (Invitrogen)

before insertion into pTXB1 (New England Biosciences) with NheI and XhoI (New

England Biosciences) restriction enzyme cloning sites to excise from the entry vector and

ligate into the expression vector.

### *Native protein expression and purification in E. coli*

1L LB was inoculated from 10ml *E. coli* BL12(DE3) (pTXB1/*mnxDEFG*) with 100µg/ml Ampicillin, 0.2mM CuSO<sub>4</sub>, and 10mM Tris-HCl pH 7.5 added, grown until an OD ~0.5, chilled to 17°C, and induced with 0.1mM IPTG for 18 hours (140 RPM). The shaking function was turned off for 22 hours with CuSO<sub>4</sub> added to 2mM. The harvested cells were lysed into HIC start buffer supplemented with 10mM CaCl<sub>2</sub>, 1mM CuSO<sub>4</sub>, and EDTA free protease inhibitor cocktail (Sigma) by two rounds of French press at 1000 psi. The crude extract was clarified by 20 minute incubation at 70°C. The oxidase was purified by collecting active fractions of chromatography steps supplemented with 50µM CuSO<sub>4</sub>, Phenyl Sepharose 6 Fast Flow (high sub), HiPrep 16/60 Sephacryl S-300 High Resolution, and HiTrap Q HP (GE Lifesciences), where it was isolated from a single peak. Protein was quantified using the BCA (bicinchoninic acid) reagent (Thermo Scientific); molecular weight of the purified complex was determined to be 230 kDa using the size exclusion chromatography. Purified protein copper content was determined with a Perkin-Elmer Optima 2000 DV inductively coupled plasma optical emission spectrometer. UV-visible absorption spectrum was collected on a Varian Cary 50 spectrophotometer.

### *Mass spectrometry analysis*

Purified protein was run on Tris Glycine 4-15% SDS gel (Bio-Rad) in adjacent wells. After electrophoresis, the lanes were separated and stained in Imperial protein stain (Pierce) or Silver stain (Pierce) and assayed for Mn oxidation (Francis et al., 2002). The Imperial stained band that corresponded to the Mn oxidation active band was excised by razor blade and submitted to LC-MS at the OHSU proteomics shared resource center.



The gel slice was reduced with 10 mM DTT and alkylated with 55 mM IAA before an overnight digestion with trypsin at a protease to protein ratio of greater than 5:1. All solutions were in 100 mM ammonium bi-carbonate (AB).

For analysis on the mass spectrometer each protein digest was analyzed by LC-MS using an Agilent 1100 series capillary LC system (Agilent Technologies Inc, Santa Clara, CA) and an LTQ Velos linear ion trap mass spectrometer (ThermoFisher, San Jose, CA). *Bacillus* sp. PL-12 MnxD, MnxE, MnxF, and MnxG were appended to *E. coli* sequences downloaded from the Swiss-Prot website (November 2011). The database sequences and their reversed sequences were appended to 179 common contaminant sequences and their reversed forms. We used the sequence-reversed database to estimate error thresholds (Elias and Gygi, 2007). Electrospray ionization was performed with an ion max source fitted with a 34 gauge metal needle (ThermoFisher, cat. no. 97144-20040) and 2.7 kV source voltage. Samples were applied at 20  $\mu$ L/min to a trap cartridge (Michrom BioResources, Inc, Auburn, CA), and then switched onto a 0.5 x 250 mm Zorbax SB-C18 column with 5 mm particles (Agilent Technologies) using a mobile phase containing 0.1% formic acid, 7-30% acetonitrile gradient over 30 min, and 10  $\mu$ L/min flow rate.

Data-dependent collection of MS/MS spectra used the dynamic exclusion feature of the instrument's control software (repeat count equal to 1, exclusion list size of 100, exclusion duration of 30 sec, and exclusion mass width of -1 to +4) to obtain MS/MS spectra of the five most abundant parent ions (minimum signal of 10,000) following each survey scan from m/z 350-2000. The tune file was configured with no averaging of microscans, a maximum MS1 inject time of 200 msec, a maximum MS2 inject time of

100 msec, and automatic gain control targets of  $3 \times 10^4$  in MS1 mode and  $1 \times 10^4$  in MS2 mode.

#### *Mn(III)-PP trapping*

UV-vis spectral measurements of Mn oxidation reactions with purified oxidase and Na pyrophosphate were performed and fitted as described previously for *Bacillus* sp. SG-1 exosporium (Soldatova et al., 2012).

#### *X-ray absorption spectroscopy*

Mn oxide minerals were harvested as follows: 5  $\mu$ g purified protein was added to 100 ml or 1 L 10 mM HEPES pH 7.8, 50 mM NaCl, 100  $\mu$ M MnCl<sub>2</sub>. The reaction was shaken overnight at 30°C. The 100 ml reaction was allowed to settle for about 3 days and the 1 L reaction was allowed to settle about 2 hours before the oxides were siphoned off the bottom, centrifuged 5000 x g for 10 min, then centrifuged again 15000 x g for 1 min in microfuge tubes. The oxides were allowed to air dry before packing into Al sample holders. Samples were secured with kapton tape with lexan covers between the samples and kapton tape to prevent any reduction of Mn induced by the beam during data collection (Webb et al., 2005c). Mn K-edge EXAFS was collected on transmission mode at SSRL beamline 4-1 with a Si(220) double crystal monochromator and detuned 60%. Energy calibration was done using the pre-edge feature of potassium permanganate (6543.34 eV). Samples were run at 77°K using a liquid nitrogen cryostat. Background subtraction and normalization was done using Athena (Ravel and Newville, 2005).

### **Results and Discussion**

Direct molecular evidence for the oxidation in the *Bacillus* exosporium demonstrated the presence of MnxF and MnxG in an active SDS PAGE gel band (Dick et

al., 2008), but co-expressing these genes in *E. coli* did not produce active protein. However, active protein was obtained when the *mnxDEFG* operon construct was expressed without a tag in *E. coli* by inducing at 17°C and loading with 2mM CuSO<sub>4</sub> under microaerobic conditions. (Preliminary experiments indicate that *mnxD* can be omitted from the construct.) After lysis, *E. coli* proteins were removed by trypsin proteolytic digestion or by heat precipitation at 70°C for 20 min. The active heat stable and trypsin cleavage resistant Mn oxidase was purified by a series of native chromatography steps: hydrophobic interaction, gel filtration, and ion exchange. Enzymatic Mn(II)-oxidizing activity was demonstrated by the formation of brown Mn(IV) oxides after the addition of MnCl<sub>2</sub> to protein in solution or run on a non-denaturing SDS PAGE (without thiol reductant or boiling sample pretreatments). The presence of oxidized Mn was confirmed by a colorimetric assay, in which Mn(III) and Mn(IV) react with leucoberbelin blue (LBB) to turn the solution blue (Abs 618nm).

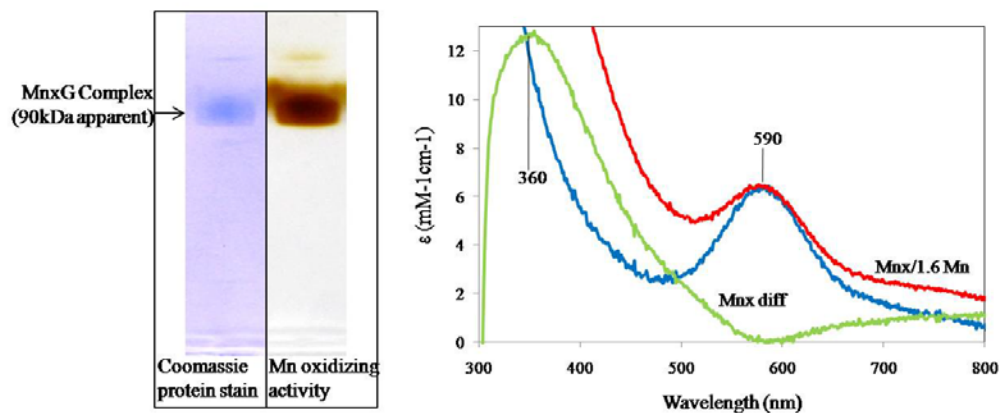


**Fig. 1.** Characterization of purified Mnx oxidase: (Left) SDS PAGE of purified oxidase diluted into Laemmli buffer and Coomassie stained (lane 1) or incubated with Mn(II) (lane 2), showing MnO<sub>2</sub> formation by the protein. The arrow indicates a single native purified protein band. (Right) UV-visible spectrum before (blue trace, 590nm band) and after incubation with 3-fold excess MnCl<sub>2</sub> and dialysis (red trace). The difference spectrum (green) shows Mn(IV) (360nm band) bound to the protein (1.6 Mn/mol protein).

To elucidate which *mnxDEFG* operon gene products were in the purified active protein, we ran an in-gel Mn oxidation assay (Francis and Tebo, 2002) in non-denaturing SDS PAGE to select an active protein band for tandem mass spectrometry (MS/MS) identification (Figure 1, left). MS/MS identified 100 unique peptides from MnxG (48.3% coverage), 10 from MnxE (48.2% coverage) and 5 from MnxF (23.3% coverage), a surprising result since no MCO has been previously purified as a multi-protein complex. The molecular weight of the purified MnxG complex determined by size exclusion chromatography and a molecular weight calibration curve is ~230kDa, suggesting the presence of one full length MnxG (138kDa) and an oligomer of 6- 8 MnxE and MnxF subunits (12kDa each) of unknown stoichiometry.

MnxE and MnxF have no conserved sequence homology to known proteins. However, a BLAST (Basic Local Alignment Search Tool) search indicated that MnxE, MnxF, and MnxG all have homologs in the spore-forming bacteria, *Cellulosilyticum*

*lentocellum*, a cellulose degrading *Clostridium*, and *Desulfotomaculum kuznetsovii*, a thermophilic methylotrophic sulfate-reducer. It is unknown if these organisms can oxidize Mn but because MnxE and MnxF are only conserved among spore-forming bacteria, they may be required for activity, stability, and/or localization of MnxG-like MCOs to the spore surface or exosporium.

The MnxG sequence predicts it to be a large, 6-domain MCO, similar to human ceruloplasmin, a ferroxidase (Van Waasbergen et al., 1996). MCOs contain four copper atoms that couple the oxidation of phenolic or metal substrates to the sequential reduction of O<sub>2</sub> to H<sub>2</sub>O. These four copper atoms reside in the blue Type 1 (Abs ~600nm) center and the trinuclear center containing one Type 2 and two Type 3 (Abs ~330nm) Cu atoms.

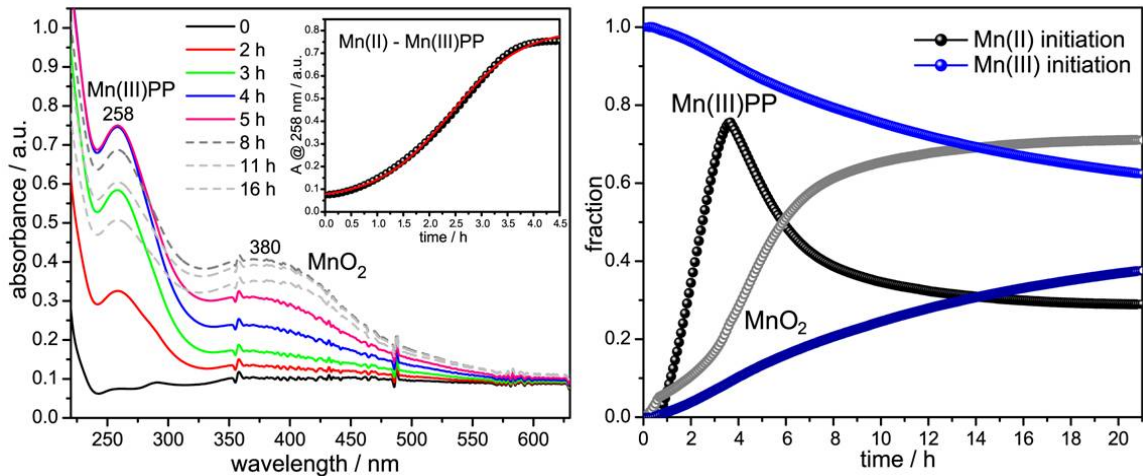


**Fig. 2.** Mn(II) and Mn(III) initiated Mn oxidation assays. (Left) UV-vis absorption spectra of purified oxidase in HEPES buffer, pH 7.5, in the presence of sodium pyrophosphate (PP) and O<sub>2</sub>, taken at the indicated time points after the addition of 0.1 mM MnCl<sub>2</sub>. (Right) Time courses followed by Mn(III)PP and MnO<sub>2</sub> species during Mn oxidation by purified oxidase and obtained from a linear least squares fit analysis of the time-resolved spectra (23). After the addition of MnCl<sub>2</sub>, the 258 nm absorption band due to Mn(III)PP rises sigmoidally (left panel, inset) and then decays (right panel, black points) as the 380 nm absorption band due to MnO<sub>2</sub> rises (right panel, gray points). Addition of 0.1 mM Mn(III) is followed by a steady decay of the 258 nm band and a concomitant rise of the 360 nm absorption band.

In addition to these canonical Cu atoms, MCOs can also bind Cu in extra T1 sites and in labile regulatory sites (Lindley et al., 1997; Roberts et al., 2003). Our purified MnxG complex is blue colored (Abs 590nm) (Figure 1, right) and has a copper occupancy of ~6.4 Cu per mol of MnxG complex by inductively coupled plasma-optical emission spectroscopy (ICP-OES) analysis.

To determine the course of MnO<sub>2</sub> formation, we monitored changes in the UV-vis absorption spectrum when Mn(II) or Mn(III) was allowed to react with oxygenated buffer in the presence of purified enzyme and the Mn(III) chelator, pyrophosphate (PP) (Figure 2). When the reaction was initiated with Mn(II), a 258nm peak, due to Mn(III)-PP, rises and then falls as a 360nm peak, due to colloidal MnO<sub>2</sub>, rises. The initial time course of the rising Mn(III)-PP peak is sigmoidal, suggesting cooperative, allosteric substrate binding. When Mn(III)-PP initiates the reaction, the Mn(III)-PP peak decays as the MnO<sub>2</sub> forms (Figure 2). These results corroborate the earlier findings using *Bacillus exosporium* that Mn(II) oxidation to MnO<sub>2</sub> is catalyzed by two single electron transfers (Webb et al., 2005a; Soldatova et al., 2012).

Since formation of mononuclear Mn(IV) in a protein environment would be energetically prohibitive, we have proposed a polynuclear mechanism, in which electron transfer from Mn(III) would be driven by the formation of bridging oxides (Soldatova et al., 2012). Consistent with such a mechanism, we found that when three-fold excess Mn(II) was titrated into purified enzyme, dialyzed overnight, and concentrated, the solution displayed a 360nm difference absorption band (Figure 1, right) and LBB reactivity, suggestive of a polynuclear Mn(IV) species. ICP-OES analysis gave a stoichiometry of 1.6 Mn per mol of MnxG complex. This result suggests that Mn(II)

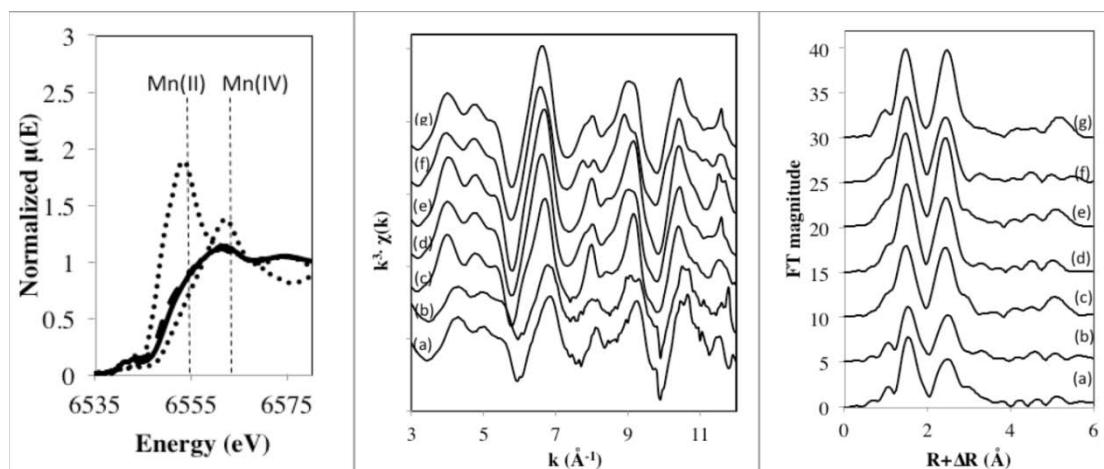


**Figure 3.** Mn K-edge XANES (left) and EXAFS (center) and Fourier transforms (right) of two different amounts of MnxG complexes after incubation with Mn(II). Left: XANES spectra of 50  $\mu\text{g}\cdot\text{L}^{-1}$  (bold line) and 5  $\mu\text{g}\cdot\text{L}^{-1}$  (dashed line) protein incubated in 100  $\mu\text{M}$  Mn(II). XANES of  $\text{MnCl}_2\cdot 4\text{H}_2\text{O}$  and  $\delta\text{-MnO}_2$  are provided as indicators for Mn(II) and Mn(IV) with maximum absorbance features at 6553 and 6562 eV, respectively. Mn K-edge EXAFS (center) and Fourier transforms (right) of the two different concentrations of MnxG complex, 50 (a) and 5 (b)  $\mu\text{g}\cdot\text{L}^{-1}$ . EXAFS of selected Mn oxides, biogenic Mn oxides formed by spores of *Bacillus* sp. SG-1 in NaCl solution (c), biogenic Mn oxides formed by spores of *Bacillus* sp. SG-1 in  $\text{CaCl}_2$  solution (d),  $\delta\text{-MnO}_2$  (e), triclinic birnessite (f), and hexagonal birnessite (g) are shown for comparison.

oxidation results in a protein-bound dinuclear or trinuclear Mn(IV) oxo complex, which can initiate  $\text{MnO}_2$  nucleation.

The Mn oxidation state and the structure of the  $\text{MnO}_2$  minerals made by purified *Bacillus* sp. PL-12 Mn oxidase were analyzed using X-ray absorption spectroscopy and compared to those previously reported for intact purified *Bacillus* sp. SG-1 spores (Bargar et al., 2000; Bargar et al., 2005a; Webb et al., 2005c; Webb et al., 2005b). X-ray absorption near-edge spectra (XANES) of solid phases of two different concentrations of purified Mn oxidase, 5 and 50  $\mu\text{g}\cdot\text{L}^{-1}$  demonstrated that both preparations oxidized Mn(II) to Mn(IV) (Figure 3, left). The absorbance maximum for these two preparations occurs near the white line of Mn(IV) at 6562 eV. Linear combination fitting of the data confirm

a predominance of Mn(IV) in the samples with 20-30% Mn(II) and Mn(III) present, mostly as Mn(II) as evidenced by the shoulder at 6553 eV. Measurements of the Mn K-edge extended x-ray absorption fine structure (EXAFS) were also performed on these preparations (Figure 3, right). In previous studies, it was shown that Mn oxides formed by spores of *Bacillus* sp. SG-1 in NaCl solution were similar to  $\delta$ -MnO<sub>2</sub> (Bargar et al., 2000), while in CaCl<sub>2</sub> solution biogenic Mn oxides exhibited features similar to triclinic or orthogonal manganates (Webb et al., 2005c). Qualitatively, EXAFS of Mn oxides formed by purified Mn oxidase were similar to the spore product but with some differences between the Mn oxides depending on the amount of protein used. Specifically, EXAFS of Mn oxides formed with 50  $\mu\text{g}\cdot\text{L}^{-1}$  purified protein showed single antinodes at 8.0 and 9.3  $\text{\AA}^{-1}$  while Mn oxides produced from 5  $\mu\text{g}\cdot\text{L}^{-1}$  protein showed double antinodes (Figure 3, right). Single antinodes can be found in hexagonal layer symmetry which includes  $\delta$ -MnO<sub>2</sub>, hexagonal birnessites, and biogenic Mn oxides from *Bacillus* sp. SG-1 in NaCl, while double antinodes at 8.0 and 9.3  $\text{\AA}^{-1}$  can be observed in orthogonal layer symmetry such as triclinic birnessites and biogenic Mn oxides formed by spores of *Bacillus* sp. SG-1 in CaCl<sub>2</sub> (Gaillot et al., 2003; Manceau et al., 2004; Webb et al., 2005b; Webb et al., 2005c). Fourier transforms show that Mn oxides from purified Mn oxidase have most of the features observed in *Bacillus* sp. SG-1 spore generated Mn oxides in both NaCl and CaCl<sub>2</sub> solution (i.e., first peak (Mn-O) and second peak (edge-sharing Mn-Mn), and amplitude of multiple-scattering peak at 5.2  $\text{\AA}$ ).

The purified *Bacillus* exosporium MnxG complex represents a distinct chapter in biomineralization. It is the only example of an MCO catalyzing two energetically distinct



metal oxidation steps, as part of bio-oxide formation. The requirement of two small accessory proteins for function is also unprecedented. Now that a method is in hand to produce quantities of purified Mn oxidase, we plan to elucidate its unique mechanism through structure determination and spectroscopic methods. Given that MCOs appear to be the enzymes responsible for Mn oxidation in a variety of environmentally conspicuous organisms (Lee, 1994; Corstjens et al., 1997; Francis and Tebo, 2002; Dick et al., 2006; Ridge et al., 2007b; Dick et al., 2008; Geszvain et al., 2013), this insight will be invaluable in understanding how Mn cycling occurs and how it impacts other geochemical cycles. The enzyme may also have useful biotechnological applications in the fields of biomaterials, enzyme catalysis, bioremediation, metal recovery, and bioenergy.

### **Chapter 3. Substrate kinetics and Cu binding characteristics of the Mn oxidizing Mnx complex from *Bacillus* sp. PL-12**

#### Abstract

In addition to chemical and physical forces, many global geochemical cycles, such as the redox cycling of manganese, are driven by bacteria. Bacterial Mn(II) oxidation and subsequent Mn(IV) mineral formation is widespread and diverse. Direct enzymatic Mn oxidation presents rare Mn chemistry in that the Mn is the substrate of the reaction instead of the catalytic cofactor. Until recently, however, there has been no protein available to investigate. The heterologously purified Mn oxidase (Mnx) from marine *Bacillus* sp. PL-12 is made up of the multicopper oxidase (MCO) MnxG, and two small proteins of unknown function MnxE and MnxF. Mnx binds Cu and oxidizes both Mn(II) and Mn(III), generating Mn(IV) oxide minerals that resemble those found on the *Bacillus* spore surface. Here we present direct spectroscopic evidence to verify the presence of the canonical MCO Cu types and the existence of at least six extra Cu binding to the complex. Additionally, we describe the kinetics of the oxidation by Mnx of Mn(II) and the more typical MCO substrates Fe(II), 2,2'-azino-bis(3-ethylbenzthiazoline-6-sulphonic acid) (ABTS) and 2,6-dimethoxyphenol (2,6-DMP). The oxidation of Fe(II), DMP, and ABTS (pH 4.5) follow Michaelis-Menten kinetics whereas Mn and ABTS (pH 8) follow allosteric sigmoidal trends. Putting the metal content and kinetic analyses together with the oligomeric nature of the Mnx complex allows us to hypothesize about the nature of the mechanism of this unique two-step reaction.

Key Words 5 max

biogeochemistry, bacteria, copper, iron, laccase

## Introduction

Mn is abundant in the Earth's crust and surface waters and cycles between the +II, +III, and +IV oxidation states. The reduced form of Mn (Mn(II)) is used in enzymatic catalysis of essential processes like prokaryotic DNA biosynthesis (Cotruvo and Stubbe, 2010) and protecting against reactive oxygen species in bacteria (Horsburgh et al., 2002) and O<sub>2</sub> generation in plants, algae, and cyanobacteria (Kirby et al., 1981; De Paula and Brudvig, 1985; Dismukes, 1996). Mn(II) oxidation is ubiquitous and the insoluble Mn(III,IV) oxides control the elemental cycling of other metals such as Se (Scott and Morgan, 1996), Cr (Manceau and Charlet, 1992), and As (Huang, 1991) in the environment. The reactivity of the insoluble Mn(IV) oxides extends from metals to the incorporation of radionuclides (Todd et al., 1988a; Wei and Murray, 1991) and the degradation of organic matter and the synthetic contaminants atrazine, chlorinated anilines, polychlorinated biphenyls, and Bisphenol A (BPA) (Stone and Morgan, 1984a; Stone and Morgan, 1984b; Stone, 1987b; Ulrich and Stone, 1989; Lin et al., 2009).

The impact of this dynamic metal's cycling is clear but the mechanism of oxidation has been unresolved. A biotic rather than an abiotic process may be the main driver of Mn oxidation in the natural world because biotic Mn(II) oxidation occurs several orders of magnitude faster (Hastings and Emerson, 1986). In most cases, bacterial Mn oxidation produces highly reactive Mn oxides on the cell surface (Tebo et al., 2010). Mn oxides made by bacteria are formed in such a way that spiny birnessite minerals form with high surface area, heightening their reactive and sorptive properties (Tebo et al., 2004). Many diverse bacteria are capable of this process including several marine *Bacillus* species isolated from near shore sediments and which deposit Mn oxides on their

dormant spore surface (Francis et al., 2002; Francis and Tebo, 2002). Losing the ability to oxidize Mn does not seem to affect vegetative cell growth or sporulation and germination of various isolates in the lab (Van Waasbergen et al., 1993; Geszvain et al., 2013), so the purpose of this mineral encrustation remains a mystery.

We recently described the isolation of the *Bacillus* Mn oxidase (Mnx). When the portion of the *mnx* operon conserved in Mn(II) oxidizing *Bacillus* species SG-1, PL-12, and MB-7 is expressed in *E. coli*, a protein complex is found and composed of three consecutive gene products, mnxE, mnxF, and mnxG (Butterfield et al., 2013). MnxE and MnxF are both 12 kDa with no sequence similarity to any protein in the protein database; MnxG is a 138 kDa putative six domain multicopper oxidase (MCO). MCOs have been implicated in the oxidation of Mn in diverse bacteria including *Leptothrix discophora* (Corstjens et al., 1997), *Pedomicrobium* sp. ACM3067 (Ridge et al., 2007a), and *Pseudomonas putida* (Geszvain et al., 2013). MCOs are named for their Cu catalytic centers in which electrons are stripped from a substrate at the type 1 Cu then transferred to the trinuclear center, made up of one type 2 and two type 3 Cu atoms, where they reduce O<sub>2</sub> to H<sub>2</sub>O (Solomon et al., 1996).

MCOs are known to have a broad substrate range including phenolic compounds and transition metals Fe(II) and Cu(I) (Xiao and Wedd, 2011; Reiss et al., 2013). Fine tuning substrate turnover over eons of evolution has given rise to a family of proteins that catalyze the oxidation of different substrates via the same mechanism. For example, it has been suggested that CueO in *E. coli* is tuned to Cu(I) oxidation so that it can detoxify excess Cu(I) to Cu(II) in the periplasm so it is easily exported (Outten et al., 2001). Ceruloplasmin participates in metal homeostasis as well by oxidizing Fe(II) and

partnering with transferrin to mineralize it in order to regulate Fe concentration in the blood of mammals (Osaki, 1966). Laccase-like MCOs degrade plant lignin and other organics, and includes a laccase, CotA, from *Bacillus subtilis* that synthesizes a brown pigment on the spore coat (Sakurai and Kataoka, 2007). Determining the most efficient catalysis of the *Bacillus* MCO at environmentally relevant conditions could point to a physiological function.

Calcium may also play a role in Mn oxidation by Mnx since it increases the rate of Mn oxidation by four or five times in *Bacillus* sp. SG-1 spores (Toyoda and Tebo, 2013). Ca has been implicated in Mn centers and in MCOs: ceruloplasmin has been shown to be stabilized by Ca (Musci et al., 1996), and Mn driven catalysis in PSII is also facilitated by Ca (Ghanotakis et al., 1984; Miyao and Murata, 1984). Additionally, Mn was utilized as a binding proxy in Ca analysis of ceruloplasmin (Musci et al., 1996).

Unlike any other MCO, however is the capability of Mnx to directly catalyze both Mn(II) and Mn(III) oxidation, two energetically distinct reactions, to form reactive Mn(IV) oxides (Butterfield et al., 2013). Here we take a closer look at the metal content and substrate specificity of this complex and what it might mean for the mechanism of the reaction center and for bacteria that have evolved it.

## **Methods**

### *Protein expression and purification*

Protein was purified by methods described previously (Butterfield et al., 2013) or by Strep-tag affinity chromatography. For affinity purification, *mnxD* to *mnxG* (NCBI accession EF158106) were amplified from *Bacillus* sp. PL-12 (Taxonomy ID: 161537) genomic DNA by the following primers: Fwd 5'-

**CCGCGGTATGCGTCATTCGGATTATTTGAAAAATTTGT-3'** and Rvs 5'-  
**GTCGACTGCCTTTTCTTCATTGTCCCACC-3'** and cloned by restriction enzyme digestion and ligation into the Strep-tag pASK/IBA3plus vector using SacII and SalI (sequences in bold). In place of the *mnxG* stop codon the Strep-tag (underlined) was engineered to a linker (italicized) at the C-terminus of *mnxG* (*VDLQGDHGLSAWSHPQFEK*). The resulting construct was transformed into *E. coli* BL21 (DE3) and grown at 37 °C to an OD<sub>600</sub> ~ 0.5 in Luria-Bertani (LB) broth containing 0.2 mM CuSO<sub>4</sub>, 10 mM Tris-HCl pH 7.5, and 100 mg/L ampicillin. The temperature was then lowered to 17 °C by cooling the culture on ice or in a refrigerated shaker and then 0.2 mg/L anhydrotetracycline was added to induce transcription of the *mnx* genes. The cells were allowed to shake and express for 16-20 h. CuSO<sub>4</sub> was added to a final concentration of 2 mM and the shaking function was stopped for at least 22 h to allow for the microaerobic uptake of Cu ions into the *E. coli* cytoplasm as described in Durão et al. (Durão et al., 2008). This Cu loading step was omitted during the apo-protein preparation.

The cells were then harvested, suspended in Streptactin equilibration buffer (100 mM Tris pH 8.0, 150 mM NaCl) amended with 10 mM CaCl<sub>2</sub>, 1 mM CuSO<sub>4</sub>, and an EDTA-Free SIGMAFAST™ Protease Inhibitor Cocktail Tablet, and lysed by sonication microtip for 1 min/ ml cell lysate at 40% amplitude with 10 s on/off pulses on ice. The cell lysate was clarified by heat denaturation at 70 °C for 15 min. The cell debris was removed by centrifugation 15,000 x g 4 °C 30 minutes and the supernatant was filtered through a 0.4 µm pore PVDF filter. The clarified lysate was then added to 5 ml column volume (CV) of Strep-Tactin Superflow Plus (Qiagen) and slowly rotated for 1 hour at

room temperature. By gravity flow, the unbound protein fraction was removed and the resin was washed with 20 CV Streptactin equilibration buffer. The Mnx protein was eluted with 5 CV equilibration buffer plus 2.5 mM D-Desthiobiotin, and the column was regenerated with 15 CV equilibration buffer plus 1 mM 2-(4-hydroxyphenylazo)benzoic acid. The eluted protein was concentrated to < 1.5 ml on 100 kDa molecular weight cutoff filtration units (Millipore) for loading onto HiPrep 16/60 Sephacryl S-200 High Resolution gel filtration column (GE Healthcare) equilibrated with 20 mM HEPES pH 7.8 50 mM NaCl 5 % D-glucose (weight/volume) at 4 °C. All buffers up to this point were supplemented with 50 µM CuSO<sub>4</sub> to avoid Cu leaching by Tris. A single peak corresponding to a 230 kDa protein was collected, concentrated, and dialyzed three times for at least 3 h each at a volume of 1 L 20 mM HEPES pH 7.8, 50 mM NaCl for every 1 mL of protein sample at 4 °C. The protein was quantified by the Thermo Scientific Pierce bicinchoninic acid (BCA) protein assay. It was then diluted with dialysis buffer to 0.2 mg/ml for kinetic studies or, for spectroscopy sample preparation, left concentrated, flash frozen in liquid nitrogen, and stored at -80 °C. Apo-Mnx was prepared by omitting the Cu incorporation step during purification and harvesting the cells after overnight expression.

#### *Spectroscopic analysis*

Quantitative metal analysis on the protein was performed with a Perkin-Elmer Optima 2000 DV inductively coupled plasma-optical emission spectrometer (ICP-OES). Continuous-wave spectrum electron paramagnetic resonance (EPR) was collected at an X-band frequency (9.429 GHz) with a Bruker ER085CS spectrometer. The measurement

parameters were: temperature -170 °C; microwave power 10 mW; modulation amplitude 4G? conversion time 40.96ms attenuation 13dB

Reduction of Mnx was performed by adding excess dithionite to concentrated protein anaerobically. Excess dithionite was removed by running the sample through a protein desalting column (Thermo) equilibrated with 20 mM HEPES (pH 7.8)-50 mM NaCl buffer degassed with Ar. The UV-visible absorption spectrum was collected on a Varian Cary 50 spectrophotometer to confirm absence of the type 1 Cu absorbance maximum at 590 nm.

### *Kinetics*

Kinetic experiments were performed on the Molecular Devices SpectraMax M2 microplate reader spectrophotometer at 22 °C with purified protein. 2,2'-azino-bis(3-ethylbenzthiazoline-6-sulphonic acid) (ABTS) oxidation was measured directly at 420 nm using an extinction coefficient of  $36 \text{ mM}^{-1} \text{ cm}^{-1}$ . Reactions were carried out with 10 µg Mnx (final 240 nM) in 100 mM phosphate-citrate buffer pH 3-8 and 20 mM CHES, HEPES, and/or MES at pH 7-10. 2, 6-dimethoxyphenol (DMP) oxidation was followed by measuring the increase in absorbance at 468 nm and  $\epsilon = 49.6 \text{ mM}^{-1} \text{ cm}^{-1}$  in the same buffers. These assays were performed in at least two independent trials in triplicate. Fe(II) (ferrous ammonium sulfate) oxidation was measured using the absorbance at 570 nm and a ferrous ammonium sulfate standard curve after quenching 200 µl reactions with 50 µl of the Fe(II) chelating colorimetric assay ferrozine (15 mM) at different time intervals after initiating the reaction. Fe(II) oxidation reactions were performed with 10 µg Mnx in 100 mM Na acetate-acetic acid buffer (pH 4- 6). Mn(II) ( $\text{MnCl}_2$ ) oxidation in 20 mM HEPES (pH 7- 8.5) was measured by quenching 5 µl of 200 µl reactions with



195  $\mu$ l leucoberbelin blue (LBB) colorimetric reagent and reading the absorbance at 618 nm. Working LBB reagent was prepared by diluting concentrated stock (100 mg LBB in 25 ml 0.4 % NaOH) 1:10 into 1 % acetic acid. A  $\text{KMnO}_4$  standard curve was used to determine  $\text{MnO}_2$  oxide equivalent concentration. The metal substrate assays were performed in five independent trials, then the high and low values were discarded from each concentration. The linear part of each curve was plotted and fit with a linear regression in GraphPad Prism, version 6.02. These slopes were converted to the appropriate kinetic units, plotted, and fit with nonlinear regressions with Michaelis-Menten ( $Y = V_{\max} * [S] / (K_M + [X])$ ) or allosteric sigmoidal ( $Y = V_{\max} * [S]^h / (K_{\text{half}}^h + [S]^h)$ ) functions determined by comparing best fit values in the same software.  $K_{\text{half}}$  is the concentration of substrate that produces  $1/2V_{\max}$ .  $K_M$ ,  $K_{\text{half}}$ , and  $V_{\max}$  were determined and reported as  $K_M$ ,  $K_{\text{half}}$ , and  $k_{\text{cat}} = V_{\max} / [\text{enzyme}]$ .

## Results

In the previous work, the active Mnx complex was purified from a plasmid containing *mnxDEFG* genes from *Bacillus* sp. PL-12. Even though only three of the four Mnx proteins were identified in the active SDS PAGE (sodium dodecyl sulfate polyacrylamide gel electrophoresis) band by mass spectrometry (MnxEFG), the significance of the highly conserved MnxD is unknown, so it was retained in the current construct. The construct contained a Strep affinity tag to ease the purification regimen and produce a cleaner product. MnxE and MnxF were present in the active complex and appeared to contribute an additional mass of ~100 kDa to MnxG according to gel filtration estimates, resulting in a large oligomer complex of ~ 230 kDa (Butterfield et al., 2013). *mnxDEFG* were co-expressed in a C-terminal strep tag (~2 kDa) plasmid on an

anhydrotetracycline inducible promoter under cool conditions in LB medium, and loaded with Cu *in vivo*. The cells were lysed, purified by batch affinity chromatography, and further cleaned on a gel filtration column. This preparation yields a protein complex that elutes in the same gel filtration fractions, and therefore is similarly sized, as the previously described untagged product (Butterfield et al., 2013). Given that protein mass calculated from gel filtration elution gives an odd value with respect to Mnx protomeric state, our approximation of the stoichiometry of the subunits are 3 MnxE, 3 MnxF, and 1 MnxG, resulting in 211 kDa, and we use this value in metal binding and kinetic studies described below.

#### *Ca and Cu binding*

As described above, MCOs require four canonical Cu atoms to catalyze the oxidation of a substrate (Solomon et al., 1996). The type 1 Cu is detected by its blue color and absorbance maximum of ~ 600 nm. Both the type 1 and type 2 Cu can also be observed by EPR in their oxidized states. In the past, it has been difficult to determine the native state of Cu binding in MCOs because the stoichiometries were determined indirectly from EPR peak intensity, UV-vis 610/280 nm ratios, and amino acid sequence similarities (Musci et al., 1993). These parameters change depending on small variations in ligand-Cu coordination among the MCOs (Solomon et al., 2004). Mnx is expressed in excess Cu loading conditions to assist in solubility and complex formation. However, without the addition of extra Cu to the *mnx*-expressing *E. coli* growth medium, the protein binds only about 3 mol Cu per mol Mnx and is unstable (data not shown) and inactive (Table 1).

Table 1. Metal content of Mnx and effect of Cu on Mn oxidation activity.

Metal content and corresponding Mn(II) oxidation activity		Cu				Mn	Ca	Fe
		Undialyzed	HEPES dialyzed	Tris dialyzed	No Cu added			
M/ protein		13.5 ± 2.69	15.1 ± 0.33	9.9 ± 0.99	2.96	0	3.3 ± 1.9	0.043 ± 0.061
Mn(II)	h	ND <sup>a</sup>	1.83 ± 0.086	1.82 ± 0.11				
	K <sub>half</sub> (μM)	ND	123 ± 7.00	134.6 ± 9.16	BD <sup>b</sup>			
	k <sub>cat</sub> (s <sup>-1</sup> )	ND	16.1 ± 0.94	12.9 ± 0.76	BD			

Metal content per Mnx protein complex (mol M/mol protein if there are three of each MnxE and MnxF to one MnxG= 211kDa) was determined by ICP-OES.

<sup>a</sup>ND not done. <sup>b</sup>BD below detection.

We noticed that after purification, the protein exhibited vastly different Cu binding stoichiometries.

In order to stabilize the metal content of the Mnx protein complex, the purified protein was extensively dialyzed in either 20 mM HEPES pH 7.8 or Tris pH 8 buffer with 50 mM NaCl after purification in Cu-supplemented Tris buffers. Dialysis in HEPES results in a Cu: Mnx stoichiometry of 15: 1, whereas Tris dialysis yields 10: 1 stoichiometry. Both results suggest that Mnx binds many more Cu than necessary to fill the four MCO sites, which has been observed for the other MCOs CueO (5:1) and ceruloplasmin (6:1) (Musci et al., 1993; Roberts et al., 2003).

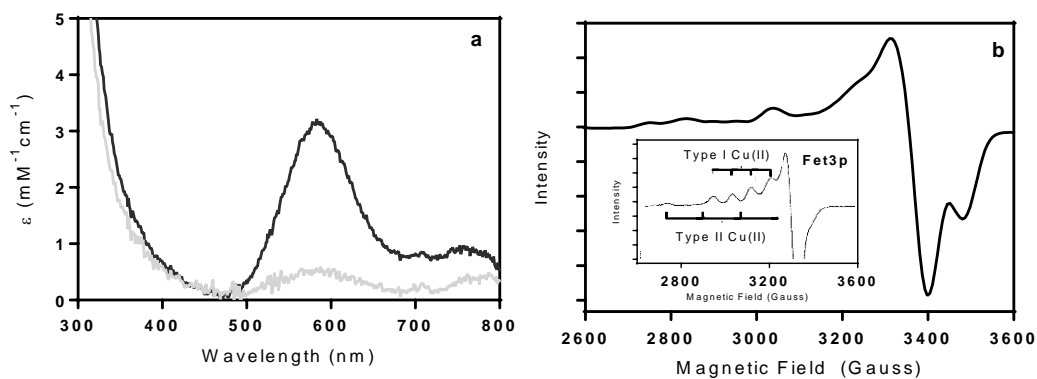


Figure 1. Spectroscopic evidence of MCO Cu in Mnx. A. UV-visible spectra of dithionite-reduced MCO (gray trace) and oxidized Mnx (black trace). The blue type I Cu absorbance maximum at 590 nm is depleted in the reduced sample. B. EPR scan of Mnx has similar features to the typical trace of type I and type II Cu described in *S. cerevisiae* Fet3p (inset) (Hassett et al., 1998).

Coordination of Cu in the Mnx complex was explored through UV-visible absorption and electron paramagnetic resonance (EPR) spectroscopies (Fig. 1). The purified Mnx complex has an indigo blue color with an absorbance maximum of 590 nm, indicative of the Cys-S-Cu(II) charge transfer found on type 1 Cu sites (Solomon et al., 1996). Upon exposure to the reductant dithionite, the protein loses its color and the 590 nm absorption feature, further supporting the conclusion that Mnx contains a type 1 Cu site (Fig 1a). The EPR spectrum obtained from the oxidized complex shows characteristic peaks for the MCO type 1 Cu and type 2 Cu (Fig 1b), but the peaks are not as well-resolved as in the Fet3p spectrum due to possible contributions of additional Cu from the MnxE and MnxF subunits. The MnxE and MnxF subunits contain five and six His residues, respectively; three of which are conserved among MnxF from *Bacillus* spp. SG-1, PL-12, and MB-7.

Metal ion content analysis was undertaken to determine if other potential metallo-cofactors were present in the isolated complex. We observed a small, variable amount of Ca atoms ( $3.3 \pm 1.9$ ) in the as-purified Mnx complex.

To rule out the interfering contamination of other metallo substrates, we also quantified the Fe and Mn content (Table 1). Neither Mn nor Fe were added during enzyme preparation beyond the trace amounts in the LB growth medium. No Mn was detected, and only a trace amount of Fe contamination was measured, which should not interfere with the kinetic analyses.

#### *Mnx oxidizes metal and MCO substrates*

From metals to large phenolics, multicopper oxidases have wide substrate specificities. To relate the MCO and Cu content to activity, Mn oxidation rates were determined for differentially loaded enzyme by measuring the appearance of  $\text{MnO}_2$ . Tris-dialyzed, HEPES-dialyzed, and Cu-unloaded Mnx were analyzed for their relative rates of Mn oxidation at pH 7.8 in HEPES buffer (Table 1). NaCl was omitted from the assays, since all kinetic experiments preliminary suggest that NaCl facilitates Mn oxide precipitation, interfering with the ability to quench a small aliquot of the homogeneous reaction mixture. As predicted, the enzyme lacking enough Cu to load the MCO (3 mol Cu/ mol Mnx) had undetectable Mn oxidation activity, while Cu containing enzyme catalyzed the reaction well. There was only a small decrease in activity in the Tris-dialyzed enzyme compared to the HEPES-dialyzed enzyme.

Reaction kinetic analyses of these Cu-loaded Mnx proteins showed allosteric sigmoidal trends for Mn oxidation (HEPES loaded data shown in Fig. 2a). The allosteric sigmoidal equation is generally used to factor in the contribution of cooperative activity

of subunits, and an  $h$  (the Hill slope) value greater than 1 indicates positive cooperativity. The  $h$  value can also approximate the number of substrate binding sites within the protein, but never exceed it. At  $h$  of about 1.8, it is possible that there are two Mn binding sites in Mnx, corroborating the multi-substrate binding model proposed in Soldatova et al. 2012(Soldatova et al., 2012). This result was also reproduced in 10 mM Tris pH 7.8 buffer as well. The  $K_{\text{half}}$  decreased to  $101 \pm 6.0 \mu\text{M}$ ,  $h$  increased to  $2.6 \pm 0.24$ , and  $k_{\text{cat}}$  decreased to  $5.86 \pm 0.36 \text{ sec}^{-1}$ .

Table 2. Mnx oxidation kinetics of various substrates.

Substrate	Fe(II)		Mn(II)	
	$K_M$ ( $\mu\text{M}$ )	$k_{\text{cat}}$ ( $\text{s}^{-1}$ )	$K_{\text{half}}$ ( $\mu\text{M}$ )	$k_{\text{cat}}$ ( $\text{s}^{-1}$ )
Mnx <i>Bacillus</i> sp. PL-12	$9.00 \pm 1.04$	$0.0744 \pm 0.008$	$123 \pm 7.00$	$16.1 \pm 0.941$
Fet3p <i>C. albicans</i> <sup>d</sup>	$7.9 \pm 0.5$	$1.06 \pm 0.02$		
Fet3p <i>S. cerevisiae</i> <sup>e</sup>	$4.9 \pm 0.8$	$0.835 \pm 0.023$		

Mnx, being most similar to the Fe-oxidizing ceruloplasmin and Fet3p, was tested first for its ability to oxidize Fe at pH 4-6 (Fig 2a, b). Indeed, Mnx also has a high affinity to Fe ( $K_M$  9  $\mu\text{M}$ ) and oxidizes it at a similar efficiency to Fet3p enzymes from yeast at pH 5 (Table 2) (Stoj et al., 2006; Ziegler et al., 2011).

Mnx also readily oxidizes phenolic compounds, similar to the *Bacillus* spore coat MCO, CotA (Durão et al., 2008; Koschorreck et al., 2008). ABTS and 2, 6-DMP are phenolic compounds used as lignin analogs to characterize MCOs as behaving like the lignin degrading enzymes, laccases. Their oxidation is observed by color change (468 nm for 2, 6-DMP and 420 nm for ABTS) in a microplate and recorded with a spectrophotometer. Mnx oxidizes ABTS at pH 4.5 in a Phosphate-citrate buffer, but when

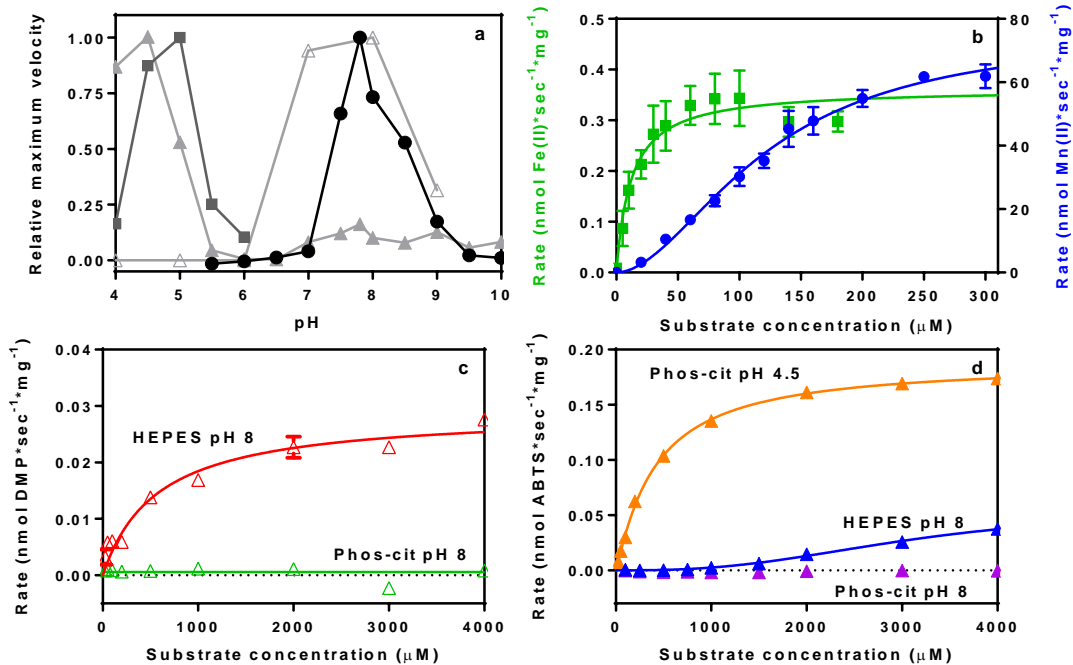


Figure 2. Mn x oxidation kinetics of various substrates.

a) The pH optima for each Mn x substrate Fe (squares), Mn (circles), 2,6-DMP (empty triangles), and ABTS (closed triangles) plotted versus their internal relative maximum velocities. b-d) The initial oxidation velocities of Fe(II) (b, squares), Mn(II) (b, circles), DMP (c), and ABTS (d) are plotted against their initial concentrations and fitted with either Michaelis-Menten or allosteric sigmoidal functions. Fe(II) and Mn(II) oxidation by HEPES-dialyzed Mn x is followed by quenching the reaction with ferrozine (abs max 570 nm) and leucoberbelin blue (abs max 618 nm), respectively. DMP oxidation and ABTS in HEPES and Phosphate-citrate buffers are directly followed by the change in absorbance at 468 nm  $\epsilon = 49.6 \text{ mM}^{-1} \text{ cm}^{-1}$  and 220 nm  $\epsilon = 36 \text{ mM}^{-1} \text{ cm}^{-1}$ , respectively.

the buffer system is switched to HEPES Mn x oxidizes ABTS at pH 8 (Fig 2d). Mn x only oxidizes 2,6-DMP at pH 8 in HEPES and is inactive in phosphate-citrate buffer (Fig 2c).

Mn x catalyzes both of these reactions much slower than CotA (Table 2).

Not only does ABTS oxidation by Mn x have two pH optima, but the kinetic traces at two different pH also look different. At pH 4.5, the curve follows Michaelis-Menten kinetics, while at pH 8, the curve fits the allosteric sigmoidal function much like Mn oxidation (Fig. 2). DMP and Fe oxidation also have Michaelis-Menten kinetics trends. The  $k_{\text{cat}}$  and maximum velocity increase from DMP < ABTS (pH 8) < ABTS (pH

Table 3: Mnx laccase-like activity compared to other *Bacillus* spp. coat MCOs, CotA.

Substrate	ABTS		2, 6-DMP	
	$K_M$ ( $\mu\text{M}$ )	$k_{\text{cat}}$ ( $\text{s}^{-1}$ ) <sup>c</sup>	$K_M$ ( $\mu\text{M}$ )	$k_{\text{cat}}$ ( $\text{s}^{-1}$ )
Mnx <i>Bacillus</i> sp. PL-12	456 $\pm$ 23.3	0.206 $\pm$ 0.0136	576 $\pm$ 163	0.0061 $\pm$ 0.0005
CotA <i>B. subtilis</i> <sup>a</sup>	6.5	83	216	80
CotA <i>B. licheniformis</i> <sup>b</sup>	124	322	56.7	28

4.5) < Fe < Mn (Table 2, 3). The enzyme's substrate affinity increases thusly; ABTS (pH 8) << DMP < ABTS (pH 4.5) < Mn < Fe.

### Discussion

The MnxG subunit within the Mnx protein complex has been proposed to be an MCO from the typical blue color (absorbance max. at 590 nm) and the sequence homology to the six domain MCOs (Butterfield et al., 2013). For the first time, we have spectroscopic evidence that the MnxG subunit contains an MCO center. EPR data clearly implicate type 1 and type 2 Cu in the Mnx protein that make up the MCO. The type 3 center is often evidenced by a 330 nm peak in the UV-visible spectrum of other MCOs, but we have not observed it. Rather, we surmise its presence based on azide inhibition and that enzymatic Mn oxidation consumes O<sub>2</sub> (Soldatova et al., 2012).

Mnx binds many more Cu than necessary for catalysis in the canonical MCO. Even when the protein is not expressed in Cu-loading conditions, the protein still binds about 3 mol Cu per protein and is inactive. CotA has been reported to have activity at a similar Cu: protein stoichiometry (Durão et al., 2008), and it is likely that in Mnx, three Cu atoms bind at peripheral sites, outside of the MCO center, rendering Mnx protein



inactive . The protein binds between 10 and 15 Cu depending on whether it is dialyzed in Tris or in HEPES buffers, respectively. Ceruloplasmin has two extra type 1 sites, and *Bacillus* sp. SG-1 MnxG has sequence similarity to these residues. The *Bacillus* sp. PL-12 MnxG, however, does not (Dick et al., 2008), so we do not anticipate that this MnxG binds any other type 1 Cu outside of the MCO center. If the true Cu content can be gleaned from the slightly more rigorous Cu removal of the Tris dialysis (ten total) and four are accounted for in the MCO, then the remaining six Cu in the complex might be in MnxE and MnxF. Additional Cu atoms in other MCOs have been proposed to aid in structural stability (Sedlak and Wittung-Stafshede, 2007) and in catalysis by acting as a labile Cu located near the type 1 site to facilitate substrate oxidation (Roberts et al., 2003). MnxE does not have any predicted Cu domains, but MnxF has two His residues, similar to the MnxG region containing conserved type 2 and type 3 Cu binding residues (Dick et al., 2008). Isolating the MnxE and MnxF subunits from MnxG will allow the analysis of extra Cu binding beyond the MCO.

Mnx was found to oxidize a wide variety of substrates, but the highest turnover efficiency was observed with Mn. Thus, Mnx can be defined as a metallo-oxidase with laccase-like activity. Mnx requires Cu to oxidize Mn while consuming oxygen at a pH optimum of 7.8, close to the near-shore marine sediment environment from which this *Bacillus* was isolated (Francis and Tebo, 2002). Also not surprising is its ability to oxidize Fe at pH 5, similar to other metallo-oxidases (de Silva et al., 1997; Kataoka et al., 2007). The striking difference between the reactions is that Mn oxidation diverges from Michaelis-Menten kinetics and follows an allosteric sigmoidal trend. This trend demonstrates that there is positive cooperativity, either due to substrate binding or due to

conformational change, which is an unprecedented feature among MCOs. Allosteric behavior has been observed in Mn(II)-oxidizing heme peroxidases, which bind two Mn<sup>2+</sup> in a pH-dependent manner (Mauk et al., 1998; Ertan et al., 2012). There, Mn<sup>2+</sup> acts as a homotropic allosteric regulator by increasing the rate of oxidation through a second Mn<sup>2+</sup> binding event. Work is ongoing to investigate the mechanism of both Mn(II) and Mn(III) oxidation reactions through in depth kinetic and spectroscopic analyses. Once structural information about Mnx is known, it will be interesting to contrast the pathways by which Fe and Mn are oxidized in these different enzymes.

We also tested Mnx specificity toward oxidation of phenolic compounds. Both 2,6-DMP and ABTS are oxidized by Mnx, typical of many MCOs. An interesting trend is emerging, however, amongst the kinetic data. Fe, 2,6-DMP, and ABTS (pH 4.5) oxidations all follow Michaelis-Menten trends nicely, at pHs similar to other MCOs in the literature. On the other hand, ABTS oxidation at pH 8 follows an allosteric sigmoidal trend like Mn oxidation. The two independent kinetic traces for ABTS (pH 4.5 and 8) imply two effectively different binding sites, implying that the allosteric sigmoidal character of the protein is structural rather than cooperative metal binding (or perhaps an unfortunate side reaction of the buffer conditions). The pH change may induce large enough changes to allow weak binding and slow turnover at pH 8 relative to pH 4.5. This activity is so weak that the reaction is probably an indirect consequence of this particular set of protein-in-buffer conditions. The other scenario in which ABTS could be oxidized at pH 8 is if there is a small contamination of Mn(II) in solution. ABTS is oxidized in the presence of MnO<sub>2</sub> alone (data not shown), so if Mn(II) is oxidized by Mnx in the presence of reduced ABTS, there could be redox between the two species.

Confirming the presence of the MCO Cu centers and describing the activity of the catalytic center brings us closer to tying the two together and providing evidence for the direct enzymatic conversion of Mn(II) to MnO<sub>2</sub> oxides in the environment. Furthermore, the tendency of this protein to catalyze a broad range of substrates, particularly Mn, may point towards a physiological role on the bacterial spore surface. Considering that the marine environment provides the optimum Mn oxidizing pH conditions (~ pH 8) and that Mn oxides promote the degradation of organic matter (Stone and Morgan, 1984b), it is tempting to speculate that the spore utilizes this MCO to harvest recalcitrant carbon in sediments. Additionally, if the spore encounters more acidic environments, direct oxidation of phenolic compounds can be employed to degrade organic matter. Once local concentrations of available carbon build up, the spore can germinate and use them as an energy source for vegetative cell growth.

As more enzymes are characterized from bacteria that carry out interesting geochemical cycling, more novel enzymatic mechanisms will be discovered to broaden our scope of what chemistry is possible within the protein environment.

## **Chapter 4. Spectroscopic studies reveal novel type 2 Cu and heme binding in subunits of a multicopper oxidase-containing complex**

### Abstract

The Mn(II) oxidizing Mnx complex from *Bacillus* sp. is the first MCO co-purified with subunit proteins. MnxE and MnxF precede MnxG in all three of the sequenced *Bacilli* species, but neither MnxE nor MnxF have any conserved regions from which their functions can be predicted. Also unique about the Mnx complex is that it performs substrate oxidation in an allosteric sigmoidal kinetic fashion and contains far more Cu than necessary to fill the MCO, dampening the EPR signal of the MCO type 1 and type 2 Cu. It is unknown how much of these unusual characteristics can be attributed to the MnxE and MnxF subunits. Here, the MnxE and MnxF subunits are analyzed for their sequence homology, metal content by EPR, XAS, and UV-vis, and potential contribution to catalysis within the complex. The MnxEF subunits oligomerize in the absence of MnxG, bind Cu and heme, and do not oxidize Mn on their own. These newly elucidated features point towards an electron transfer role in the MnxEF subunits and perhaps a direct role in substrate turnover. These results suggest even more complex metallo-protein story found on the outer layer of a perceived inactive dormant bacterial spore surface.

### Introduction

Bacteria impact geochemical cycles through direct and indirect processes. The biogeochemical cycling of Mn is especially significant because it is abundant in ground and surface waters and affects several other elemental cycles through sorption and oxidation reactions. Microbial Mn oxidation has been shown to be both enzymatic and

indirectly facilitated through superoxide and Mn(III) generation. Direct enzymatic Mn(II) to Mn(IV) oxidation has been shown to be the driver of Mn mineralization on the outer cell surfaces of diverse bacteria. These Mn oxidases are Mnx, a multicopper oxidase, in *Bacillus* and *Pseudomonads* and MopA, an animal heme peroxidase in *Aurantimonas* and *Erythrobacter*. Although the Mn oxidation enzymes have been identified, little is known about the molecular mechanism of oxidation.

The only enzyme that has been purified and characterized to date is Mnx from *Bacillus* sp. PL-12. Mnx oxidizes Mn in a Cu dependent manner, consistent with the MCO catalytic center. MCOs have four canonical Cu atoms liganded in three different orientations. The type 1 is bound by one S(Cys), one S(Met), and two N(His), type 2 by three N(His), and two type 3 binuclear Cu by two N(His). MCOs utilize these Cu to catalyze the oxidation of a variety of substrates, including phenolic compounds and metals, and the reduction of O<sub>2</sub> to H<sub>2</sub>O. MCOs are common enzymes that carry out numerous physiological functions, are very well-studied, and when purified from an *E. coli* expression system, are always derived from single MCO gene products. This last characteristic was not true for the Mn oxidizing MCO from *Bacillus*. The expression of soluble and active Mn oxidase requires the co-expression of at least three genes on the *mnx* operon, *mnxG*, the MCO, and *mnxE* and *mnxF*, small proteins of unknown function. Since no other MCO requires the co-expression of subunits, the role of MnxE and MnxF is a mystery.

While MCOs have not been purified as complexes, other Cu proteins like cytochrome c oxidase do require the co-expression of several other proteins to assembly a functional, multi-subunit complex. Cytochrome c oxidase is also a heme-copper oxidase

membrane protein involved in the reduction of O<sub>2</sub> to H<sub>2</sub>O and supplying respiration processes with proton motive force. Much has been done to distill the cytochrome complex down to its essential metal binding residues, and there is considerable sequence similarity between organisms. The sequence of the O<sub>2</sub> reduction site, for example, is composed of six strictly-conserved His residues in subunit I to bind the type 2 Cu and heme catalytic center.

MnxE and MnxF do not, however, contain any conserved domains from which to predict function. They are hydrophobic, small, about 12 kDa each, and well-conserved among the Mn oxidizing *Bacillus* spp. that have been sequenced. They oligomerize with each other (with unknown stoichiometry) and co-purify with MnxG during heterologous preparations and assemble into a large 230 kDa complex. As a complex, MnxEFG bind many more Cu (ten) than necessary for MCO function (four). The EPR spectrum of the complex is similar to that from Fet3p, indicating the presence of type 1 and type 2 Cu, but is a little less resolved, likely from another EPR detectable Cu species. It is possible that the extra Cu atoms reside in the MnxEF subunits, perhaps contributing to electron transfer and Mn oxidation catalysis, like subunit I of cytochrome c oxidase.

Here, MnxEF were purified independently from MnxG and analyzed with EPR, XANES, and optical spectra to determine the type and oxidation state of metal bound. Three diverse *Bacillus* spp. MnxE and MnxF sequences were used to predict Cu binding ligands and site directed mutagenesis replaced the residues with Ala. The same spectroscopic analyses were used to determine if the conserved residues were involved in metal binding.

## **Methods**

### *Cloning and mutagenesis*

Protein was purified by *Strep*-tag affinity chromatography. MnxDEFG complex was cloned, expressed, and purified as previously described (Butterfield and Tebo, In preparation). *mnxE* to *mnxF* (NCBI accession EF158106) were amplified from *Bacillus* sp. PL-12 (Taxonomy ID: 161537) genomic DNA by the following primers: Fwd 5'-**CCGCGGTATGCATGACTCGCCATT**-3' and Rvs 5'-**TCGACATAGTCTTCGAGCTTCG**-3' and cloned by restriction enzyme digestion and ligation from the pJet1.2 (Thermo) entry vector into the *Strep*-tag pASK/IBA3plus expression vector using SacII and Sall (sequences in bold). In place of the *mnxF* stop codon the *Strep*-tag (underlined) was engineered to a linker (italicized) at the C-terminus of *mnxG* (*VDLQGDHGLSAWSHPQFEK*). Single amino acid mutations were generated in the pJet1.2/*mnxDEFG* (Butterfield and Tebo, In preparation) construct with the Stratagene QuickChange® site-directed mutagenesis kit (Agilent). MnxF H21, 80, and 82 were changed to Ala in the *Strep*-tag construct to yield MnxF H21/80/82A-*Strep*. Then *mnxEF* H21/80/82A mutant or *mnxDEFG* H21/80/82A were PCR amplified and cloned into the pASK/IBA3plus vector as described above and in previous publication.

### *Protein expression and purification*

The resulting construct was transformed into *E. coli* BL21 (DE3) and grown at 37 °C to an OD<sub>600</sub> ~ 0.5 in Luria-Bertani (LB) broth containing 0.2 mM CuSO<sub>4</sub>, 10 mM Tris-HCl pH 7.5, and 100 mg/L ampicillin. 0.2 mg/L anhydrotetracycline was added to induce transcription of the *mnx* genes and let express shaking for 3 h. CuSO<sub>4</sub> was added to a final concentration of 2 mM and the flasks were set on the bench for a static incubation at 23 °C for at least 22 h more to allow for the microaerobic uptake of Cu ions

into the *E. coli* cytoplasm as described in Durao et al.2008 (Durão et al., 2008). This Cu loading step was omitted during the apo-protein preparation.

The cells were then harvested, suspended in *Strep*-Tactin equilibration buffer (100 mM Tris pH 8.0, 150 mM NaCl) amended with 1 mM CuSO<sub>4</sub> and an EDTA-Free SIGMAFAST™ Protease Inhibitor Cocktail Tablet, and lysed by sonication microtip for 1 min/ ml cell lysate at 40% amplitude with 10 s on/off pulses on ice. The cell debris was removed by centrifugation 15,000 x g 4 °C 30 minutes and the supernatant was filtered through a 0.4 µm pore PVDF filter. The clarified lysate was then added to 1 ml column volume (CV) of *Strep*-Tactin Superflow Plus (Qiagen). By gravity flow, the unbound protein fraction was removed and the resin was washed with 20 CV Streptactin equilibration buffer. The MnxEF protein was eluted with 5 CV equilibration buffer plus 2.5 mM D-Desthiobiotin and the column was regenerated with 15 CV equilibration buffer plus 1 mM 2-(4-hydroxyphenylazo)benzoic acid. The eluted protein was concentrated to < 1.5 ml on 50 kDa molecular weight cutoff filtration units (Millipore). The protein was then dialyzed in 50 mM Tris-HCl pH 8 and decreasing NaCl concentrations from 150 to 50 mM NaCl and flash frozen with 20% ethylene glycol for future analyses. The protein was quantified by the Thermo Scientific Pierce bicinchoninic acid (BCA) protein assay.

#### *Estimate size of MnxEF*

Protein was run on an HiPrep 16/60 Sephacryl S-200 High Resolution gel filtration column (GE Healthcare) equilibrated with 20 mM HEPES pH 7.8 50 mM NaCl 5 % D-glucose (w/v) at 4 °C to approximate size. All buffers up to this point were supplemented with 50 µM CuSO<sub>4</sub> to avoid Cu leaching by Tris buffer. A single peak



corresponding to a 150 kDa= 5.85 dimer subunits was run on SDS-PAGE alongside *Strep* purified protein even though it had precipitated after eluting.

#### *Alignments*

Alignments were carried out with MUSCLE with default parameters on the following URL <http://www.ebi.ac.uk/Tools/msa/muscle/> (Edgar, 2004a; Edgar, 2004b) with accession numbers MnxE PL-12 ABP68888, MB-7 ABP68897, SG-1 EDL64242 and MnxF PL-12 ABP68889, MB-7 ABP68898, SG-1 EDL64243.

#### *Mass spec*

Purified protein was run on Tris Glycine 4-15% sodium dodecyl sulfate polyacrylamide electrophoresis gel (Bio-Rad) and stained in Imperial protein stain (Pierce). The protein band that migrated to 12 kDa according to the PageRuler™ Unstained Protein Ladder (Thermo) was excised by a clean razor blade and submitted to the Oregon Health & Science University Proteomics Shared Resource Center for analysis with the *Bacillus* sp. PL-12 *mnxE* and *mnxF<sub>H→A</sub>* sequences. Mass spec analysis was performed as previously described in Butterfield et al. 2013 (Butterfield et al., 2013).

#### *UV-visible spectra*

The UV-visible spectra were collected on a SpectraMax M2 in a 50  $\mu$ l 1 cm path length quartz cuvette.

#### *EPR*

X-band continuous wave electron paramagnetic resonance (CW EPR) spectra were recorded using a Bruker (Billerica, MA) Biospin EleXsys E500 spectrometer equipped with a cylindrical TE011-mode resonator (SHQE-W). Cryogenic temperatures were achieved and controlled using an ESR900 liquid helium cryostat in conjunction with

an Oxford Instrument temperature controller (ITC503) and gas flow controller. All CW-EPR data were collected at 15 K under non-saturation and slow-passage conditions. The spectrometer settings used were as follows: microwave frequency = 9.374 GHz, microwave power = 0.002 mW, conversion time = 120 ms, modulation amplitude = 3 G, modulation frequency = 100 kHz. EasySpin computational package was used to simulate the EPR data (Stoll and Schweiger, 2006).

#### *Mn oxidation activity assay*

A small aliquot of purified protein was diluted into 10 mM HEPES pH 7.8, 50 mM NaCl and 100  $\mu$ M MnCl<sub>2</sub> was added. The appearance of brown Mn oxides and reactivity with the colorimetric reagent leucoberberlin blue confirmed activity.

#### **Results**

MnxE and MnxF primary sequences are highly conserved among the Mn oxidizing *Bacilli* that have been sequenced. Here we looked at their homology to get an understanding of how the protein binds Cu. A previous sequence alignment of MnxE and MnxF identified a region in MnxF resembling two His of type 2 and type 3 Cu binding ligands found in the MCOs. A new sequence alignment for the three *Bacillus* spp. MnxE and MnxF was performed to find additional conserved Cu binding ligand candidates (Fig. 1). MnxF has exactly three conserved His residues, H21, H80, and H82 that are attractive contenders for type 2 Cu binding ligands. These three residues were mutated to Ala to probe whether the Cu binding properties of the subunits would be disrupted.

<b>MnxE_PL-12</b>	1	MHDSPLKSLSAASNVA-----SVNDPLFDFFNKH <b>MGK</b> QILIIITESSQLNILGQTFRPIF
MnxE_MB-7	1	MQRKRRGSF <b>MV</b> KEKKPVKEEIEVDDRFFRELLALKGESILLVTESDQLNLFQTFRPVF
MnxE_SG-1	1	-----MKTNNRLP-----EDRLLLEL <b>MDL</b> MGREILVITEAPQLNLLGQTFRPIF
<b>MnxE_PL-12</b>	55	CGKVAEVEPGH <b>L</b> TLSPVTIKILNAPFHKFPIPLSIPFEKIAHFTTDDV <b>D</b> CS <b>M</b> RIPLV
MnxE_MB-7	61	CGEITDVQQG <b>Q</b> LTLFPVNIK <b>M</b> VNAPFFNFPTPLSIPLEKIAHFTPDFD <b>C</b> NARLPLS
MnxE_SG-1	45	CGTLAEVGRGH <b>I</b> TLDPVIFK <b>M</b> VNAPFYEF <b>P</b> PI <b>S</b> IIPLEKIVSF <b>T</b> TEIP <b>D</b> TVFPLT
<b>MnxF_PL-12</b>	1	MEALF <b>P</b> MSTDYSK <b>M</b> TDVNEI <b>H</b> DSAIL <b>E</b> FRNGIGHKTLVISPSYP <b>M</b> FVGI <b>I</b> KELIGDTV
MnxF_MB-7	1	-MSQEKVNTEW-EYPTVN <b>V</b> L <b>H</b> DQALVEEFIEGIGKNIF <b>I</b> MTPSFPPYVFIGKLVEVEDQA
MnxF_SG-1	1	-MAISDQERD--SFQ <b>S</b> INDI <b>E</b> DEGLVDLFRV <b>N</b> KGRRV <b>F</b> ML <b>M</b> P <b>N</b> YPFIFIGKILDVIDD <b>M</b> V
<b>MnxF_PL-12</b>	61	MIDVET <b>H</b> F <b>A</b> QLENREWYI <b>H</b> I <b>H</b> NI <b>E</b> VFYIERPGAPKIPKLED-Y
MnxF_MB-7	59	VVDVKVTTISELENRQWYI <b>H</b> I <b>H</b> QIEVFYIQK <b>G</b> QPRIPELRDDF
MnxF_SG-1	58	LLDVETSQFPAL <b>E</b> KVKWHI <b>H</b> I <b>H</b> NI <b>E</b> VFYIEKSTGPRI <b>P</b> RLKD--

Figure 1. Alignments of three Mn(II) oxidizing *Bacillus* spp. PL-12, MB-7, and SG-1 MnxE and MnxF amino acid sequences. Conserved/mutated His residues (PL-12 H21, H80, H82) highlighted in black, conserved Cys in dark gray, remaining His in light gray and Met in bold.

### *MnxEF copurify and oligomerize*

The MnxE and MnxF subunits were co-expressed on a C-terminal Strep tag plasmid and purified on a Streptactin column. A MnxF triple His to Ala mutant was constructed and isolated in the

same manner. This modified protein was run on SDS PAGE and the protein corresponding to 12kDa mass (Fig. 2) was analyzed by mass spec to ensure that both MnxE and MnxF peptides were present and that mutagenesis was successful. Mass spec analysis

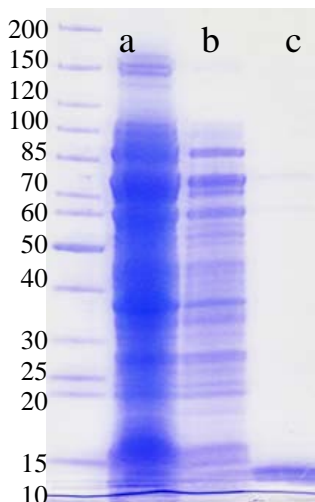


Figure 2. SDS PAGE of MnxEF purification. *Strep*-Tactin affinity purification fractions: flow through (a), wash (b), and elution (c).

confirmed the mutagenesis (Fig. 3) and identified 108 unique peptides from MnxE (100% coverage) and 67 from MnxF (89% coverage). These results show that even without

MnxG present, MnxE and MnxF co-elute in the same fraction when only MnxF contains the affinity tag.

The stoichiometry of the MnxEF subunits in relation to each other and to the MnxG MCO is yet unknown. When *mnxDEFG* is expressed and purified, a large 230 kDa complex is isolated, composed of MnxE (12.2 kDa), MnxF (13.5 kDa), and MnxG (138 kDa) by mass spec analysis (Butterfield et al., 2013). By summation, MnxE and MnxF would have to comprise about 90 kDa of the complex mass and we have previously surmised that they oligomerize into a hexamer of about 77 kDa. When expressed and purified on their own, MnxEF precipitates during gel filtration chromatography, preventing estimation of its size. Thus, for the rest of the discussion, we assume purified MnxEF is in a hexamer (77 kDa) and refer to the MnxEF triple H21/80/82A mutant as MnxEF3.

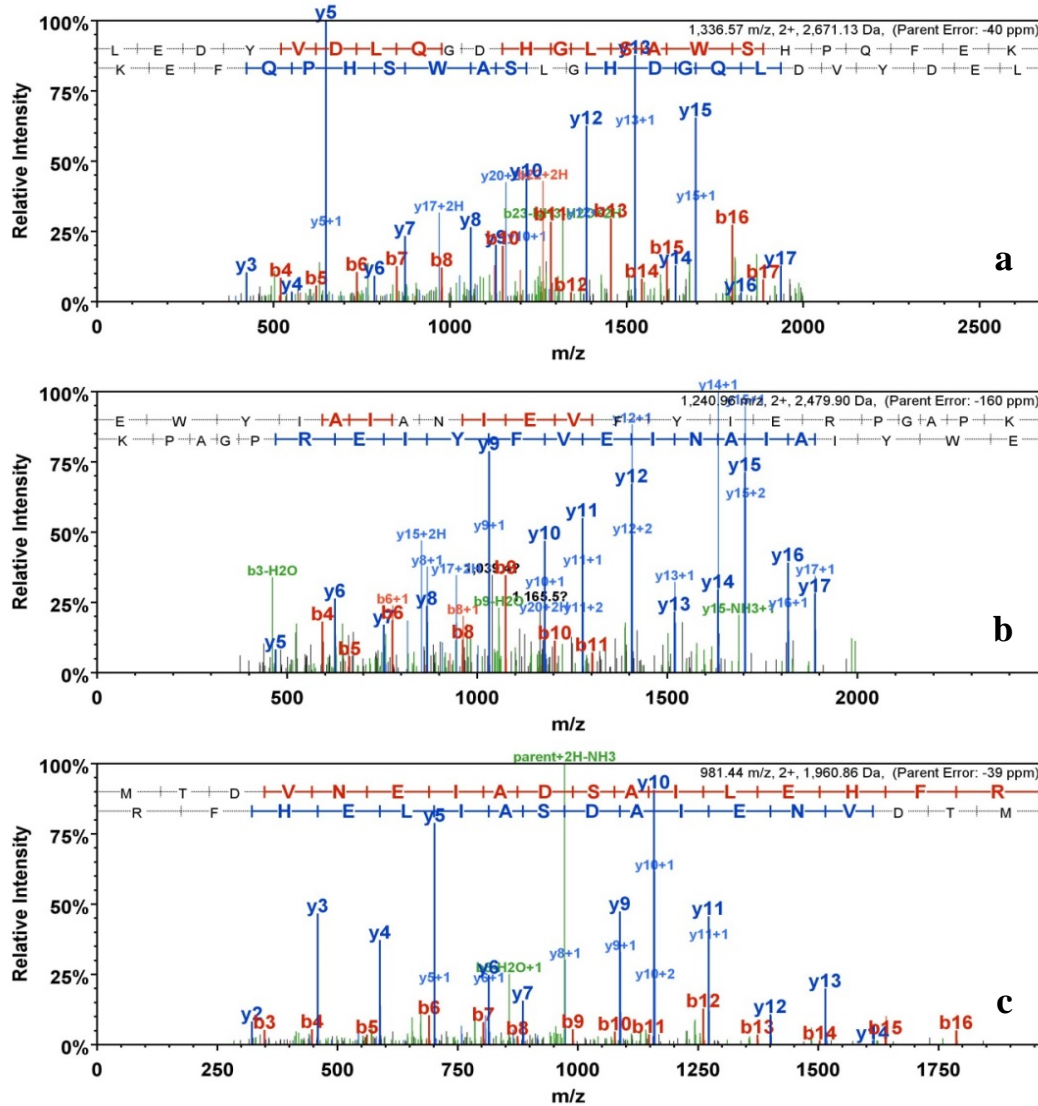


Figure 3. Mass spec identifies MnxF peptides including the Strep tag and each of the three His to Ala mutations. a) Strep tag, b) H80A and H82A, c) H21A

MnxF H21/80/82A was incorporated in the genes expressed for subunit analysis, *mnxEF*, and for activity analysis in the MnxF complex, *mnxDEFG*. Neither showed divergence in activity with respect to wild type. MnxEF and MnxEF3 do not oxidize Mn, but both wt and triple mutant MnxF complexes oxidize Mn as seen in the assays (not shown). MnxF H21, 80, and 82 do not seem to play a significant role in Mn oxidation.

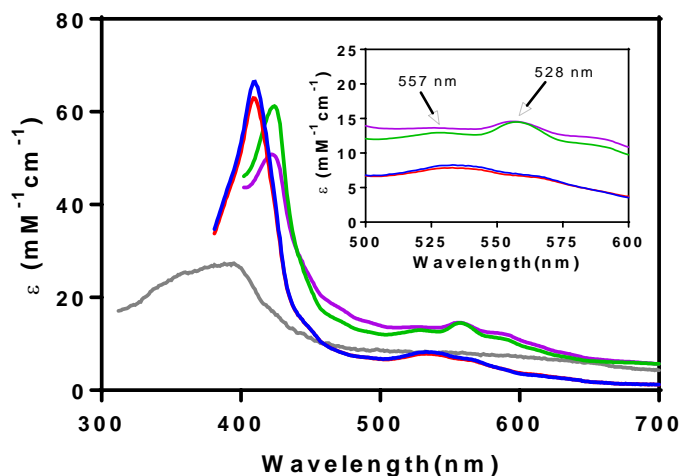


Figure 4. Strep-purified wt MnxEF (blue) and MnxEF H21/80/82A mutant (MnxEF3) (red) contain the same Soret 408 nm peak after heme incorporation. After reduction of heme-MnxEF (green, 2X) and heme-MnxEF3 (purple, 2X), the Soret band shifts to 424 nm and the visible bands at 528 nm and 557 nm appear (inset). Bovine hemin (gray) is shown for comparison.

Both wtMnxEF and MnxEF3 are orange in color when purified and concentrated. Their UV-visible spectra showed an absorbance peak at 408 nm that did not reduce with the addition of dithionite or ascorbate (data not shown) (Fig. 4). Bovine hemin was added to MnxEF3 and then excess was removed by desalting spin columns and dialysis. The resulting protein was diluted and its spectrum was typical of oxidized heme with the Soret band at 408 nm and visible bands at 531 nm and 565 nm. Upon the addition of 10 mM dithionite, the Soret band shifted to 424 nm, while the visible bands shifted to 528 nm and 557 nm.

#### *Cu binding analyses*

In a previous study, the Mnx protein complex was found to bind a minimum of ten mol Cu per mol protein. It is presumed that four Cu reside in the MCO while six are left unaccounted for and are perhaps in the subunits. Cu content analyses of the newly purified MnxEF subunits by ICP-OES (2.6 Cu: 1 MnxEF) and Cu(II) in EPR (2.8 Cu: MnxEF) both gave a Cu: protein molar ratio of about 3:1.

MnxEF and the triple H21/80/82A mutant MnxEF3 were analyzed by X-band (9.374 GHz) CW EPR spectroscopy, shown in Figure 5. Their spectra exhibit typical type 2 Cu ('normal Cu', square planar coordination) signal with hyperfine coupling ( $g_{\parallel} \approx 2.21$ ,  $A_{\parallel} \approx 199$  Gauss) and seven hyperfine peaks ranging from 3187 to 3275 Gauss, with hyperfine splitting around 14 ~ 15 Gauss. The first derivative spectrum (not shown) was taken to calculate the intensity of seven peaks, and although theoretical intensity 1:3:6:7:6:3:1 did not match well, the number of seven peaks indicates that there could be three  $^{14}\text{N}$  coordinated with Cu. Unlike the EPR of the previously described Mnx complex, the typical type 1 Cu with smaller hyperfine coupling ( $g_{\parallel} \approx 2.30$ ,  $A_{\parallel} \approx 40 - 93$  G) is not observed, indicating that there is no type 1 Cu in MnxEF.

The low Cu binding stoichiometry of one MnxEF3 sample facilitated the one component simulation which supposed all the Cu atoms bound with three  $^{14}\text{N}$  coordinated (with high affinity) (Fig. 5c). But this simulation did not fit for the rest of the spectra, even the higher Cu stoichiometry triple mutant, so a two component simulation including three  $^{14}\text{N}$  coordinated and a square planar Cu was used. The two component simulation fit well and may confirm that there are at least two types of type 2 Cu binding site in MnxEF subunits.

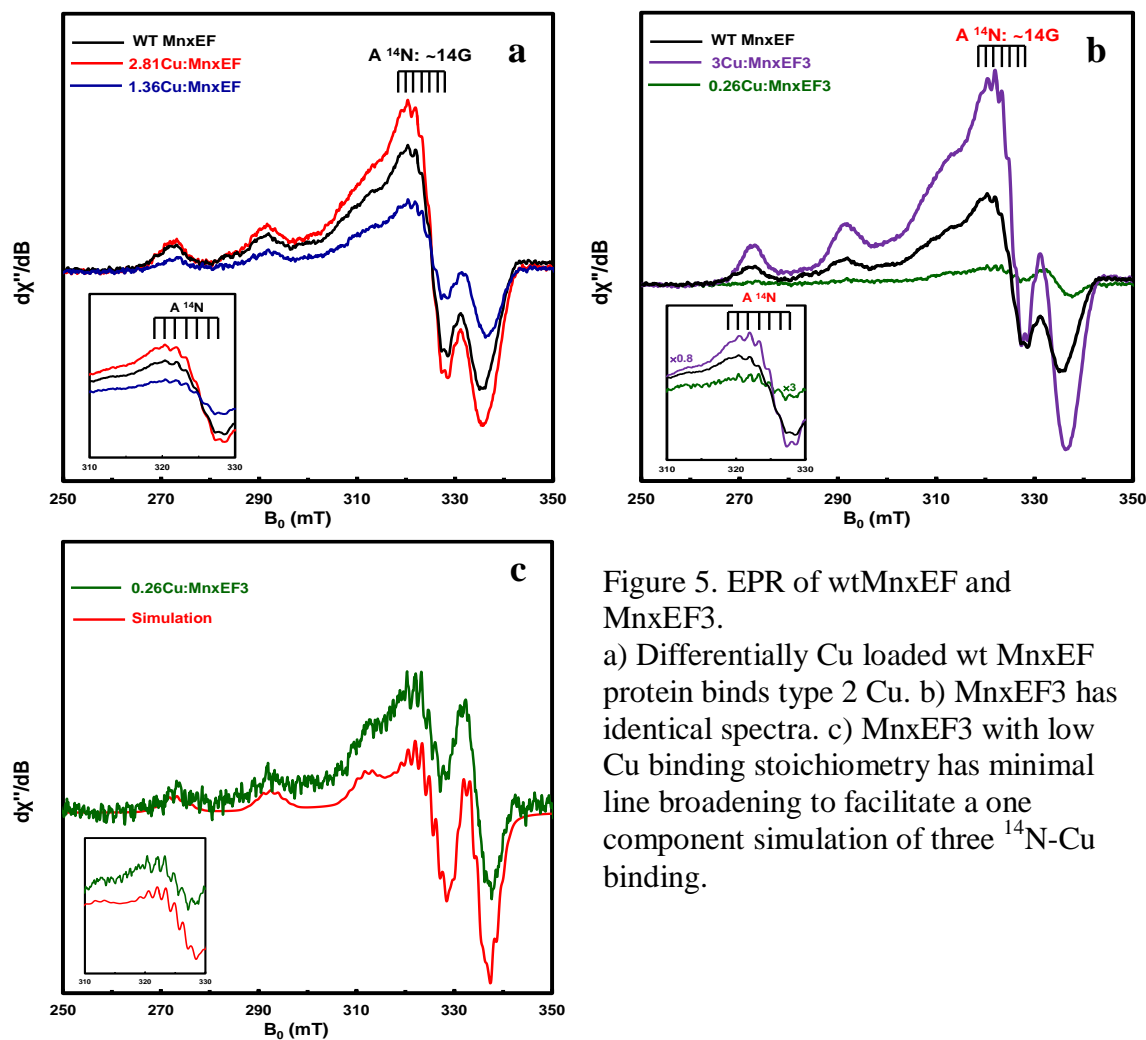


Figure 5. EPR of wtMnxEF and MnxEF3. a) Differentially Cu loaded wt MnxEF protein binds type 2 Cu. b) MnxEF3 has identical spectra. c) MnxEF3 with low Cu binding stoichiometry has minimal line broadening to facilitate a one component simulation of three  $^{14}N$ -Cu binding.

Mnx EPR spectrum is more complex than typical MCO spectra (Butterfield and Tebo, In preparation). The type 1 and 2 Cu(II) signatures seemed to be dampened by a third signal. The newly analyzed EPR spectra and simulations of the MnxEF Cu(II) allowed us to integrate this signal into the MCO complex EPR spectrum. Adding together the type 2 Cu signal from MnxEF and the MnxG MCO EPR visible type 1 and type 2 Cu signals results in an agreeable simulation of the entire complex (Fig. 6).



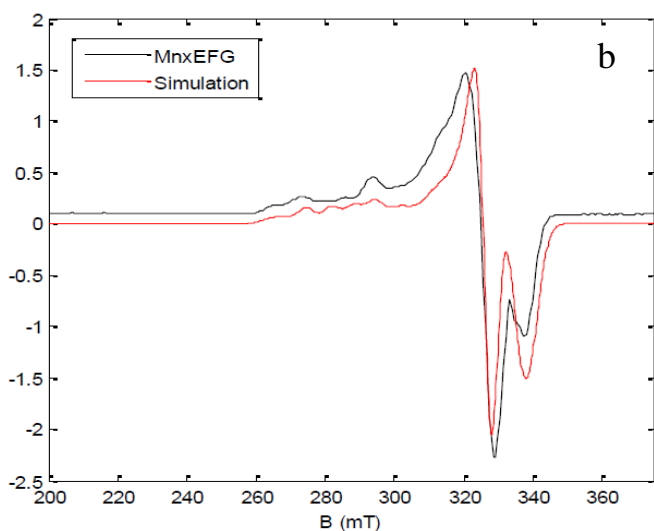
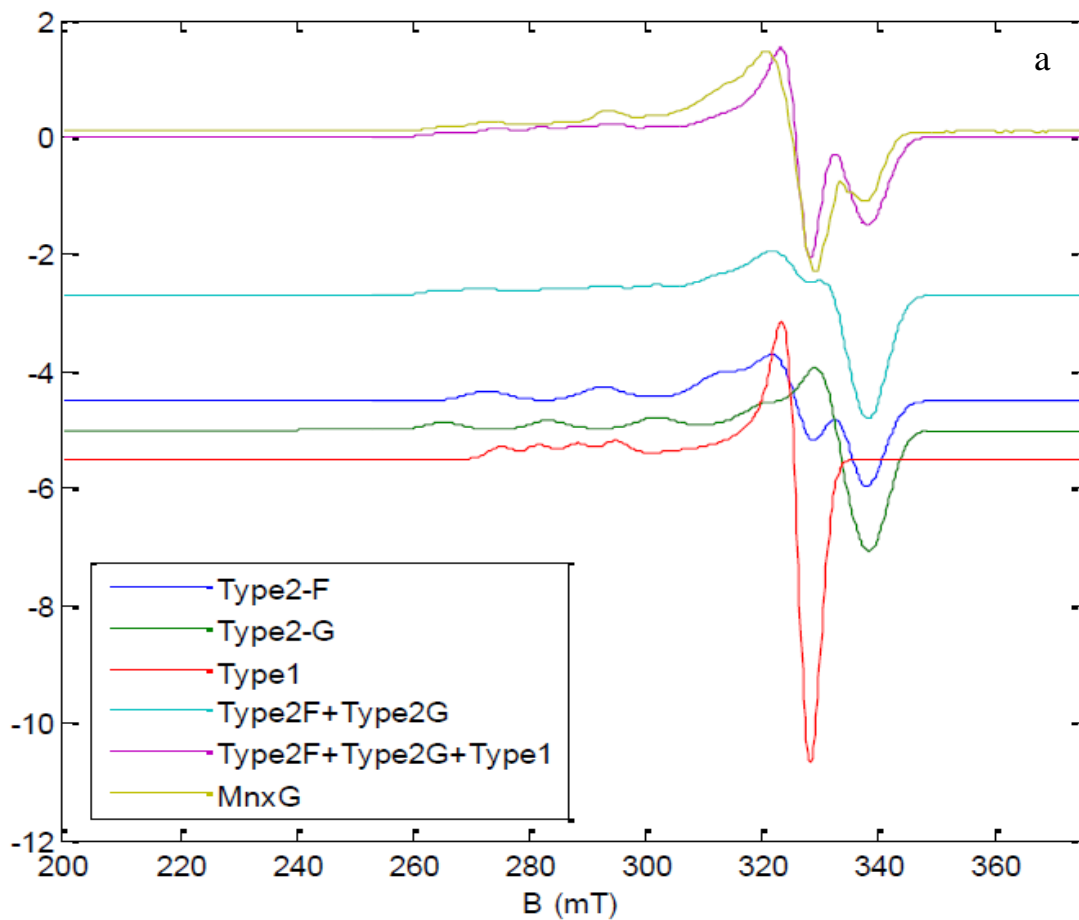


Figure 6. Contributions of Cu from the MnxEFG subunits in the greater MnxEFG complex. a) From the MCO and subunit sequences, MnxG will bind type 1 (red) and type 2 (green), and MnxF will bind type 2 (blue). From these, permutations (turquoise and purple) are compared against the experimental data (gold). b) The simulation with all three predicted Cu sites (type 1 from MnxG, type 2 from MnxG, and type 2 from MnxEFG) (red) best represents the Mnx Cu system (black).

## Discussion

Dissecting the role of each unit of the Mnx complex is important for determining the structure function relationship of electron transfer and substrate turnover mechanism. Many unsuccessful attempts at expressing soluble, active MnxG necessitated the isolation of the remainder of the complex to begin to unravel the contribution of the individual subunits. We previously observed MnxE and MnxF oligomerize in an unknown stoichiometry within the Mnx complex, and now it is apparent that this action is not contingent on MnxG. While the stoichiometry of MnxE and MnxF subunits relative to each other in the oligomer is still unknown, there are at least six ~12 kDa subunits in the Mnx complex. More sophisticated structural analyses like analytical centrifugation and crystallography are required to determine the subunit stoichiometry.

With no structural information, sequence homology and spectroscopy were used to provide clues for Cu binding within the small Mnx subunits. As a whole, MnxE and MnxF sequences contain zero Met, two Cys, and three His conserved amongst the three sequenced Mn(II) oxidizing *Bacilli* that could contribute to Cu binding like that found in MnxG. There is no evidence for or against S-S bridging between the two conserved Cys in MnxE, and SMet Cu binding cannot be ruled out since there are six Met between *Bacillus* sp. PL-12 MnxE and MnxF proteins. If each of the subunits also hold this 3:1 ratio with respect to the oligomer as a whole, then either MnxE or MnxF could bind one Cu each or one MnxE and one MnxF could bridge one Cu between the two subunits.

The optical and EPR spectra point to MnxEF binding heme and type 2 Cu. Predicting the N ligands is not so straightforward since all of the well-conserved His from MnxF were mutated to Ala without disrupting the EPR spectra. However, the loss of one

or two Cu binding N(His) may not necessarily be observed by the EPR spectra presented here. On the other hand, there is plenty of examples in the literature for non-His N binding Cu (Aronoff-Spencer et al., 2000; El Ghazouani et al., 2011), such as non-conserved N(His), NH from the peptide backbone, or the N-terminal.

Electron spin echo envelope modulation (ESEEM) and electron nuclear double resonance (ENDOR) will be used to investigate more specific information for the Cu binding sites, such as exactly the number of coordinated His, H<sub>2</sub>O, etc.

Initially ruled out as heme impurity from previous crude isolations, we were surprised to find that affinity-purified MnxEF appears to bind heme specifically. The Soret and visible peaks in the absorption spectrum (oxidized: 408, 531, and 565 nm; reduced: 424, 528, 557 nm) lie well within the literature values for other heme proteins like mammalian cytochrome oxidase *b*<sub>5</sub> (His/His Fe axial coordination) (oxidized: 410 nm; reduced: 423, 527, and 555 nm) (Beck von Bodman et al., 1986) and a heme peroxidase from *Streptomyces refuineus* (oxidized: 408, 530, and 561 nm) (Connor et al., 2011). Parallels with heme/Cu protein cytochrome c oxidase are quickly drawn. The Cu site that bridges dioxygen with the Fe heme in cytochrome c oxidase is Cu<sub>B</sub>, known to have a type 2 square planar geometry of three equivalent N(His) (g parallel 2.20, A parallel 190 G and g perpendicular 2.06), which is similar to values found in MnxEF (Pezeshk et al., 2001). Further research is required to determine if heme and type 2 Cu lie in similar proximity to those found in the cytochrome c oxidase. An analogous heme/Cu center in MnxEF would be very interesting indeed, as examples are rare in the literature. To determine if heme in MnxEF has any effect on catalysis when complexed with MnxG, heme needs to be incorporated during expression which could be done by either of the

following methods. The maturation and heme loading of cytochrome *c* in *E. coli* is facilitated by the incorporation of a signal peptide that targets nascent protein to the periplasm (Londer 2011). Sudhamsu and coworkers also derived a method for inexpensive Cys and His-liganded heme loading by the co-expression of the native *E. coli* protein ferrochelatase and addition of a small amount of  $\delta$ -Ala, (Sudhamsu et al. 2010).

To implicate the heme/Cu oligomeric MnxEF subunits in the direct mechanism of oxidation within the Mnx complex is becoming increasingly tempting as hallmarks of electron transferring metallo-centers present themselves. It is apparent from the identical nature of the optical and EPR spectra of wtMnxEF and MnxEF3 that the three conserved His are not essential and that more structural analyses are required to determine the residues involved in metal binding. Further directed mutagenesis, spectroscopic, and structural studies of the Cu and heme binding centers will help put the MnxEF subunits in context with oxidation catalysis in the Mnx complex.

## Chapter 5. Conclusions and Future Directions

### *Summary*

Elucidating the enzymatic mechanism of Mn oxidation in bacteria has evaded scientists for many years because of the lack of purified protein. The breakthrough of expressing and purifying the Mn oxidase from *Bacillus* sp. PL-12 described here was achieved in part with aid from recent advances in cytochrome oxidase multi-subunit expression and metal homeostasis in *E. coli*. The co-expression of *mnx* operon genes and *in vivo* Cu loading enabled soluble protein production and subsequent characterization of the active Mn oxidase complex.

Unlike any other MCO isolated to date, MnxG co-elutes with small subunits MnxE and MnxF, formerly known as well-conserved “hypothetical” proteins on the *mnx* operon. Now, since they have been found to oligomerize and bind heme and Cu on their own, they can be characterized as heme/Cu binding MCO subunits. MnxG cannot be expressed as a soluble protein without these partners, but they do not have Mn(II) oxidizing activity on their own, so their roles in structure and catalysis are still unknown.

The Mnx complex oxidation activity with different MCO substrates was surveyed and it was concluded that Mnx has a broad substrate diversity like many other MCOs. It had much better turnover efficiency with Mn and Fe than with phenolic substrates ABTS and 2, 6-DMP. The Mn oxidation reaction stood out for its increased reaction velocity, its two-electron oxidation, and its allosteric kinetics character. This allostery could be the result of cooperative Mn binding, or in other words, conformational change upon Mn binding. I have outlined a kinetic scheme (expanded from Tom Spiro’s model Chapter 1. Fig. 3) that could explain where in the Mn loading process allostery might hasten Mn

oxidation in Appendix A. In my model, structural priming of the enzyme occurs upon loading of both the substrate and holding sites to facilitate cooperative binding in the binuclear site. Further analyses are required to uncover the course of Mn oxidation within the overall structure of the complex.

#### *Detecting Mn(III-III) intermediates*

Experiments are ongoing to split up and define the individual oxidation reactions, following a hypothesis put forward in Soldatova et al. 2012 (Chapter 1. Fig. 13) (Soldatova et al., 2012). It combines the canonical MCO mechanism of four electron oxidation of substrate with the reduction of O<sub>2</sub> and the Mn(III) chemistry of Mn peroxidase, which also has allosteric sigmoidal kinetics. The first step of Mn(II) oxidation to Mn(III) mimics that of Fe(II) oxidizing MCOs, where Mn(II) oxidation is promoted at the type 1 proximal substrate site by substrate entasis and the Mn(III) product stabilization in a holding center. The second step involves a bit of imagination and creativity, however. Since Mn(III) is highly unstable, it requires ligands to avoid disproportionation into Mn(II) and Mn(IV). The Mn-peroxidase-like binuclear center may meet this need and facilitate Mn(IV) generation. The model suggests Mn(III-OH-III) bridging in order to control electron flow toward Mn(IV). The next step to validate this model is the detection of the Mn(III) binuclear center. Mn(III) is EPR silent, but the binuclear site can be detected in parallel mode. Mn oxidation time trials, rapid freeze quench, and D<sub>2</sub>O replacement are all being employed to capture reaction intermediates and to characterize the metal-ligand environment.

#### *Role of O<sub>2</sub> in Mn oxidation*

Oxygen is central to Mn oxidation. First, the MCO requires O<sub>2</sub> as an oxidant, it consumes O<sub>2</sub> as the substrate is oxidized. O from OH in H<sub>2</sub>O may provide bridging for Mn(III)-Mn(III) oxidation. O<sub>2</sub> is also present at the termination of the reaction because it composes half of the O in MnO<sub>2</sub> oxides.

It should, therefore, be straightforward to measure O<sub>2</sub> consumption during Mn oxidation and determine a reaction stoichiometry of O<sub>2</sub> with respect to Mn. MCO substrate oxidation kinetics are often determined by measuring the disappearance of O<sub>2</sub> rather than the oxidation substrate. I quantified O<sub>2</sub> consumption with a Clark-type electrode during Mn oxidation and was confused by the results which indicated that just a fraction of O<sub>2</sub> was consumed relative to Mn (Appendix B). The reaction time frame was much shorter than Mn oxide formation experiments. This is likely due to the fact that the O<sub>2</sub> consumption experiments were performed at a higher temperature (37 °C) than the Mn oxide formation experiments (22 °C).

Our initial interpretation of the result is that there must be another abundant oxidant in the system to support the electron flow away from Mn, the first candidate being HEPES buffer. If HEPES was supplying superoxide, for example, like that described in the literature (Grady et al., 1988; Welch et al., 2002; Zhao and Chasteen, 2006), then that might take away from the allosteric hypothesis for the sigmoidal shape of the Mn oxidation kinetics curve because superoxide would oxidize Mn(II) and change the kinetics of the reaction. I repeated the Mn oxidation kinetics experiment, measuring MnO<sub>2</sub> formation by leukoberbelin blue assay in Tris pH 7.8 buffer and observed the same sigmoidal kinetics curve (Appendix B).

HEPES alone is not likely to produce enough oxidant to change the shape of the kinetics curve, but may still influence the measurable O<sub>2</sub> concentrations. Future O<sub>2</sub> consumption experiments with other substrates and buffer (and buffer-free) systems should narrow down the field of potential electron sinks.

### *Mnx structure and mutagenesis*

Determining the course of Mn oxidation will benefit from having structural information about the Mnx complex. Especially useful would be a Mn(II) soaked crystal so Mn binding to discrete residues within the protein could be mapped. Attempts at crystallization over several trials in Amy Rosenzweig's lab (Northwestern University) have not been successful so far, but efforts are ongoing.

In lieu of an experimentally derived structure, we have obtained a model generated by I-TASSER, a software program that predicts the amino acid quaternary structure from the primary sequence by first predicting the higher order structure and threading the structure through the five most similar experimentally-derived structures in the protein database. MnxG was most similar to the human ceruloplasmin crystal structure pdb (protein database) 1kcw. Complicating matter is the domain rearrangement between MnxG and Ceruloplasmin. We have been aware of this since the first MnxG sequence homology in Lorraine Van Waasbergen's work nearly 20 years ago (Van Waasbergen et al., 1996). The Cu binding residues are highly conserved but are in domains two and three instead of one and six in ceruloplasmin. The odd and even domains, however, are structurally conserved so when we look at the trinuclear center of *Bacillus* SG-1 MnxG and highlight all of the His residues thought to be involved, we can see that they are all situated near each other. Fortunately, Cp has an extra type 1 site in



domain two and the accompanying Cu atom is represented in the model so we can explore the region around the type 1 Cu in search of potential substrate binding residues. Preliminary results of Mn oxidation activity of *Bacillus* sp. PL-12 MnxEFG with Ala substitutions at D190 and E279, show decreased activity, suggesting that the model may indeed be a useful tool to investigate the Mn pathway and divergence from Cp. SG-1 His residues 274, 225, 246, and 247 are also type 1 Cu proximal and may assist in Mn binding to the substrate site. MnxE and MnxF do not share significant sequence or structural similarity with any of the structures in the pdb, so we have to wait for the structural information.

#### *MnxEF Cu binding and role in activity*

In Chapter 4, MnxEF was isolated as a heme and Cu containing oligomer. The EPR analyses of the differentially Cu loaded wild type and triple His→ Ala mutant provided valuable information about N binding to Cu but the only evidence of heme binding is the Soret and visible bands in the UV-visible absorption spectrum. This complex will be analyzed by Kelly Chacón of the Blackburn lab at the SLAC national acceleration laboratory by Cu X-ray absorption spectrometry to determine if there are any S bound to the Cu. In future work, it may be informative to run Fe XAS and also determine the relative affinity for Cu by the MnxEF subunits and MnxG to see if MnxEF could play a role in Cu loading of the MCO. From very preliminary crystals grown by Thomas Lawton in Amy Rosenzweig's lab, we could observe a "connectivity map" structure of MnxEF in a trimer (of MnxEF dimers) binding one Cu per dimer subunit. We are hopeful that newly purified, heme loaded MnxEF will allow better crystallization and elucidation of the structure to resolve how MnxEF is binding to MnxG and how Cu and

Fe heme may be oriented over active MCO sites within MnxG and play a role in electron transfer.

#### *Reactivity of Mnx-made Mn oxides*

Mnx is responsible for making Mn oxides that resemble those found on the surface of the *Bacillus* spores. Instead of spiny structures as seen on previous transmission electron micrographs (TEMs) of Mn oxidizing *Bacillus* spp. spores though, the Mn oxides produced by Mnx collapse into layers, some containing large holes that may in fact be artifacts of the sample preparation process (Fig. 1). Although, it is easily interpreted that that the spiny structures in the spore TEMs are just layers of Mn oxide sheets like those made by the protein, templated onto the nap-like exterior of the spore. The differences between the structures of the products of the slow and fast Mn oxidation may extend to the reactivity and absorption properties. The vacancies will most likely improve adsorption and catalytic efficiency. Our collaborators at UC Davis are working towards attaching the enzyme-generated Mn oxides on an electrode to generate H<sub>2</sub>. They are currently optimizing the production of the Mn oxides for the most efficient activity, hoping to surpass that of the abiotic Mn oxides.

#### *Mechanism of Biomineralization of Mn on Mnx*

The structure and composition of emerging Mn oxides from Mnx determines their reactivity and therefore their biological function and environmental impact (Tebo et al., 2004). Mn oxide templating on biological material on the outside of the cell contributes to its final surface area and thus its exposure to solution. The Mn oxides may stick nonspecifically to peptide backbone carboxylates, generating the most surface area. Or they may form as chains leaving MnxG and then assemble into to a more complex

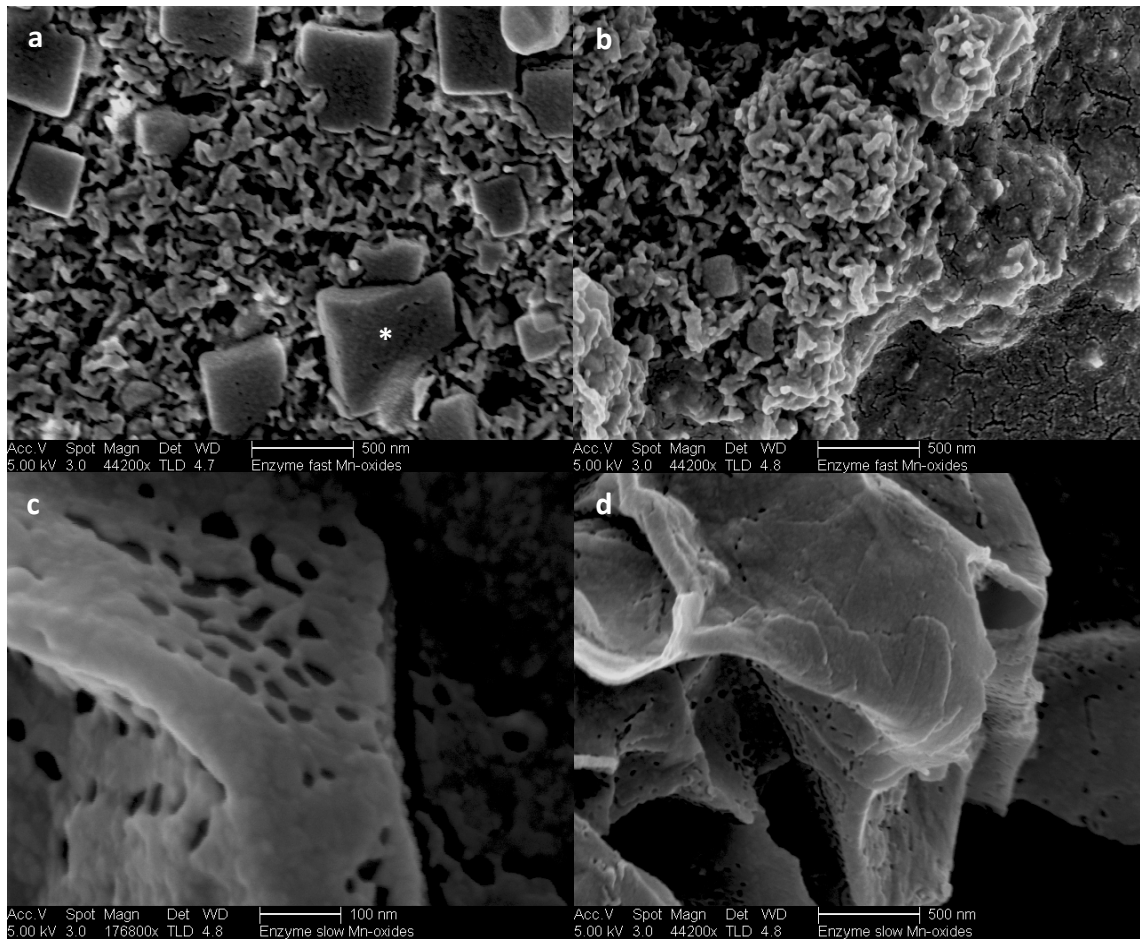


Figure 1. Scanning electron micrograph of Mnx-made Mn oxide minerals. Mnx protein and  $\text{MnCl}_2$  was added to a flask containing HEPES pH 7.8, NaCl buffered solution and allowed to shake overnight. SEM images were obtained of the resulting oxides made with either  $50 \mu\text{g} \cdot \text{L}^{-1}$  (a, b) or  $5 \mu\text{g} \cdot \text{L}^{-1}$  (c, d) Mnx were imaged by Wendy Smythe. \*NaCl crystals formed during desiccation.

superstructure.

Capturing this stage of mineral formation is important with respect to the biological physiology and enzyme mechanism. We will attempt to visualize this process at near-atomic resolution in collaboration with Alice Dohnalkova and Bruce Arey in the microscopy group. The EMSL CRYO 2005 transmission electron microscope has a resolution of 3.1 Å. It will allow us to determine the nanostructure of the oxides in relation to protein surface structure to generate a full picture of what exactly these bacterial enzymes make immediately following mineralization. Depending on the stage of ongoing X-ray crystallographic studies to determine protein structure, we will either use the emerging crystallographic structure or a software-predicted homology model of MnxG (from I-TASSER) (Zhang, 2008; Roy et al., 2010) to fit the protein scaffold into the CryoTEM image which may help localize the site of mineral formation. Localizing the MnO<sub>2</sub> exit point will also provide evidence for where the course of Mn oxidation terminates, completing the mechanism scheme. The Helios and Helium Ion microscopes will provide important 3D information and information about the elemental localization and composition of the samples, in particular Mn.

### *Significance*

The isolation and characterization of the Mn oxidizing complex from *Bacillus* sp. PL-12 has unlocked a piece of hidden bioinorganic chemistry. It has and will continue to broaden our knowledge of the diversity of the natural world specifically that involved in biogeochemistry. There are an abundance of features to investigate within Mnx and many proteins yet to be isolated from other Mn oxidizing organisms lacking the *mnx* gene operon suite. When emphasis is placed on the investigation of a novel problem or

particularly unique process rather than the ubiquitous or trendy, the likelihood for failure and discovery are equal. This work provides inspiration to pick up failed projects with fresh eyes to see where the science goes.

## References

- Anderson, C.R., H.A. Johnson, N. Caputo, R.E. Davis, J.W. Torpey and B.M. Tebo (2009). Mn(II) oxidation is catalyzed by heme peroxidases in "Aurantimonas manganoxydans" strain SI85-9A1 and *Erythrobacter* sp. strain SD-21. *Applied And Environmental Microbiology*. 75: 4130-4138.
- Aronoff-Spencer, E., C.S. Burns, N.I. Avdievich, G.J. Gerfen, J. Peisach, W.E. Antholine, H.L. Ball, F.E. Cohen, S.B. Prusiner and G.L. Millhauser (2000). Identification of the Cu<sup>2+</sup> binding sites in the N-terminal domain of the prion protein by EPR and CD spectroscopy. *Biochemistry*. 39(45): 13760-13771.
- Ba, L.A., M. Doering, T. Burkholz and C. Jacob (2009). Metal trafficking: From maintaining the metal homeostasis to future drug design. *Metallomics*. 1(4): 292-311.
- Bargar, J.R., B.M. Tebo, U. Bergmann, S.M. Webb, P. Glatzel, V.Q. Chiu and M. Villalobos (2005a). Biotic and abiotic products of Mn(II) oxidation by spores of the marine *Bacillus* sp. strain SG-1. *American Mineralogist*. 90: 143-154.
- Bargar, J.R., B.M. Tebo and J.E. Villinski (2000). In situ characterization of Mn(II) oxidation by spores of the marine *Bacillus* sp. strain SG-1. *Geochimica Et Cosmochimica Acta*. 64(16): 2775-2778.
- Bargar, J.R., S.M. Webb and B.M. Tebo (2005b). EXAFS, XANES and in-situ SR-XRD characterization of biogenic manganese oxides produced in sea water. *Physica Scripta T*. T115: 888-890.
- Beck von Bodman, S., M.A. Schuler, D.R. Jollie and S.G. Sligar (1986). Synthesis, bacterial expression, and mutagenesis of the gene coding for mammalian cytochrome b5. *Proceedings of the National Academy of Sciences of the United States of America*. 83(24): 9443-9447.
- Beswick, P.H., G.H. Hall and A.J. Hook (1976). Copper toxicity: evidence for the conversion of cupric to cuprous copper in vivo under anaerobic conditions. *Chemico-Biological Interactions*. 14(3-4): 347-356.
- Butterfield, C.N., A.V. Soldatova, S.W. Lee, T.G. Spiro and B.M. Tebo (2013). Mn(II,III) oxidation and MnO<sub>2</sub> mineralization by an expressed bacterial multicopper oxidase. *Proceedings of the National Academy of Sciences of the United States of America*. 110(29): 11731-11735.
- Butterfield, C.N. and B.M. Tebo (In preparation). Characterization of the Mn(II, III)-oxidizing multicopper oxidase from *Bacillus* sp. PL-12.

- Carvalho, A.S., E.P. Melo, B.S. Ferreira, M.T. Neves-Petersen, S.B. Petersen and M.R. Aires-Barros (2003). Heme and pH-dependent stability of an anionic horseradish peroxidase. *Arch Biochem Biophys.* 415(2): 257-67.
- Cheney, M.A., J.Y. Shin, D.E. Crowley, S. Alvey, N. Malengreau and G. Sposito (1998). Atrazine dealkylation on a manganese oxide surface. *Colloids and Surfaces A: Physicochemical and Engineering Aspects.* 137(1-3): 267-273.
- Cheney, M.A., G. Sposito, A.E. McGrath and R.S. Criddle (1996). Abiotic degradation of 2,4-D (dichlorophenoxyacetic acid) on synthetic birnessite: A calorimetric method. *Colloids and Surfaces A: Physicochemical and Engineering Aspects.* 107: 131-140.
- Chinni, S., C.R. Anderson, K.-U. Ulrich, D.E. Giammar and B.M. Tebo (2008). Indirect  $UO_2$  oxidation by Mn(II)-oxidizing spores of *Bacillus* sp. strain SG-1 and the effect of U and Mn concentrations. *Environmental Science & Technology.* 42: 8709-8714.
- Connor, K.L., K.L. Colabroy and B. Gerratana (2011). A heme peroxidase with a functional role as an l-tyrosine hydroxylase in the biosynthesis of anthramycin. *Biochemistry.* 50(41): 8926-8936.
- Corstjens, P.L.A.M., J.P.M. de Vrind, T. Goosen and E.W. de Vrind-de Jong (1997). Identification and molecular analysis of the *Leptothrix discophora* SS-1 *mofA* gene, a gene putatively encoding a manganese-oxidizing protein with copper domains. *Geomicrobiology Journal.* 14: 91-108.
- Cotruvo, J.A. and J. Stubbe (2010). An Active Dimanganese(III)-Tyrosyl Radical Cofactor in Escherichia coli Class Ib Ribonucleotide Reductase. *Biochemistry.* 49(6): 1297-1309.
- Cowen, J.P. and Y.H. Li (1991). The influence of a changing bacterial community on trace metal scavenging in a deep-sea particle plume. *Journal of Marine Research.* 49: 517-542.
- Cowen, J.P., G.J. Massoth and E.T. Baker (1986). Bacterial scavenging of Mn and Fe in a mid- to far-field hydrothermal particle plume. *Nature.* 322(6075): 169-171.
- Cowen, J.P., G.J. Massoth and R.A. Feely (1990). Scavenging rates of dissolved manganese in a hydrothermal vent plume. *Deep Sea Research Part A, Oceanographic Research Papers.* 37(10): 1619-1637.
- Davis-Kaplan, S.R., C.C. Askwith, A.C. Bengtzen, D. Radisky and J. Kaplan (1998). *Proceedings of the National Academy of Sciences of the United States of America.* 95(23): 13641-13645.

- De Paula, J.C. and G.W. Brudvig (1985). Magnetic properties of manganese in the photosynthetic O<sub>2</sub>- evolving complex. *Journal Of the American Chemical Society*. 107(9): 2643-2648.
- de Silva, D., S. Davis-Kaplan, J. Fergestad and J. Kaplan (1997). Purification and characterization of Fet3 protein, a yeast homologue of ceruloplasmin. *Journal of Biological Chemistry*. 272: 14208-14213.
- Dick, G.J., Y.E. Lee and B.M. Tebo (2006). Manganese(II)-oxidizing *Bacillus* spores in Guaymas basin hydrothermal sediments and plumes. *Applied And Environmental Microbiology*. 72(5): 3184-3190.
- Dick, G.J., J.W. Torpey, T.J. Beveridge and B.M. Tebo (2008). Direct identification of a bacterial manganese(II) oxidase, the multicopper oxidase MnxG, from spores of several different marine *Bacillus* species. *Appl Environ Microbiol*. 74: 1527-1534.
- Dismukes, G.C. (1996). Manganese enzymes with binuclear active sites. *Chemical Reviews*. 96(7): 2909-2926.
- Durão, P., Z. Chen, A.T. Fernandes, P. Hildebrandt, D.H. Murgida, S. Todorovic, M.M. Pereira, E.P. Melo and L.O. Martins (2008). Copper incorporation into recombinant CotA laccase from *Bacillus subtilis*: Characterization of fully copper loaded enzymes. *Journal of Biological Inorganic Chemistry*. 13(2): 183-193.
- Edgar, R. (2004a). MUSCLE: a multiple sequence alignment method with reduced time and space complexity. *BMC Bioinformatics*. 5(1): 1-19.
- Edgar, R.C. (2004b). MUSCLE: multiple sequence alignment with high accuracy and high throughput. *Nucleic Acids Res*. 32(5): 1792-7.
- El Ghazouani, A., A. Baslé, S.J. Firbank, C.W. Knapp, J. Gray, D.W. Graham and C. Dennison (2011). Copper-binding properties and structures of methanobactins from *Methylosinus trichosporium* OB3b. *Inorganic Chemistry*. 50(4): 1378-1391.
- Elias, J.E. and S.P. Gygi (2007). Target-decoy search strategy for increased confidence in large-scale protein identifications by mass spectrometry. *Nature Methods*. 4(3): 207-214.
- Ertan, H., K.S. Siddiqui, J. Muenchhoff, T. Charlton and R. Cavicchioli (2012). Kinetic and thermodynamic characterization of the functional properties of a hybrid versatile peroxidase using isothermal titration calorimetry: Insight into manganese peroxidase activation and lignin peroxidase inhibition. *Biochimie*. 94(5): 1221-1231.
- Fendorf, S.E. and R.J. Zasoski (1992). Chromium(III) oxidation by  $\delta$ -MnO<sub>2</sub>. 1. Characterization. *Environmental Science and Technology*. 26(1): 79-85.



- Francis, C.A., K.L. Casciotti and B.M. Tebo (2002). Localization of Mn(II)-oxidizing activity and the putative multicopper oxidase, MnxG, to the exosporium of the marine *Bacillus* sp. strain SG-1. *Archives of Microbiology*. 178: 450-456.
- Francis, C.A. and B.M. Tebo (2002). Enzymatic manganese(II) oxidation by metabolically-dormant spores of diverse *Bacillus* species. *Applied And Environmental Microbiology*. 68: 874-880.
- Fredrickson, J.K., J.M. Zachara, D.W. Kennedy, C. Liu, M.C. Duff, D.B. Hunter and A. Dohnalkova (2002). *Geochimica et Cosmochimica Acta*. 66(18): 3247-3262.
- Gaillot, A.C., D. Flot, V.A. Drits, A. Manceau, M. Burghammer and B. Lanson (2003). Structure of Synthetic K-rich Birnessite Obtained by High-Temperature Decomposition of KMnO<sub>4</sub>. I. Two-Layer Polytype from 800 °C Experiment. *Chemistry of Materials*. 15(24): 4666-4678.
- Geszvain, K., J.K. McCarthy and B.M. Tebo (2013). Elimination of manganese(II, III) oxidation in *Pseudomonas putida* GB-1 by a double knockout of two putative multicopper oxidase genes. *Applied And Environmental Microbiology*. 79(1): 357-366.
- Ghanotakis, D.F., G.T. Babcock and C.F. Yocum (1984). Calcium reconstitutes high rates of oxygen evolution in polypeptide depleted Photosystem II preparations. *FEBS Letters*. 167(1): 127-130.
- Glenn, J.K., L. Akileswaran and M.H. Gold (1986). Mn(II) oxidation is the principal function of the extracellular Mn-peroxidase from *Phanerochaete chrysosporium*. *Archives of Biochemistry and Biophysics*. 251(2): 688-696.
- Goldberg, E.D. (1954). Marine geochemistry I. Chemical scavengers of the sea. *Journal of Geology*. 62: 249-265.
- Grady, J.K., N.D. Chasteen and D.C. Harris (1988). Radicals from 'Good's' buffers. *Analytical Biochemistry*. 173(1): 111-115.
- Grass, G. and C. Rensing (2001). CueO is a multi-copper oxidase that confers copper tolerance in *Escherichia coli*. *Biochemical and Biophysical Research Communications*. 286(5): 902-8.
- Gray, H.B., B.G. Malmström and R.J.P. Williams (2000). Copper coordination in blue proteins. *Journal of Biological Inorganic Chemistry*. 5(5): 551-559.
- Hansel, C.M. and C.A. Francis (2006). Coupled photochemical and enzymatic Mn(II) oxidation pathways of a planktonic *Roseobacter*-like bacterium. *Applied And Environmental Microbiology*. 72: 3543-3549.

- Hansel, C.M., C.A. Zeiner, C.M. Santelli and S.M. Webb (2012). Mn(II) oxidation by an ascomycete fungus is linked to superoxide production during asexual reproduction. *Proc Natl Acad Sci U S A*. 109(31): 12621-5.
- Hassett, R.F., D.S. Yuan and D.J. Kosman (1998). Spectral and kinetic properties of the Fet3 protein from *Saccharomyces cerevisiae*, a multinuclear copper ferroxidase. *Journal of Biological Chemistry*. 273: 23274-23282.
- Hastings, D. and S. Emerson (1986). Oxidation of manganese by spores of a marine bacillus: Kinetic and thermodynamic considerations. *Geochimica Et Cosmochimica Acta*. 50(8): 1819-1824.
- Höfer, C. and D. Schlosser (1999). Novel enzymatic oxidation of Mn<sup>2+</sup> to Mn<sup>3+</sup> catalyzed by a fungal laccase. *FEBS Letters*. 451(2): 186-190.
- Honarmand Ebrahimi, K., E. Bill, P.L. Hagedoorn and W.R. Hagen (2012). The catalytic center of ferritin regulates iron storage via Fe(II)-Fe(III) displacement. *Nature Chemical Biology*. 8(11): 941-948.
- Horsburgh, M.J., S.J. Wharton, M. Karavolos and S.J. Foster (2002). Manganese: elemental defence for a life with oxygen. *Trends in Microbiology*. 10(11): 496-501.
- Huang, P.M. (1991). Kinetics of redox reactions on manganese oxides and its impact on environmental quality. In: D.L. Sparks and D.L. Suarez (eds.), Rates of Soil Chemical Processes, Soil Science Society of America, Inc., Madison, p.191-230.
- Hullo, M.F., I. Moszer, A. Danchin and I. Martin-Verstraete (2001). CotA of *Bacillus subtilis* is a copper-dependent laccase. *Journal Of Bacteriology*. 183(18): 5426-5430.
- Kailas, L., C. Terry, N. Abbott, R. Taylor, N. Mullin, S.B. Tzokov, S.J. Todd, B.A. Wallace, J.K. Hobbs, A. Moir and P.A. Bullough (2011). Surface architecture of endospores of the *Bacillus cereus*/anthracis/*thuringiensis* family at the subnanometer scale. *Proceedings of the National Academy of Sciences*. 108(38): 16014-16019.
- Kataoka, K., H. Komori, Y. Ueki, Y. Konno, Y. Kamitaka, S. Kurose, S. Tsujimura, Y. Higuchi, K. Kano, D. Seo and T. Sakurai (2007). Structure and Function of the Engineered Multicopper Oxidase CueO from *Escherichia coli*-Deletion of the Methionine-Rich Helical Region Covering the Substrate-Binding Site. *Journal of Molecular Biology*. 373(1): 141-152.
- Kim, J. and W. Schumann (2009). Display of proteins on *Bacillus subtilis* endospores. *Cellular and Molecular Life Sciences*. 66(19): 3127-3136.
- Kirby, J.A., A.S. Robertson, J.P. Smith, A.C. Thompson, S.R. Cooper and M.P. Klein (1981). State of manganese in the photosynthetic apparatus. 1. Extended X-ray absorption

- fine structure studies on chloroplasts and di- $\mu$ -oxo-bridged dimanganese model compounds. *Journal of the American Chemical Society*. 103(18): 5529-5537.
- Klewicki, J.K. and J.J. Morgan (1998). Kinetic behavior of Mn(III) complexes of pyrophosphate, EDTA, and citrate. *Environmental Science & Technology*. 32(19): 2916-2922.
- Klewicki, J.K. and J.J. Morgan (1999). Dissolution of  $\beta$ -MnOOH particles by ligands: Pyrophosphate, ethylenediaminetetraacetate, and citrate. *Geochimica Et Cosmochimica Acta*. 63(19-20): 3017-3024.
- Koschorreck, K., S.M. Richter, A.B. Ene, E. Roduner, R.D. Schmid and V.B. Urlacher (2008). Cloning and characterization of a new laccase from *Bacillus licheniformis* catalyzing dimerization of phenolic acids. *Applied Microbiology and Biotechnology*. 79(2): 217-224.
- Kostka, J.E., G.W. Luther III and K.H. Nealson (1995). Chemical and biological reduction of Mn (III)-pyrophosphate complexes: Potential importance of dissolved Mn (III) as an environmental oxidant. *Geochimica Et Cosmochimica Acta*. 59(5): 885-894.
- Laha, S. and R.G. Luthy (1990). Oxidation of aniline and other primary aromatic amines by manganese dioxide. *Environmental Science and Technology*. 24: 363-373.
- Lee, Y. (1994). Microbial Oxidation of Cobalt: Characterization and Its Significance in Marine Environments. Ph.D. Dissertation, University of California, San Diego, 159 pp.
- Lehmann, R.G., H.H. Cheng and J.B. Harsh (1987). Oxidation of phenolic acids by soil iron and manganese oxides. *Soil Science Society of America Journal*. 51(2): 352-356.
- Lin, K., W. Liu and J. Gan (2009). Oxidative removal of bisphenol A by manganese dioxide: Efficacy, products, and pathways. *Environmental Science and Technology*. 43(10): 3860-3864.
- Lindley, P.F., G. Card, I. Zaitseva, V. Zaitsev, B. Reinhammar, E. Selin-Lindgren and K. Yoshida (1997). An X-ray structural study of human ceruloplasmin in relation to ferroxidase activity. *Journal of Biological Inorganic Chemistry*. 2(4): 454-463.
- Lippard, S.J. and J.M. Berg (1994). Principles of Bioinorganic Chemistry. Mill Valley, CA, USA, University Science Books.
- Londer, Y. Y. (2011). Expression of recombinant cytochromes c in *E. coli*. *Methods Mol Biol*. 705: 123-150.
- Luther III, G.W., D.T. Ruppel and C. Burkhard (1998). Reactivity of dissolved Mn(III) complexes and Mn(IV) species with reductants: Mn redox chemistry without a

dissolution step. Ch 13. In: D.L. Sparks and T.J. Grundl (eds.), *Mineral-Water Interfacial Reactions: Kinetics and Mechanisms*, ACS Symposium Series, 715, American Chemical Society, Washington, D.C., p.265-280.

Luthra, A., I.G. Denisov and S.G. Sligar (2011). Spectroscopic features of cytochrome P450 reaction intermediates. *Archives of Biochemistry and Biophysics*. 507(1): 26-35.

Manceau, A. and L. Charlet (1992). X-ray absorption spectroscopic study of the sorption of Cr(III) at the oxide-water interface. I. Molecular mechanism of Cr(III) oxidation on Mn oxides. *Journal of Colloid and Interface Science*. 148(2): 425-442.

Manceau, A., M.A. Marcus, N. Tamura, O. Proux, N. Geoffroy and B. Lanson (2004). Natural speciation of Zn at the micrometer scale in a clayey soil using X-ray fluorescence, absorption, and diffraction. *Geochimica et Cosmochimica Acta*. 68(11): 2467-2483.

Martins, L.O., C.M. Soares, M.M. Pereira, M. Teixeira, T. Costa, G.H. Jones and A.O. Henriques (2002). Molecular and biochemical characterization of a highly stable bacterial laccase that occurs as a structural component of the *Bacillus subtilis* endospore coat. *J Biol Chem*. 277(21): 18849-59.

MARUM, U.o.B., and NOAA-Pacific Marine Environmental Laboratory (2012). Close up view of orange iron-oxide microbial mat overlying black manganese-oxide encrusted mat. 2014:

Mauk, M.R., K. Kishi, M.H. Gold and A.G. Mauk (1998). pH-linked binding of Mn(II) to manganese peroxidase. *Biochemistry*. 37(19): 6767-6771.

Miyao, M. and N. Murata (1984). Calcium ions can be substituted for the 24-kDa polypeptide in photosynthetic oxygen evolution. *FEBS Letters*. 168(1): 118-120.

Moeller, R., A.C. Schuerger, G. Reitz and W.L. Nicholson (2012). Protective Role of Spore Structural Components in Determining *Bacillus subtilis* Spore Resistance to Simulated Mars Surface Conditions. *Applied and Environmental Microbiology*. 78(24): 8849-8853.

Morgan, J.J. (2000). Manganese in natural waters and earth's crust: Its availability to organisms. In: A. Sigel and H. Sigel (eds.), *Metal Ions in Biological Systems*. Vol. 37 *Manganese and Its Role in Biological Processes*, Marcel Dekker, New York, p.1-33.

Murray, K.J. and B.M. Tebo (2007). Cr(III) is indirectly oxidized by the Mn(II)-oxidizing bacterium *Bacillus* sp. strain SG-1. *Environmental Science and Technology*. 41(2): 528-533.

- Murray, K.J., S.M. Webb, J.R. Bargar and B.M. Tebo (2007). Indirect oxidation of Co(II) in the presence of the marine Mn(II)-oxidizing bacterium *Bacillus* sp. strain SG-1. *Applied And Environmental Microbiology*. 73(21): 6905-6909.
- Musci, G., M.C. Bonaccorsi Di Patti and L. Calabrese (1993). The state of the copper sites in human ceruloplasmin. *Archives of Biochemistry and Biophysics*. 306(1): 111-118.
- Musci, G., M.C.B. di Patti, R. Petruzzelli, A. Giartosio and L. Calabrese (1996). Divalent cation binding to ceruloplasmin. *BioMetals*. 9: 66-72.
- Nasser, A., G. Sposito and M.A. Cheney (2000). Mechanochemical degradation of 2,4-D adsorbed on synthetic birnessite. *Colloids and Surfaces A: Physicochemical and Engineering Aspects*. 163(2-3): 117-123.
- Nealson, K.H. (1978). The isolation and characterization of marine bacteria which catalyze manganese oxidation. In: W.E. Krumbein (ed.) *Environmental Biogeochemistry and Geomicrobiology Volume 3: Methods, Metals and Assessment*, Ann Arbor Science Publishers Inc., Ann Arbor, MI, p.847-858.
- Osaki, S. (1966). Kinetic studies of ferrous ion oxidation with crystalline human ferroxidase (ceruloplasmin). *Journal of Biological Chemistry*. 241(21): 5053-5059.
- Outten, F.W., D.L. Huffman, J.A. Hale and T.V. O'Halloran (2001). The Independent cue and cus Systems Confer Copper Tolerance during Aerobic and Anaerobic Growth in *Escherichia coli*. *Journal of Biological Chemistry*. 276(33): 30670-30677.
- Park, J.W., J. Dec, J.E. Kim and J.M. Bollag (1999). Effect of humic constituents on the transformation of chlorinated phenols and anilines in the presence of oxidoreductive enzymes or birnessite. *Environmental Science and Technology*. 33(12): 2028-2034.
- Parker, D.L., G. Sposito and B.M. Tebo (2004). Manganese(III) binding to a pyoverdine siderophore produced by a manganese(II)-oxidizing bacterium. *Geochimica et Cosmochimica Acta*. 68: 4809-4820.
- Perez, J. and T.W. Jeffries (1992). Roles of manganese and organic acid chelators in regulating lignin degradation and biosynthesis of peroxidases by *Phanerochaete chrysosporium*. *Applied And Environmental Microbiology*. 58(8): 2402-2409.
- Pezeshk, A., J. Torres, M.T. Wilson and M.C.R. Symons (2001). The EPR spectrum for CuB in cytochrome c oxidase. *Journal of Inorganic Biochemistry*. 83(2-3): 115-119.
- Post, J.E. (1999). Manganese oxide minerals: Crystal structures and economic and environmental significance. *Proceedings of the National Academy of Sciences*. 96(7): 3447-3454.

- Prasad, V.S. and M. Chaudhuri (1995). Removal of bacteria and turbidity from water by chemically treated manganese and iron ores. *Aqua London*. 44(2): 80-82.
- Ravel, B. and M. Newville (2005). ATHENA, ARTEMIS, HEPHAESTUS: Data analysis for X-ray absorption spectroscopy using IFEFFIT. *Journal of Synchrotron Radiation*. 12(4): 537-541.
- Reiss, R., J. Ihssen, M. Richter, E. Eichhorn, B. Schilling and L. Thöny-Meyer (2013). Laccase versus Laccase-Like Multi-Copper Oxidase: A Comparative Study of Similar Enzymes with Diverse Substrate Spectra. *PLoS ONE*. 8(6):
- Reiss, R., J. Ihssen and L. Thony-Meyer (2011). *Bacillus pumilus* laccase: a heat stable enzyme with a wide substrate spectrum. *BMC Biotechnol*. 11: 9.
- Richardson, L.L., C. Aguilar and K.H. Nealson (1988). Manganese oxidation in pH and O<sub>2</sub> microenvironments produced by phytoplankton. *Limnology & Oceanography*. 33(3): 352-363.
- Ridge, J.P., M. Lin, E.I. Larsen, M. Fegan, A.G. McEwan and L.I. Sly (2007a). A multicopper oxidase is essential for manganese oxidation and laccase-like activity in *Pedomicrobium* sp. ACM 3067. *Environ Microbiol*. 9(4): 944-953.
- Ridge, J.P., M. Lin, E.I. Larsen, M. Fegan, A.G. McEwan and L.I. Sly (2007b). A multicopper oxidase is essential for manganese oxidation and laccase-like activity in *Pedomicrobium* sp. ACM 3067. *Environmental Microbiology*. 9(4): 944-953.
- Roberts, S.A., G.F. Wildner, G. Grass, A. Weichsel, A. Ambrus, C. Rensing and W.R. Montfort (2003). A labile regulatory copper ion lies near the T1 copper site in the multicopper oxidase CueO. *Journal of Biological Chemistry*. 278(34): 31958-31963.
- Rosson, R.A. and K.H. Nealson (1982). Manganese binding and oxidation by spores of a marine bacillus. *Journal Of Bacteriology*. 151: 1027-1034.
- Roy, A., A. Kucukural and Y. Zhang (2010). I-TASSER: a unified platform for automated protein structure and function prediction. *Nature protocols*. 5(4): 725-738.
- Sakurai, T. and K. Kataoka (2007). Basic and applied features of multicopper oxidases, cueo, bilirubin oxidase, and laccase. *Chemical Record*. 7(4): 220-229.
- Schlosser, D. and C. Höfer (2002). Laccase-catalyzed oxidation of Mn<sup>2+</sup> in the presence of natural Mn<sup>3+</sup> chelators as a novel source of extracellular H<sub>2</sub>O<sub>2</sub> production and its impact on manganese peroxidase. *Applied and Environmental Microbiology*. 68(7): 3514-3521.

- Scott, M.J. and J.J. Morgan (1996). Reactions at oxide surfaces. 2. Oxidation of Se(IV) by synthetic birnessite. *Environmental Science and Technology*. 30(6): 1990-1996.
- Sedlak, E. and P. Wittung-Stafshede (2007). Discrete roles of copper ions in chemical unfolding of human ceruloplasmin. *Biochemistry*. 46(33): 9638-9644.
- Shulman, R.G., P. Eisenberger, W.E. Blumberg and N.A. Stombaugh (1975). Determination of the iron-sulfur distances in rubredoxin by x-ray absorption spectroscopy. *Proceedings of the National Academy of Sciences*. 72(10): 4003-4007.
- Soldatova, A., C. Butterfield, O. Oyerinde, B. Tebo and T. Spiro (2012). Multicopper oxidase involvement in both Mn(II) and Mn(III) oxidation during bacterial formation of MnO<sub>2</sub>. *Journal of Biological Inorganic Chemistry*. 17(8): 1151-1158.
- Solomon, E.I., D.E. Heppner, E.M. Johnston, J.W. Ginsbach, J. Cirera, M. Qayyum, M.T. Kieber-Emmons, C.H. Kjaergaard, R.G. Hadt and L. Tian (2014). Copper active sites in biology. *Chemical Reviews*. 114(7): 3659-3853.
- Solomon, E.I., U.M. Sundaram and T.E. Machonkin (1996). Multicopper oxidases and oxygenases. *Chemical Reviews*. 96(7): 2563-2605.
- Solomon, E.I., R.K. Szilagyi, S. DeBeer George and L. Basumallick (2004). Electronic Structures of Metal Sites in Proteins and Models: Contributions to Function in Blue Copper Proteins. *Chemical Reviews*. 104(2): 419-458.
- Stoj, C.S., A.J. Augustine, L. Zeigler, E.I. Solomon and D.J. Kosman (2006). *Biochemistry*. 45(42): 12741-12749.
- Stoll, S. and A. Schweiger (2006). EasySpin, a comprehensive software package for spectral simulation and analysis in EPR. *Journal of Magnetic Resonance*. 178(1): 42-55.
- Stone, A.T. (1987a). Microbial metabolites and the reductive dissolution of manganese oxides: oxalate and pyruvate. *Geochimica et Cosmochimica Acta*. 51: 919-925.
- Stone, A.T. (1987b). Reductive dissolution of manganese(III/IV) oxides by substituted phenols. *Environmental Science and Technology*. 21(10): 979-988.
- Stone, A.T. and J.J. Morgan (1984a). Reduction and dissolution of manganese(III) and manganese(IV) oxides by organics. 1. Reaction with hydroquinone. *Environmental Science and Technology*. 18(6): 450-456.
- Stone, A.T. and J.J. Morgan (1984b). Reduction and dissolution of manganese(III) and manganese(IV) oxides by organics: 2. Survey of the reactivity of organics. *Environmental Science and Technology*. 18(8): 617-624.

- Sunda, W.G. and D.J. Kieber (1994). Oxidation of humic substances by manganese oxides yields low-molecular-weight organic substrates. *Nature*. 367(6458): 62-64.
- Tebo, B.M., J.R. Bargar, B.G. Clement, G.J. Dick, K.J. Murray, D. Parker, R. Verity and S.M. Webb (2004). Biogenic manganese oxides: Properties and mechanisms of formation. *Annual Review of Earth and Planetary Sciences*. 32: 287-328.
- Tebo, B.M., K. Geszvain and S.-W. Lee (2010). The molecular geomicrobiology of bacterial manganese(II) oxidation. In: L. Barton, M. Mandl and A. Loy (eds.), *Geomicrobiology: Molecular and Environmental Perspective*, Springer, p.285-308.
- Templeton, A.S., H. Staudigel and B.M. Tebo (2005). Diverse Mn(II) oxidizing bacteria isolated from submarine basalts at Loihi Seamount. *Geomicrobiology Journal*. 22: 127-139.
- Todd, J.F., R.J. Elsingher and W.S. Moore (1988a). The distributions of uranium, radium and thorium isotopes in two anoxic fjords, Framvaren Fjord (Norway) and Saanich Inlet (British Columbia). *Marine Chemistry*. 23: 393-415.
- Todd, J.F., R.J. Elsingher and W.S. Moore (1988b). The distributions of uranium, radium and thorium isotopes in two anoxic fjords: Framvaren Fjord (Norway) and Saanich Inlet (British Columbia). *Marine Chemistry*. 23(3-4): 393-415.
- Towler, P.H., J.D. Smith and D.R. Dixon (1996). Magnetic recovery of radium, lead and polonium from seawater samples after preconcentration on a magnetic adsorbent of manganese dioxide coated magnetite. *Analytica Chimica Acta*. 328(1): 53-59.
- Toyoda, K. and B.M. Tebo (2013). The effect of Ca<sup>2+</sup> ions and ionic strength on Mn(II) oxidation by spores of the marine *Bacillus* sp. SG-1. *Geochimica Et Cosmochimica Acta*. 101(0): 1-11.
- Turekian, K.K. and K.H. Wedepohl (1961). Distribution of the elements in some major units of the earth's crust. *Bulletin of the Geological Society of America*. 72(2): 175-192.
- Ulrich, H.J. and A.T. Stone (1989). Oxidation of chlorophenols adsorbed to manganese oxide surfaces. *Environmental Science and Technology*. 23(4): 421-428.
- Vallee, B.L. and R.J. Williams (1968). Metalloenzymes: the entatic nature of their active sites. *Proceedings of the National Academy of Sciences of the United States of America*. 59(2): 498-505.
- Van Waasbergen, L.G., M. Hildebrand and B.M. Tebo (1996). Identification and characterization of a gene cluster involved in manganese oxidation by spores of the marine *Bacillus* sp. strain SG-1. *Journal Of Bacteriology*. 178(12): 3517-3530.

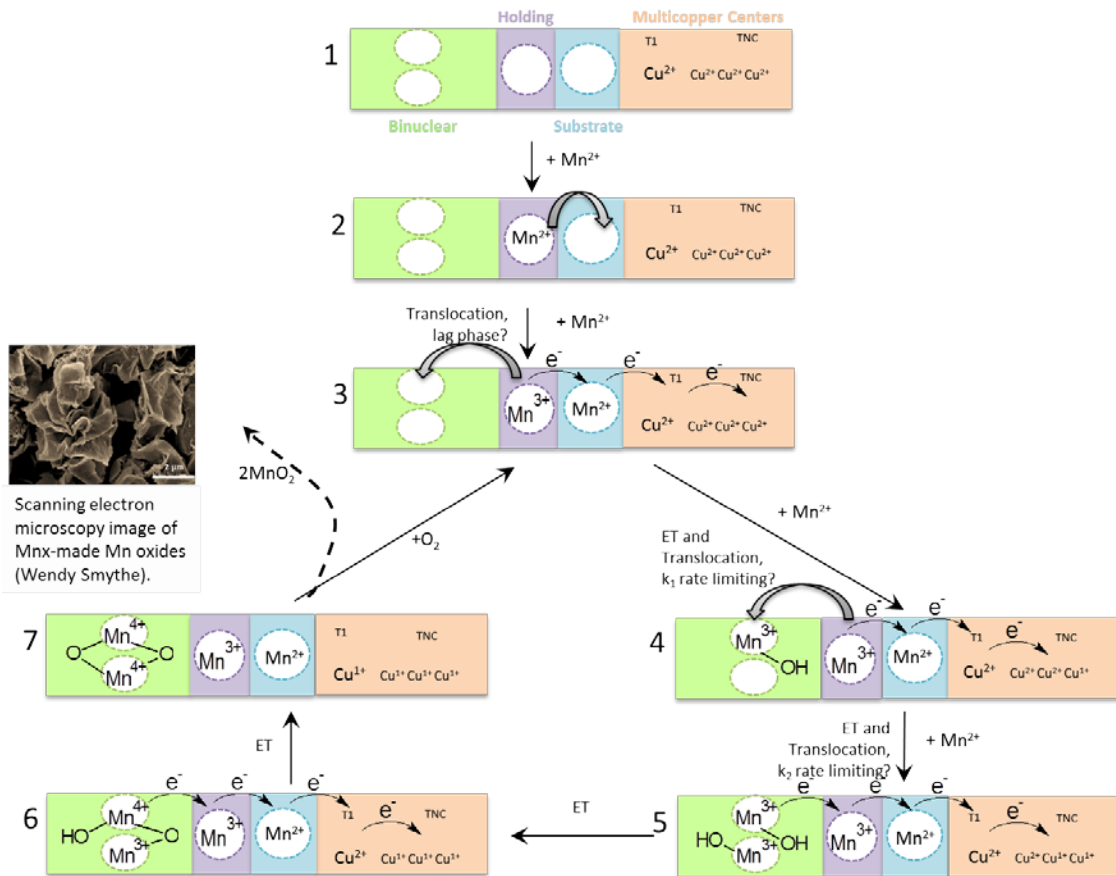


- Van Waasbergen, L.G., J.A. Hoch and B.M. Tebo (1993). Genetic analysis of the marine manganese-oxidizing *Bacillus* sp. strain SG- 1: Protoplast transformation, Tn917 mutagenesis, and identification of chromosomal loci involved in manganese oxidation. *Journal Of Bacteriology*. 175(23): 7594-7603.
- Villalobos, M., B. Toner, J. Bargar and G. Sposito (2003). Characterization of the manganese oxide produced by *Pseudomonas putida* strain MnB1. *Geochimica et Cosmochimica Acta*. 67(14): 2649-2662.
- Webb, S.M., G.J. Dick, J.R. Bargar and B.M. Tebo (2005a). Evidence for the presence of Mn(III) intermediates in the bacterial oxidation of Mn(II). *Proceedings of the National Academy of Sciences of the United States of America*. 102(15): 5558-5563.
- Webb, S.M., B.M. Tebo and J.R. Bargar (2005b). Structural characterization of biogenic Mn oxides produced in seawater by the marine bacillus sp. strain SG-1. *American Mineralogist*. 90(8-9): 1342-1357.
- Webb, S.M., B.M. Tebo and J.R. Bargar (2005c). Structural influences of sodium and calcium ions on the biogenic manganese oxides produced by the marine *Bacillus* sp., strain SG-1. *Geomicrobiology Journal*. 22: 181-193.
- Wei, C.-L. and J.W. Murray (1991).  $^{234}\text{Th}/^{238}\text{U}$  disequilibria in the Black Sea. *Deep-Sea Research*. 38(Suppl. 2): S855-S873.
- Welch, K.D., T.Z. Davis and S.D. Aust (2002). Iron autoxidation and free radical generation: Effects of buffers, ligands, and chelators. *Archives of Biochemistry and Biophysics*. 397(2): 360-369.
- Xiao, Z. and A.G. Wedd (2011). Metallo-oxidase enzymes: Design of their active sites. *Australian Journal of Chemistry*. 64(3): 231-238.
- Zhang, Y. (2008). I-TASSER server for protein 3D structure prediction. *BMC Bioinformatics*. 9:
- Zhao, G. and N.D. Chasteen (2006). Oxidation of Good's buffers by hydrogen peroxide. *Analytical Biochemistry*. 349(2): 262-267.
- Ziegler, L., A. Terzulli, R. Gaur, R. McCarthy and D.J. Kosman (2011). Functional characterization of the ferroxidase, permease high-affinity iron transport complex from *Candida albicans*. *Molecular Microbiology*. 81(2): 473-485.

## Appendices

### Appendix A. A model of Mn oxide formation by the Mnx complex

This detailed model is intended to hypothesize the mechanism behind the lag phase of the time trials and the allosteric sigmoidal trend of the kinetics analyses.

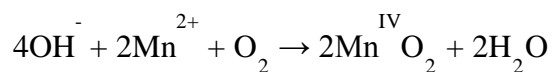


1) Mnx is loaded with reduced  $Mn^{2+}$  at the holding site and 2) translocated to the substrate site. 3) The  $Mn^{2+}$  in the substrate site is oxidized by the MCO and the  $Mn^{3+}$  produced in turn oxidizes the next  $Mn^{2+}$  entering the holding site. 4) As the third  $Mn^{2+}$  enters, the holding site  $Mn^{3+}$  is translocated to the binuclear site. The third  $Mn^{2+}$  in the holding site is oxidized by  $Mn^{3+}$  in the MCO generated the substrate site and is translocated to the binuclear site. 5) The fourth  $Mn^{2+}$  enters the holding site, gets oxidized

to  $\text{Mn}^{3+}$ , thus completing a wire that connects electron transfer (ET) from the binuclear  $\text{Mn}^{3+}$ , through the holding and substrate Mn, to the MCO. 6) Hydroxy- and oxo-bridging in the binuclear site facilitates the oxidation of the binuclear  $\text{Mn}^{3+}$  to  $\text{Mn}^{4+}$ . 7)  $\text{Mn}^{4+}$  is then released by another process as colloidal  $\text{MnO}_2$  that aggregate into minerals as shown in the SEM by Wendy Smythe. The binuclear site is now empty and ready for incoming  $\text{Mn}^{3+}$  from the holding site and for the cycle to start again. Loading the substrate and holding sites with  $\text{Mn}^{2+}$  and  $\text{Mn}^{3+}$  (Steps 1-3) may account for the lag time seen in the  $\text{O}_2$  consumption assays. The translocation events of  $\text{Mn}^{3+}$  into the binuclear site may account for the two apparent kinetic rates within the allosteric sigmoidal trend (Steps 4-7). The first entry of  $\text{Mn}^{3+}$  into the empty binuclear site may be less thermodynamically favorable than the second, meaning the second event would be cooperative. Cooperative metal binding events are abundant in nature and may be present in this system as well.

## Appendix B. Mn oxidation kinetics by Clark type electrode

The mechanism of Mn oxidation within Mn<sub>x</sub> is a central concern of this project. To scratch the surface of this question, we investigated the reaction stoichiometry of the elements involved. First, we predict Mn(II) and Mn(III) oxidation will proceed through hydroxide bridging. Then, oxidant is provided by O<sub>2</sub> reduction in the MCO to yield the overall reaction.



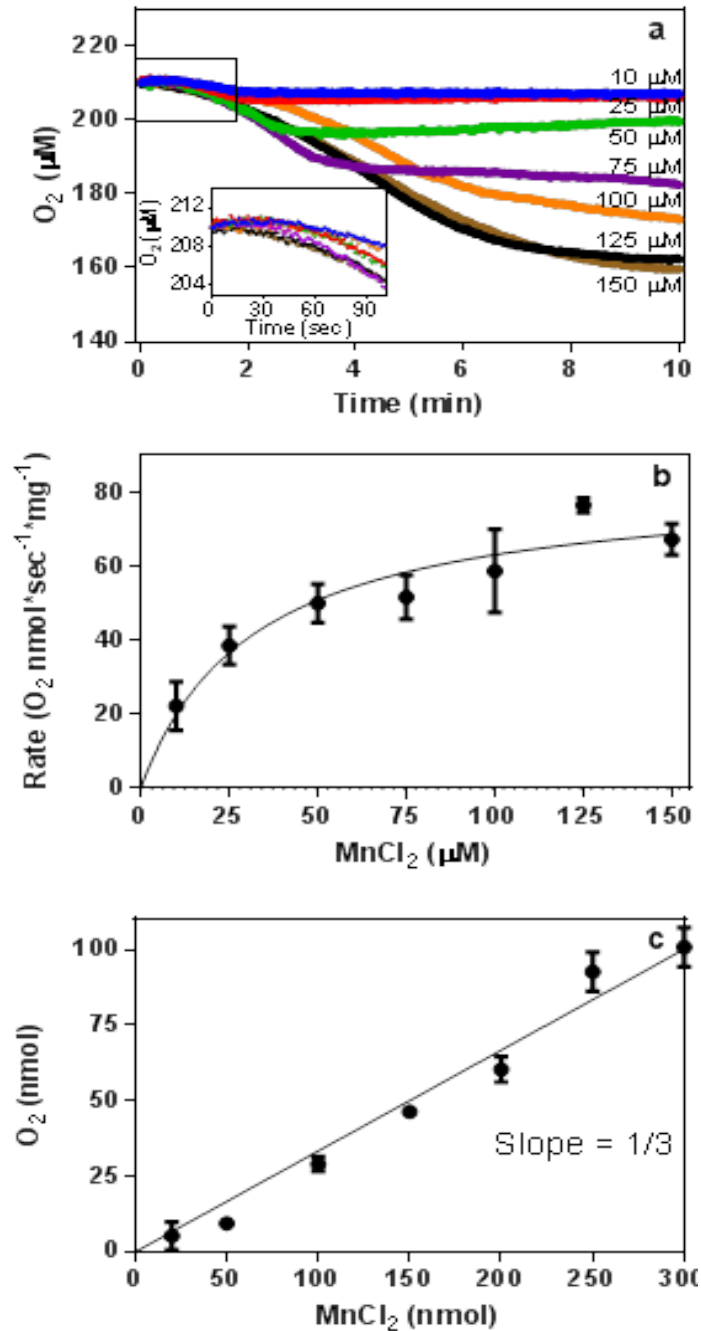


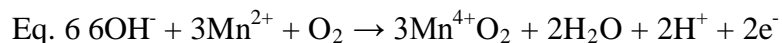
Figure 2. Oxygen consumption by Mn oxidation. a. Representative runs of  $O_2$  consumption by Mn oxidation with HEPES-dialyzed Mn and varying concentrations of  $\text{MnCl}_2$  added at  $t = 0$  (blue 50  $\mu\text{M}$ , red 100  $\mu\text{M}$ , green 200  $\mu\text{M}$ , and black no enzyme). Inset shows first 90 s to highlight the consistent lag time of about 30 s in  $O_2$  consumption. b. Initial velocities of every run are plotted against starting Mn(II) concentration. c. Total  $O_2$  consumed is plotted against starting Mn(II) concentration and fit with linear regression, forced through the origin.

Oxygen consumption was measured on a Rank Brothers LTD model 10 electrode with the polarizing voltage set to 630 mV. The 2 ml water-jacketed reaction cell was kept at 37 °C using a water bath. The instrument was calibrated by taking a zero measurement with Ar purged water and a 100% measurement with atmospheric oxygenated water assuming 214  $\mu\text{M}$   $\text{O}_2$  at 37 °C. A computer interfaced with the electrode measured  $\text{O}_2$  every 1 s. Data collection began about 1 min before 10  $\mu\text{L}$  of 1 mg/ml Mnx protein ( $\sim 24$  nM final if Mnx mass is 211 kDa) was added through the 2 mm diameter opening in the cap and allowed to equilibrate with 37 °C 20 mM HEPES pH 7.8 50 mM NaCl. Another minute of baseline reading was taken before adding 10  $\mu\text{L}$  of various concentrations of  $\text{MnCl}_2$ . The data was plotted time (min) vs. %  $\text{O}_2$  remaining, with the addition of  $\text{MnCl}_2$  as  $t = 0$  min (Fig. 2a). The data recording before  $t = 0$  is flat so it was excluded for simplicity. The initial, linear  $\text{O}_2$  consumption velocities, or slopes, of all runs were plotted against starting  $\text{MnCl}_2$  concentration, typical of kinetics curve plotting (Fig. 2b). Total  $\text{O}_2$  consumed was calculated by taking the difference of final (or minimum  $\text{O}_2$  concentration of the run just after the major consumption event) from initial  $\text{O}_2$  concentrations then plotted against  $\text{MnCl}_2$  concentration and fitted with a linear regression, forced through the x, y origin otherwise the y-intercept is negative which is impossible for this reaction (Fig. 2c). Mnx consumes  $\text{O}_2$  during Mn oxidation. Also indicative of MCOs is the consumption of  $\text{O}_2$  and its reduction to  $\text{H}_2\text{O}$ , terminating electron transfer at the trinuclear Cu center. We measured  $\text{O}_2$  consumption on a Clark type electrode during Mn oxidation by Mnx.

Following the addition of  $\text{MnCl}_2$  to enzyme complex, there is about a 30 s lag time before  $\text{O}_2$  consumption is detected across all runs (Fig 2a). As the  $\text{MnCl}_2$

concentration increased, the initial velocities of O<sub>2</sub> consumption also increased (Fig 2b). The plot of MnCl<sub>2</sub> added vs. O<sub>2</sub> consumed reveals a linear trend with a slope of about 0.252 ± 0.0149 meaning that for every 3 μmol Mn added 1 μmol O<sub>2</sub> is consumed (Fig 2c).

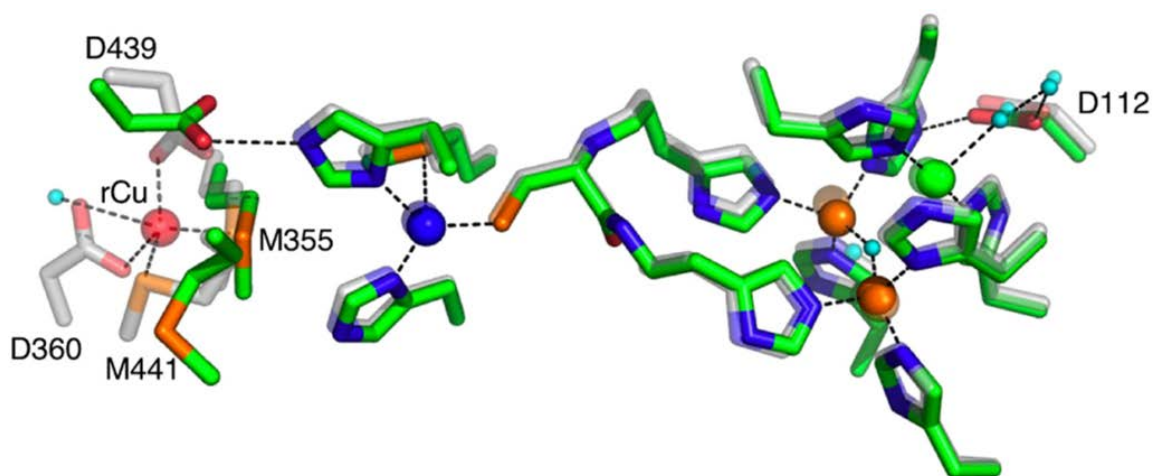
Puzzlingly, the experimental reaction stoichiometry of the Mn oxidation endpoint values presented here does not align fully to this scheme. 3Mn<sup>2+</sup> instead of 2Mn<sup>2+</sup> is required for the reduction of 1O<sub>2</sub>, yielding an unbalanced reaction (Eq. 6).



Clearly, there is a missing oxidant from this reaction. The mystery is whether the reduction occurs within the protein independent of the MCO mechanism or in solution. It is possible that Mn(II) is oxidized by emerging, newly formed MnO<sub>2</sub> oxides, tilting the reaction stoichiometry in favor of more Mn over O<sub>2</sub> consumption. If the reduction occurs within the protein, there may be a more complicated reactive oxygen species involvement. In any case, more study is needed to probe these hypotheses.

## Appendix C. Modeling MnxG in I-TASSER to identify Mn-binding residues of the type 1 Cu proximal substrate site.

MCOs have substrate sites that are tuned to bind and turnover certain substrates. The chemical and structural makeup dictate which substrates access the type 1 adjacent site for oxidation (Fig C1). If Mnx oxidizes Mn(II) preferentially, we predict that the substrate site contains hard to borderline Lewis bases N(His) and O(Glu/Asp) that are situated in a way that facilitate the entactic Mn(III) state, alleviating some of the energy barrier to catalysis. Disrupting this center by mutating these residues will allow us to validate the binding hypothesis.



Appendix figure C1. In CueO, the *E. coli* MCO, Cu is preferentially oxidized when a Met-rich region capping the substrate site is present, like in wild type (gray structure). When the region is removed (green structure), the predilection for larger phenolic substrates is increased and that for Cu is decreased. Type 1 Cu is blue, type 2 is green, and type 3 are orange and substrate Cu atom is red atom, with labeled ligands.

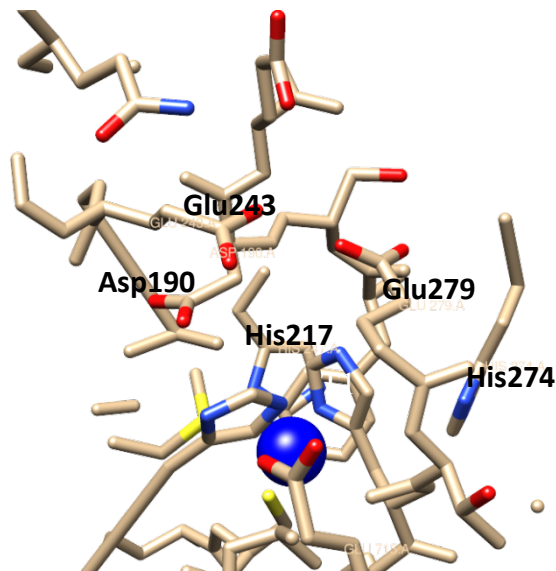
Because of the lack of substrate site sequence homology between similar MCOs MnxG and human Ceruloplasmin (hCp), even upon domain rearrangement, structural data about MnxG is required to determine which residues bind substrate, but no such



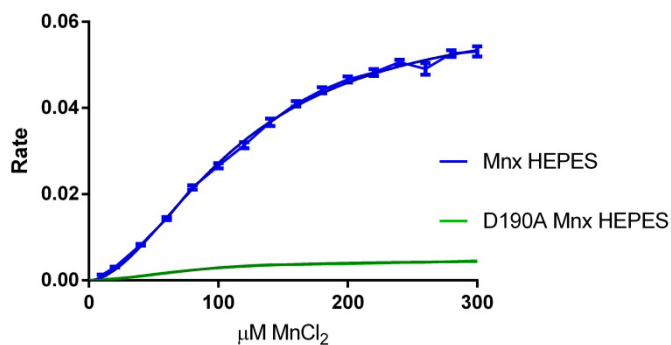
experimental data yet exists. In lieu of this I predicted the structure by simply inputting the primary sequence into the free I-TASSER software through <http://zhanglab.ccmb.med.umich.edu/I-TASSER/> (Zhang, 2008; Roy et al., 2010). I-TASSER models protein structures in three steps. First, the amino acid sequence is used to generate a template structure through LOMETS threading. Second, a structure is assembled based on the reassembly of continuous fragments of the template by “replica-exchange Monte Carlo simulations with the threading unaligned regions built by ab initio modeling. The low free-energy states are identified by SPICKER through clustering the simulation decoys.” Thirdly, the structure is re-assembled and aligned from the cluster centroids this time using PDB structures. Lastly, the software predicts biological function by collecting information from structurally analogous proteins in the PDB. For the purpose of structure comparison, discussion of the function results are not incorporated here.

Unsurprisingly, the resulting structure was most similar to hCp (DOI:[10.2210/pdb1kcw/pdb](https://doi.org/10.2210/pdb1kcw/pdb)). The hCp structure includes six Cu ions bound in the four canonical MCO and two additional type 1 Cu bridging domains 2/3 and 4/5. The two structures, hCp and MnxG were overlaid in UCSF Chimera structure viewer program to take visualize the placements of Cu within MnxG since there was too little of this information in the resulting MnxG structure pdb file. The domains in MnxG are rearranged from hCp so the MCO Cu atoms will not be in the correct placements, predicted to be in domains 2 and 3, except for the type 1 Cu. It is in this zone and within about 10 Å of the type 1 Cu center where I hunted around for Mn binding residues.

Glu 279 and Asp 190 were identified in this manner and mutated by Christine Romano to Ala (Fig. C3). These mutants had decreased rates of Mn oxidation compared to wild type (D190A in Fig. C3, E279A data not shown). We believe that the decrease in rate coincides with less efficient Mn(II) turnover caused by the direct perturbation of the active site.



Appendix figure C2. MnxG type 1 site and proximal residues/candidates for substrate binding and mutagenesis



Appendix figure C3. Mn oxidation rate (abs @ 625 nm \* min<sup>-1</sup>) by wild type (blue) and D190A (green) over several concentrations of initial MnCl<sub>2</sub> concentrations ( $\mu\text{M}$ ).

This work demonstrates the power of using simulated structures, obtained by recently available structure prediction software, to help find important functional residues that had no sequence homology to functional residues. Further, several His residues were

identified as candidates for Mn binding but their cloning is still ongoing at the time of this writing. Experimental data including the structure of Mn soaked Mnx crystals will validate the substrate binding candidates presented here, which will bring us closer to answering how Mn(II) is destabilized toward Mn(III) and plotting the course for Mn oxidation through the protein.